Technische Universität München
Lehrstuhl für Grünlandlehre

Phytomer growth and development, and nitrogen dynamics in a perennial C_4 grass

Fang Yang

Vollständiger Abdruck der von der Fakultät Wissenschaftszentrum Weihenstephan für Ernährung, Landnutzung und Umwelt der Technischen Universität München zur Erlangung des akademischen Grades eines
Doktors der Naturwissenschaften (Dr. rer.nat.)
genehmigten Dissertation.

Vorsitzender: Univ.-Prof. Dr. Urs Schmidhalter

Prüfer der Dissertation:

1. Univ.-Prof. Dr. Johannes Schnyder
2. Priv.-Doz. Dr. Yuncai Hu

Die Dissertation wurde am 06.03.2017 bei der Technischen Universität München eingereicht und durch die Fakultät Wissenschaftszentrum Weihenstephan für Ernährung, Landnutzung und Umwelt am 19.04.2017 angenommen.

Contents

Abstract……ii

Zusammenfassung…….....iv

List of Figures…….....vii

List of Tables…….....xii

Chapter I. General Introduction……...…….1

Chapter II. Effects of nitrogen fertilizer supply and vapor pressure deficit on phytomer growth and development in a perennial C_4 grass (*Cleistogenes squarrosa*)…...….9

Chapter III. Nitrogen dynamics in a perennial C_4 grass (*Cleistogenes squarrosa*) at the leaf and tiller level during vegetative growth……34

Chapter IV. General and summarizing Discussion……..…...60

References……..…….……74

Author contributions to chapter II&III.……..….89

Appendix 1. Supplementary figures for chapter II....……...…...90

Appendix 2. Supplementary methods for chapter IV...……...…….....93

Appendix 3. Nitrogen fertilization and $\delta^{18}O$ of CO_2 have no effect on ^{18}O-enrichment of leaf water and cellulose in *Cleistogenes squarrosa* (C_4) – is VPD the sole control? (a co-authored publication)…….……...95

Appendix 4. An oxygen isotope chronometer for cellulose synthesis: the successive leaves formed by tillers of a C_4 perennial grass (a co-authored manuscript; under review)……..107

Acknowledgments……..…….....138

Lebenslauf……..……...139

Abstract

Aims: The subject of the present thesis is the characterization of morphological features and N dynamics of a perennial C_4 grass, *Cleistogenes squarrosa*, a co-dominant species in Inner Mongolia Grassland, a natural arid and semiarid ecosystem. First, the effects of nitrogen supply and vapor pressure deficit (VPD) on phytomer growth and development were investigated based on measurements of phytomer lengths. The knowledge of phytomer development is imperative for evaluating the history of leaf isotopic signatures (^{18}O) and other physiological measures to reconstruct environmental conditions and ecophysiological responses of *C. squarrosa*. The second part of this thesis is focused on N dynamics at the leaf and tiller level by using ^{15}N labeling, especially concerning the N turnover in mature leaf blades of different developmental stages.

Materials and Methods: The experiments were conducted in specialized gas exchange and labeling mesocosms. Stands of *C. squarrosa* were grown in controlled-environmental chambers with 16-h photoperiod, different combinations of nitrogen (N) supply (low N: 7.5 mM; high N: 21.5 mM NO_3^-) and atmospheric vapor pressure deficit (low VPD: 0.63 kPa; high VPD 1.58 kPa) but otherwise identical and constant growth conditions. Elongation of phytomers was measured daily for 13 days in each treatment in four experimental rounds. Then component lengths of immature and mature phytomers were measured following dissection. N dynamics was studied in one treatment by labeling individual plants with $^{15}NO_3/^{14}NO_3$ for periods ranging from 24 h to 168 h, followed by measurements of isotope compositions in each component of phytomers.

Results and Discussion: The coordination of growth within and between phytomers was not affected by N supply and VPD. However, plants exhibited a significant response in tillering, showing a clear increase under high N supply. Phytomer tip emergence was coincident with the acceleration phase of its elongation and occurred when phytomers reached 26% of their final length. Blade elongation stopped when phytomers reached ~75% of their final length, and when final elongation of the preceding phytomer was confined to internode growth. No net change in N content was observed in the upper 6 to 7 mature blades, but labeling indicated a turnover rate of bulk

N in mature blades of major tillers of 0.36% per hour. N export from the mature tissues of a major tiller was approx. 2.5 times higher than N import into the immature part of the same tiller. Thus, N export of major tillers seemed to supply other parts of the plant. In accordance with this interpretation, the growth rate of the whole shoot was about three times higher than that of major tillers, due to continued production of young tillers. Thus, the excess of mobilized N must have served as a substrate for young tiller growth. These results indicated that N dynamics at the tiller level is integrated with that of the remainder of the shoot.

Conclusions and perspectives: This work presented for the first time a quantitative analysis of phytomer growth and development, and N dynamics of a wild, perennial C_4 grass. Results revealed a strong coordination of elongation both within a phytomer and between successive phytomers on a tiller. These relationships were virtually unaffected by nitrogen nutrition and VPD, providing important insight into environmental influences on plant morphological and phenotypic plasticity. The knowledge of phytomer development can help to interpret isotopic signatures of plant parts in terms of underlying dynamics and can also assist in reconstructions of e.g. short-term hydrological changes (as shown in a companion PhD thesis) or in archived materials (e.g. herbaria), and so, may help to re-evaluate environmental changes in the Mongolia grassland ecosystem. N turnover in mature blades assessed by N labeling revealed a much higher contribution of N mobilization in mature tissue than that had been derived from observation of net changes in N content alone. Additionally, the analysis of N dynamics revealed that N mobilized from a major tiller is not only used for its own growth but also for the remainder of the shoot. In future studies, the analysis of sink-source relationships in tiller N dynamics should be explored in more depth, such as quantifying the contribution of N mobilziation from mature tissue to immature tissue growth. By labeling with higher temporal resolution, such as in a diurnal circle, the analysis of the coupling of N dynamics and C dynamics in leaves by the concomitant ^{13}C labeling should provide valuable insights.

Zusammenfassung

Ziele: Ziel der vorliegenden Arbeit ist die Beschreibung der morphologischen Eigenschaften und der N-Dynamik von *Cleistogens squarrosa*, einem perennierenden C_4-Gras. Dieses Gras ist eine co-dominante Art im Grasland der Inneren Mongolei, einem natürlichen semiariden bis ariden Ökosystem. Im ersten Teil der Arbeit wurden die Auswirkungen unterschiedlicher N-Versorgung und atmosphärischen Wasserstress (Wasserdampfsättigungsdefizit) auf Wachstum und Entwicklung sukzessiv an einem Trieb gebildeter Phytomere untersucht. Die Kenntnis der Phytomerentwicklung ist Voraussetzung für die Auswertung der Isotopensignatur eines Blattes (beispielsweise der ^{18}O-Signatur) hinsichtlich der Rekonstruktion von Umweltbedingungen und der ökophysiologischen Reaktion von *C. squarrosa* auf dieselben. Im zweiten Teil der Arbeit liegt der Fokus auf N-Dynamiken auf Blatt- und Triebebene, untersucht mit Hilfe von ^{15}N-Markierung, insbesondere die Ermittlung des N-Turnover in vollständig expandierten Blättern.

Material und Methoden: Die zugrundeliegenden Experimente wurden in speziellen Gaswechsel- und Markierungskammern durchgeführt. Bestände von *C. squarrosa* wurden darin in einem 16-h Tag und bei unterschiedlichen Kombinationen von N-Versorgung (Niedrig: 7,5 mM N; Hoch: 22,5 mM N) und Wasserdampfsättigungsdefizit (VPD; Niedrig: 0,63 kPa; Hoch: 1,58 kPa) angezogen. Die übrigen Umweltbedingungen wurden gleich gehalten. Das Wachstum der Phytomere wurde über ein Intervall von 13 Tagen täglich gemessen. Diese Messungen wurden in jedem Verfahren in insgesamt vier Wiederholungen durchgeführt. Nach einer destruktiven Beprobung im Anschluss an das Messintervall wurden die Länge der Einzelkomponenten von wachsenden und vollständig expandierten Phytomeren bestimmt. In einem der Verfahren wurden einzelne Pflanzen über Zeiträume von 24 h bis 168 h mit $^{15}NO_3/^{14}NO_3$ markiert, um die N-Dynamiken innerhalb eines Triebes zu erfassen.

Ergebnisse und Diskussion: Die Koordination des Wachstums innerhalb und zwischen sukzessiven Phytomeren war nicht von N-Versorgung und VPD beeinflusst. Die Pflanzen zeigten jedoch eine deutliche Reaktion der Bestockung auf die hohe N-Versorgung. Das Erscheinen der Spitze der Phytomere fiel mit der beschleunigten Phase ihres Streckungswachstums zusammen, zu einem Zeitpunkt, als die Phytomere 26% ihrer Endlänge erreicht hatten. Die Streckung der Blattspreite war abgeschlossen bei

Erreichen von ~75% der Endlänge des gesamten Phytomers, zu einem Zeitpunkt also, als das Streckungswachstum des vorgehenden Phytomers schon auf das Internodium beschränkt war. In den oberen 6 bis 7 vollständig expandierten Phytomeren der Haupttriebe wurde keine Netto-Änderung des N-Gehaltes beobachtet; die N-Markierung zeigte jedoch einen N-Turnover in diesen Phytomeren von 0,36% pro Stunde. Der N-Export aus dem vollständig expandierten Gewebe der Triebe war ca. 2,5-mal grösser als der N-Import in das wachsende Gewebe derselben Triebe. Folglich diente der N-Export der Haupttriebe der N-Versorgung anderer Pflanzenteile. Gestützt wurde diese Interpretation durch die Tatsache, dass die relative Wachstumsrate des gesamten Sprosses ca. dreimal höher war als die der Haupttriebe, was mit der andauernden Bestockung (d.h. Nebentriebbildung) zu erklären war. Der Überschuss an mobilisiertem N diente also vermutlich als Substrat für das Wachstum der Nebentriebe. Diese Ergebnisse deuten darauf hin, dass die N-Dynamik eines Triebes in die des gesamten Sprosses integriert ist.

Schlussfolgerungen und Ausblick: Diese Arbeit kombiniert erstmalig die quantitative Analyse von Phytomerwachstum und -entwicklung mit der Untersuchung der N-Dynamiken in einem natürlich vorkommenden, perennierenden C_4-Gras. Die Ergebnisse zeigen eine enge Koordination des Streckungswachstums sowohl innerhalb als auch zwischen sukzessiven Phytomeren eines Triebes. Diese Beziehungen waren nahezu unbeeinflusst von N-Versorgung und VPD, und liefern so wichtige Erkenntnisse hinsichtlich des Umwelteinflusses auf Morphologie und phänotypische Plastizität. Die Kenntnis der Phytomerentwicklung ist hilfreich bei der Interpretation isotopischer Signaturen von Pflanzen bezüglich der zugrunde liegenden Dynamiken und kann ebenso bei der Rekonstruktion von z.B. kurzzeitigen Änderungen der Wasserversorgung genutzt werden (wie in einer parallel durchgeführten Dissertation gezeigt wurde). Diese Kenntnisse können auch auf archiviertes Material, z.B. aus Herbarien, angewandt werden und können so dazu dienen, Änderungen der Umweltbedingungen in der Inneren Mongolei zu rekonstruieren. Die Abschätzung des N-Turnovers mittels N-Markierung ergab eine wesentlich höhere N-Mobilisierung in vollständig expandiertem Gewebe als sie aus der reinen Netto-Änderung des N-Gehaltes abgeleitet worden wäre. Zusätzlich konnte gezeigt werden, dass der in Haupttrieben mobilisierte N nicht nur für das Wachstum innerhalb dieser Triebe verwendet wird, sondern auch anderen

Sprossteilen zur Verfügung steht. Die Analyse der Sink-Source-Beziehungen in einem Trieb soll noch weitergeführt werden, so z.B. der Beitrag der N-Mobilisierung in vollständig expandiertem Gewebe zur N-Versorgung wachsender Triebteile. Eine höhere zeitliche Auflösung der Markierung in Kombination mit ^{13}C-Markierung, beispielsweise im Tag-Nacht-Gang, würde die Analyse der Kopplung von N- und C-Dynamiken in Blättern noch wertvoller mache.

List of Figures

Figure I.1 N concentration in mature, fully expanded leaves along the axis of a tiller of *C. squarrosa* grown in its' natural habitat (data from Yang *et al.* 2011b). Phytomers were numbered basipetally, that is from the youngest to the oldest, starting at phytomer 2 that bore the youngest fully expanded leaf blade. Error bars indicate SE……...3

Figure II.1 Schematic of a mature phytomer and its components, and arrangement of phytomers along a tiller of *C. squarrosa*. The ligule (or collar; not shown) marks the blade-sheath junction, and the node forms the site of insertion of the leaf on the stem. Immature, growing phytomers are situated at the tip of the tillers (note: for simplicity, the scheme depicts only two growing phytomers, but up to five concurrently expanding phytomers in different developmental stages are found along the distal part of tiller axis upon dissection)…….....…...16

Figure II.2 Final (mature) length of phytomers along the axis of the main tiller of *C. squarrosa* under contrasting nitrogen fertilizer and VPD treatments. Phytomer number was counted from the tip of the tiller. Error bars indicate SE (n = 16)….19

Figure II.3 Fractional contributions of phytomer components to the final length of phytomers at successive stages of phytomer elongation of *C. squarrosa* under contrasting N fertilizer and VPD treatments. Panel A, blade; panel B, sheath; Panel C, internode. The solid lines were fitted to the data of all treatments. Stage of elongation is given by the fraction of final phytomer length, estimated as the ratio of the actual phytomer length to the predicted final phytomer length (see Methods). All data were obtained from destructive measurements. Each point corresponds to a single measurement…….23

Figure II.4 Relationships between the lengths of two successive immature (non-fully-elongated) phytomers. Different symbols denote different phytomer ranks: open squares, P_{S-1} vs. P_S; crosses, P_{S-2} vs. P_{S-1}; open diamonds, P_{S-3} vs. P_{S-2}; open circles, P_{S-4} vs. P_{S-3}. P_S indicates the phytomer that bore the youngest emerged ligule (youngest near-fully elongated phytomer with ligule visible above the surrounding leaf sheath of the next older phytomer); P_{S-1}, P_{S-2}, P_{S-3} and P_{S-4} refer to progressively younger phytomers. Each point corresponds to a single measurement……..24

Figure II.5 Relationships between the lengths of two successive immature (non-fully-elongated) phytomers of *C. squarrosa* under contrasting N fertilizer and VPD treatments. A low or high N fertilizer supply (N1 or N2) was combined with high or low VPD (V1 or V2). P_n refers to any given immature phytomer and P_{n-1} to the corresponding next younger phytomer. Symbols differentiate treatments: closed circles, N1 V1; open circles, N1 V2; closed squares, N2 V1; open squares, N2 V2. All data were obtained from destructive measurements. Each point corresponds to a single measurement. Solid line denotes a sigmoidal function fitted to the combined data of all treatments: $y = 1.34/\{1 + \exp[(0.91 - x)/0.24]\}$ ($R^2 = 0.90$; residual standard error = 0.1).……..……..25

Figure II.6 Time course of the fraction of final phytomer length in *C. squarrosa* under contrasting N fertilizer and VPD treatments. A low or high N fertilizer supply (N1 or N2) was combined with low or high VPD (V1 or V2). Colored circles represent the visible phase of the time course of phytomer development (see Materials and Methods): green circles, N1 V1; purple circles, N1 V2; red circles, N2 V1; blue circles, N2 V2. Black and white symbols represent the initial phase of phytomer development based on predictions of age and the final length: closed circles, N1 V1; open circles, N1 V2; closed squares, N2 V1; open squares, N2 V2. Tip emergence was defined as the moment a leaf blade tip had grown past the highest visible ligule of the preceding phytomers. The curve denoted the two-parameter sigmoidal function for all data: $y = 1/\{1 + \exp[(1.82 - x)/ 1.81]\}$($R^2 = 0.96$; residual standard error = 0.04)……..……27

Figure II.7 Relationships between the length of a blade and the length of its preceding sheath (i.e. length of blade Nr. n-1 vs. length of sheath Nr. n) in mature phytomers of *C. squarrosa* under contrasting N fertilizer and VPD treatments. A low or high N fertilizer supply (N1 or N2) was combined with low or high VPD (V1 or V2). Panel A, N1 V1; Panel B, N1 V2; Panel C, N2 V1; Panel D, N2 V2. The solid line indicates the fitted linear regression……...29

Figure III.1 Schematic representation of growth in a tiller of *C. squarrosa* over one leaf appearance interval. The tiller is divided in two functionally distinct compartments, immature tissue (IMT) and mature tissue (MT), with each composed of a number of phytomers (shown as solid-lined boxes). Mature phytomers are numbered consecutively from the youngest (P_2, the phytomer that bore the youngest emerged ligule) to the oldest (*n*). The grey dash-dotted box

denotes the IMT that is composed of immature phytomers. The black dash-dotted box denotes the MT. Two mature phytomers are highlighted by colored boxes. Within one leaf appearance interval, one mature phytomer is added to the MT, and P_2 turns to P_3, and so on. P_2 is exported out of IMT and referred to as "recently exported tissue", i.e. RET……..……..……..…...37

Figure III.2 Experimental scheme. Labeling experiments were performed with plants of *C. squarrosa* grown in two growth chambers. Stands in two chambers received a modified Hoagland nutrient solution with 7.5 mM nitrate-N as the sole N source. Except for the N isotope composition of the nutrient solution and the C isotope composition of the CO_2 all conditions were kept the same in each chamber. Transferred plants were labeled in the new environment for targeted durations. Four plants were sampled in each labeling interval……...39

Figure III.3 Representative images of different developmental stage blades in a tiller of *C. squarrosa*. Leaf blades were photographed at 43, 47, 49, and 54 days of age. All plants sampled were in the vegetative growth. Blades were arranged from the left to right on white paper according to their positions in a tiller (i.e. from the tip to the base of the tiller). All blades were fully expanded except for the youngest exposed blade, near the tip of the tiller…….……..41

Figure III.4 Flow chart of the individual steps to derive different flux parameters for mature tissue and mature blades in a tiller.……...……....45

Figure III.5 Natural logarithm of C mass (A) and N mass (B) *versus* time in different plant parts of *C. squarrosa*. Lines indicate linear regressions. Linear regression for whole shoot C: $Y = 0.1085*X + 1.153$, $R^2 = 0.32$; for total plant C: $Y = 0.117*X + 1.094$, $R^2 = 0.34$; for major tiller C: $Y = 0.059*X + 1.089$, $R^2 = 0.17$. Linear regression for whole shoot N: $Y = 0.095*X – 1.391$, $R^2 = 0.24$; for total plant N: $Y = 0.102*X – 1.491$, $R^2 = 0.29$; for major tiller N: $Y = 0.033*X – 1.040$, $R^2 = 0.10$……....48

Figure III.6 Representative images of a *C. squarrosa* plant at different developmental stages……...……...49

Figure III.7 Changes of N mass in immature tissue of a tiller of *C. squarrosa* over the time. Values are means ± SE ($4 \leq n \leq 8$). The dotted line denotes an average value. A linear function fitted to all individual data: $y = -0.003*x + 0.26$ ($r^2 = 0.04$; $p = 0.15$; $n = 60$).The change of N mass over time was not significant……...50

Figure III.8 N mass per unit leaf blade area (specific leaf N; SLN; A), N concentration (B), and dry mass per unit leaf area (specific leaf mass; SLM; C) in mature blades of a major tiller of *C. squarrosa*. Values are means ± SE (*n* = 32). Leaves were numbered basipetally, that is from the youngest to the oldest, starting at leaf 2, the leaf with the youngest fully expanded leaf blade in a tiller……...51

Figure III.9 Fraction of labeled N in mature blades of a tiller of *C. squarrosa* after 24 h-long ^{15}N labeling. The labeling period included a 16-h light period and 8-h dark period. Leaves were numbered basipetally, that is from the youngest to the oldest, starting at leaf 2, the leaf with the youngest fully expanded leaf blade in a tiller. Values are means ± se (*n* = 4)…….....54

Figure III.10 N fluxes in different leaf age categories of mature blades along major tillers of *C. squarrosa*. Leaves were numbered basipetally, that is from the youngest to the oldest, starting at leaf 2, the leaf with the youngest fully expanded leaf blade in a tiller. Values are means ± se (import: *n* = 4; net change: *n* = 32; export was calculated by the difference between import and net change)..……...55

Figure IV.1 Relationships between relative photosynthesis rate (RPR) and relative N import rate (RNIR in panel A), and relative N export rate (RNER in panel B) in mature leaf blades along major tillers of *C. squarrosa*. RPR was determined via concomitant ^{13}C labeling, and Different symbols represent different blade age categories. Blades were numbered from the tip to the base of a tiller. The line indicates a linear regression between RNIR and RPR: y = 0.444*x + 0.002 (r^2 = 0.5; *p* = 0.02). The relationship between RNER and RPR is not significant (*p* = 0.79).....64

Figure IV.2 Conceptual representation of nitrogen pools (black boxes) and fluxes (blue and red arrows) within a tiller of *C. squarrosa*.……66

Figure IV.3 Fraction of labeled N in the import flux into immature tissue (IMT) of a tiller of *C. squarrosa* during contentious ^{15}N labeling…….……..68

Figure IV.4 $\delta^{18}O$ of cellulose in successively produced mature leaf blades along major tillers of *C. squarrosa* grown under 7.5 mM N fertilizer conditions…….69

Figure IV.5 Time course of the fraction of final blade length in *C. squarrosa* grown under 7.5 mM N fertilizer conditions (low and high VPD: panel A and B)……..71

Figure IV.6 Fraction of new oxygen ($f_{\text{new O}}$) in cellulose of leaf blades of different ages in plants 7 days after transfer to a new VPD environment *versus* fraction of leaf blade length at the time of transfer……72

List of Tables

Table II.1 Growth and developmental parameters of *C. squarrosa* under contrasting N fertilizer and VPD treatments and the results of two-way ANOVA for each parameter……...…….....21

Table II.2 Coefficients and confidence intervals of the fitted two-parameter sigmoidal regressions for visible time course of phytomer elongation in four treatments….26

Table II.3 Coefficients and confidence intervals of the fitted two-parameter sigmoidal regressions for the complete time courses of phytomer elongation in four treatments.....28

Table II.4 Coefficients and confidence intervals of the fitted linear regressions between the length of a blade and the length of its preceding sheath (i.e. length of blade Nr. n-1 vs. length of sheath Nr. n) of mature phytomers in four treatments.……...30

Table III.1 Nitrogen mass and fluxes in immature tissue, mature tissue of a major tiller during the labeling experiment. Values are means ± SE ($4 \leq n \leq 8$). Values denoted by different letters are significantly different between the immature and mature tissue at $P < 0.05$……....50

Table III.2 Comparison of parameter *a* between plant ages. Parameters were estimated by a quadratic regression of specific leaf nitrogen as a function of phytomer number (y and x, respectively) ($y = a^* x^2 + b^* x + c$).…….....52

Table III.3 Comparison of parameter *b* between plant ages. Parameters were estimated by a quadratic regression of specific leaf nitrogen as a function of phytomer number (y and x, respectively) ($y = a^* x^2 + b^* x + c$)…….....53

Chapter I
General Introduction

Study background

In semiarid and arid ecosystems, net primary production is mainly limited by water availability but often co-limited by N availability (Hooper & Johnson, 1999; Bai *et al.*, 2008). Inner Mongolia grassland forms part of the Central Asian Steppe, the largest contiguous biome of the world. It is characterized by a semi-arid climate, and includes several vegetation types: meadow steppe, typical steppe, and desert steppe (Xiao *et al.* 1995). This grassland exhibits high spatial heterogeneities in soil properties such as water, nitrogen and other resources, related to predominant production systems with hardly controlled grazing management (Su *et al.*, 2006; Zhou *et al.*, 2008). The grassland is dominated by C_3 plants (Bai *et al.*, 2008), but often co-dominated by C_4 plants (Chen *et al.*, 2002). C_4 plants contribute approximately 20% to the total productivity in these grassland communities (Auerswald *et al.*, 2009), but the abundance of C_4 plants increased by ~10% during the last decades (Wittmer *et al.* 2010). Accordingly, we expect that the performance of C_4 plants may relate to their responses to atmospheric water stress (i.e. atmospheric vapor pressure deficit, VPD) and nitrogen (N) nutrition. So far, related studies have analyzed the relationships between C_4 abundance and water availability, increasing temperature, and grazing (Wittmer *et al.* 2010; Auerswald *et al.*, 2012), and the relations between leaf carbon isotopes discrimination and environmental factors (Yang *et al*. 2011b). However, to elucidate the response of C_4 plants to environmental factors, we first need to understand the response of their morphological development, which is unknown to date for these species and in particular for the most abundant one, a perennial grass, *Cleistogenes squarrosa*. Previous studies only characterized plant growth patterns, the allocation of nitrogen and carbon in aboveground and belowground tissues in relation to environmental parameters (e.g. N fertilizer supply, grazing, precipitation) (Gao *et al.* 2005, 2007; Kinugasa *et al.*, 2012). Secondly, no study has investigated the mechanism of N dynamics of C_4 plants in that grassland. N mobilization in mature plant parts is important for new growth, and it seems to be generally related to organ senescence and associated protease activity

(Diaz *et al*., 2008; Masclaux-Daubresse *et al*., 2008; Girondé *et al*. 2015). N mobilization in vegetative plant parts is also an important mechanism for improving N use efficiency of plants in the reproductive stage (Gallais *et al.,* 2006). A study of N dynamics in C_4 plants of that grassland may enhance the understanding of the physiological controls of their abundance in the Inner Mongolia grassland. Thus, the goal of my work was to understand the ecological and physiological factors controlling morphological development and N metabolism of a C_4 grass.

Cleistogenes squarrosa in Inner Mongolia grassland

In Inner Mongolian grassland, most C_4 species are *Poaceae* and *Chenopodiaceae* (Pyankov *et al*., 2000; Tang & Liu, 2001). In the last decades, *C. squarrosa*, an endemic perennial C_4 bunchgrass, has spread significantly and become a dominant species in typical, meadow, sandy steppes (Su *et al*., 2006; Gong *et al*., 2008; Miao *et al*., 2009; Bai *et al*., 2010). The main growth period of this species starts later in the growing season than that of C_3 plants; significant growth occurs between June and August (Liang *et al*., 2002; Yang *et al*., 2011a), when on average 64% of the total annual precipitation occurs (Auerswald *et al*., 2012). This is due to the fact that plants of the C_4 photosynthesis type have a higher temperature optimun than C_3 plants. *C. squarrosa* has a rooting depth of only ~20 cm (Chen *et al.* 2001; Jigjidsuren & Johnson 2003), and thus is completely dependent on shallow soil water from summer precipitation (Yang *et al.*, 2011a). Hence, its' competitive strength is likely enhanced by summer rains (Auerswald *et al*. 2012). An early report showed that *C. squarrosa* was only a small component of the Inner Mongolia plant community, which was essentially dominated by C_3 plants (Liu, 1963). Later, Li (1989) predicted that *C. squarrosa* would replace dominant C_3 plants at moderate grazing pressures. Progressively, *C. squarrosa* dominates (86-98%; average of 91%) the C_4 community of this grassland system (Auerswald *et al*. 2012).

The significant expansion of *C. squarrosa* must be associated with well adapted ecophysiological features. Indeed, *C. squarrosa* has an ability to produce more tillers and more leaves per tiller than other species of the same genus (Liang *et al.* 2002), and remains active and productive even in degraded grasslands (Wang, 1992). Along a tiller of *C. squarrosa* grown under natural conditions, the leaf N content showed a

decrease with phytomer rank (Fig. I.1), that was seen as a key factor driving the variation of leaf carbon isotope discrimination during photosynthesis (Yang *et al*., 2011b). However, what is not evident from this study, is if this N distribution within a tiller is an intrinsic characteristic of initial N allocation, or is a result of leaf nitrogen turnover. Possibly, this strong gradient in leaf N content along a tiller is related to a high rate of N mobilization from old, mature leaves to newly produced leaves at the top of the canopy. That result only provided the gradient of leaf N distribution along a tiller from a spatial point of view. Further, it is also unclear to which extent the N turnover and N mobilization occur simultaneously and whether these relationships change with phytomer rank. The differences among phytomer ranks are reflective of morphological dynamics. These leaves are produced in chronological order, indirectly providing a temporal basis for studying N dynamics. Thus, knowing morphological developmental traits such as leaf appearance interval is useful for studying N dynamics in a tiller. This motivated me to explore ecophysiological characteristics of *C. squarrosa* by combing the analysis of morphological traits and N dynamics in response to relevant environmental parameters such as VPD and N fertilizer supply.

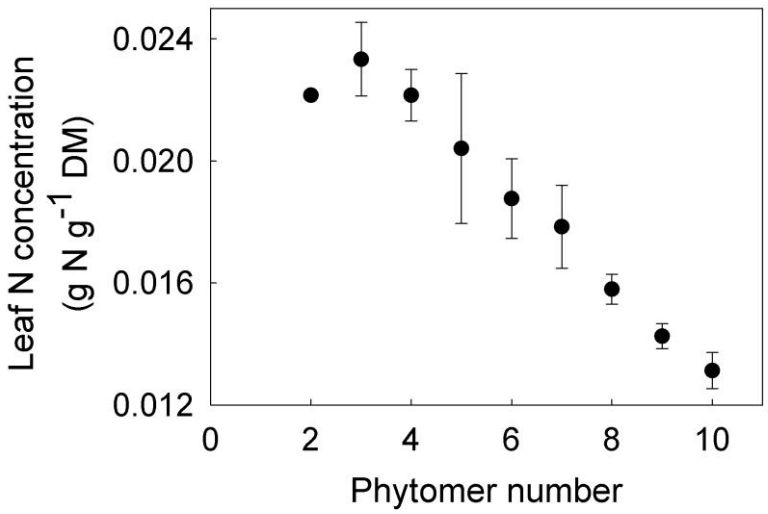

Figure I.1 N concentration in mature, fully expanded leaves along the axis of a tiller of *C. squarrosa* grown in its' natural habitat (data from Yang *et al.* 2011b). Phytomers were numbered basipetally, that is from the youngest to the oldest, starting at phytomer 2 that bore the youngest fully expanded leaf blade. Error bars indicate SE.

Morphological development of grass plants

Subunit of the morphological structure of a grass plant: the phytomer

The phytomer can be considered as a fundamental building unit of grass plants and, hence, of canopies (McMaster, 2005). A phytomer is defined as comprising a leaf blade, leaf sheath, the associated axillary buds, node, and internode (Moore & Moser, 1995). The size, number, and spatial arrangement of phytomers determine the architecture of a grass tiller (Briske, 1991; McMaster, 2005). Thus, the developmental morphology of grass plants is a function of the spatial distribution of a series of phytomers in different developmental stages – from recently initiated phytomers to senescent ones (Moore & Moser, 1995). Knowledge about the timing and rules of phytomer development or its components' development is of great interest, as phytomer morphology can serve as a basis for understanding the inherent morphogenetic constraints to environmental influences on phenotypic plasticity (Boe *et al.*, 2000).

Grass growth and development in relation to its environment

The morphological development of grass plants can be seen as an accumulation of phytomers, successively differentiating from a single apical meristem located at the tip of the shoot axis. Phytomer extension results from cell division and elongation of its components (Skinner & Moore, 2007). Phytomer extension starts from the initiation of a new leaf primordium and is terminated with the full elongation of the internode. During phytomer development, certain key events have been identified, which trigger the transition between the growth of its components, such as the emergence of the blade tip or the ligule. Knowledge of these key events is implemented in functional-structural plant modeling, which can be used to simulate shoot development and eventually the development of a canopy (Vos *et al.*, 2010). Interactions among phytomer components, i.e. leaf blade, leaf sheath, and internode are well coordinated to assure the orderly development of the plant. The coordination rules underlying phytomer development form an important basis for plant growth models e.g. for cereal crops (Fournier & Andrieu, 1998; Buck-Sorlin *et al.*, 2005; Evers *et al.*, 2005; Buck-Sorlin *et al.*, 2008;

Vos *et al.*, 2010; Zhu *et al.*, 2014). However, the patterns of phytomer development in the wild (i.e. non-domesticated) C_4 grass *C. squarrosa* are not known to date.

Response to changing environments can result in changes of the rate and/or the duration of the elongation of phytomer components (Zhu *et al.*, 2014), thus affecting the timing of the aforementioned key events. Numerous studies have pointed out that leaf growth rate is very sensitive to water supply (Passioura & Gardner, 1990), vapor pressure deficit (VPD) (Ben Haj Salah & Tardieu, 1996, 1997), and nutrient supply, especially of nitrogen (Volenec & Nelson, 1983; Gastal & Nelson, 1994). However, potential influences of environmental factors on the coordination rules of phytomer elongation are not well documented. But, to know the phytomer morphological plasticity in different environments is of importance to broaden our understanding of plant life-history strategies.

In grasses, the time interval between the emergences of successive leaves is called phyllochron (Klepper *et al.*, 1982) and is usually used to describe specific morphological events related to leaf development (Moore & Moser, 1995). This implies that not only the succession of the development of phytomer components is well coordinated, but also the development of successive phytomers. Combining the knowledge on coordination within and between phytomers allows the estimation of the developmental stage of young phytomers by the time course of the extension of the previous phytomer. This is especially helpful in studies with grasses, as the initial development of a phytomer occurs within the pseudostem of the grass tiller, i.e. covered by the tube-like structure formed by the sheaths of already fully expanded phytomers. Thus, the developmental stage of a phytomer can be determined retrospectively. In chapter II, I present phytomer growth for *C. squarrosa*. These findings are then applied to explore N dynamics of growing and mature tissues in tillers of *C. squarrosa* plants grown in the same condition in Chapter III.

Nitrogen uses in grass plants

In most higher plants, the bulk of N is stored in aboveground organs, primarily in leaves (Irving *et al.*, 2010). For a mature leaf to be fully functional, it needs to be equipped with the proper protein machinery. Protein turnover, namely synthesis and degradation,

is a permanent process over the leaf lifespan (Irving & Robinson, 2006; Hirel *et al.*, 2007; Imai *et al.*, 2008). The Rubisco protein, which is the most abundant N component, constitutes a potential pool of stored N in many species (Huffaker & Peterson, 1974; Millard, 1988). In order to support leaf growth, N components such as chlorophyll, are required for harvesting light and CO_2 (Makino & Osmond, 1991; Hörtensteiner & Feller, 2002). Therefore, growing leaves have a relative high N demand, and hence they act as a strong sink for N. When senescence proceeds in leaves, degradation of proteins provides reduced N components for the subsequent mobilization to other parts of the plant (Buchanan-Wollaston, 1997). N mobilized from protein degradation in mature or senescing leaves serves as the main N source for new growing tissues (Chapin *et al.*, 1990; Masclaux-Daubresse *et al.*, 2010). Taken together, the mechanism of N dynamics of growing and mature tissues in a tiller of *C. squarrosa* should provide essential knowledge to understand linked physiological activities.

Principally, N can be salvaged from the degradation of proteins in old leaves in favor of growing tissues (MacAdam, 2009). N retranslocation from old or shaded leaves to sunlit leaves increases the photosynthetic gain of the whole canopy (Hikosaka, 2005). Mature leaves act as an active importing agent of xylem nitrogen as well as an agent of exporting nitrogen to the phloem (Yoneyama & Takeba, 1984), providing a suite of organic N-compounds for plant growth and biomass maintenance. For *C. squarrosa*, a field study in its natural habitat showed a steep gradient in N content of leaf blades on a tiller (Yang *et al*., 2011b). The processes underlying the generation and eventual maintenance of that gradient have not been studied. Thus, we do not know how the processes of N import, turnover and export in the different leaves along a tiller – including developing, mature and senescing ones – interact to generate the N gradient observed by Yang *et al*. (2011b). For such studies, a grass tiller can conceptually be divided into two types of tissue: one is the immature tissue that is characterized by high N demand for organ growth and development acting as a strong N sink; the other is the mature tissue that potentially serves as the endogenous N source and the place where the overwhelming majority of photosynthesis is realized. This functional distinction of N partitioning between source and sink tissue can be considered as the basis of the N flux analysis in tillers of *C. squarrosa* presented in Chapter III of this thesis.

Quantitative analyses of the N supply for leaf growth of grasses mainly comes from studies tackling the question from the sink side (Lattanzi *et al.*, 2005; Lehmeier *et al.*, 2013). These studies investigated the origin of N used for new leaf growth in *Lolium perenne* (a C_3 grass) and *Paspalum dilatatum* (a C_4 grass) and showed that N recycled from internal "stores" (likely including Rubisco in senescing leaves) may account for more than half of all N used for new leaf growth. However, the actual physical/morphological origin of remobilized N and the actual N fluxes between specific sink and source organs of a tiller have not been examined to date. The understanding of how this process is regulated by source organs is also limited. Such analyses need to be integrated into analyses of N dynamics in a tiller in order to comprehensively illustrate plant N economy.

Stable N isotopes have been employed as a tracer in physiological studies to examine the movement of labeled substrates within biochemical processes, organisms, even ecosystems. Much of the information about N fluxes in plants, about N utilization during plant growth and development has been obtained by the use of ^{15}N tracer studies (De Visser *et al.*, 1997; Robinson *et al.*, 1998; Comstock, 2001; Evans, 2001; Lattanzi *et al.*, 2005; Lehmeier *et al.*, 2013). A common feature of these studies is that N dynamics was analyzed at the individual leaf level by ^{15}N labeling. However, we lack knowledge of N dynamics on larger scales such as the tiller level, hindering our understanding of N economy of the whole plant. In this study, I combine the analysis of N turnover in mature tissue and utilization of mobilized N in growing tissue with the N dynamics of plants at the tiller level using ^{15}N and ^{13}C labeling.

Aim

Although there are some field studies describing the response of *C. squarrosa* growth to environmental factors at the whole-plant level, no study has characterized its growth at the phytomer level. In addition, there is limited knowledge on N dynamics in a tiller of *C. squarrosa* and it is therefore unclear if N dynamics is affected by the N turnover of sink and source organs and/or by N demand of other parts of plants. These issues are extremely important for understanding the ecophysiological characteristics of *C.*

squarrosa. My work provides an opportunity to identify the underling mechanisms for the expansion of this grass species in the Inner Mongolia grassland.

The objectives of this work were

1) To provide fundamental information on morphological features of growth and development of a C_4 grass *C. squarrosa*, and how these respond to N fertilizer supply and VPD conditions (Chapter II). In particular, chapter II analyzes the coordination and time course of phytomer growth and development in response to its environment.

2) To investigate how *C. squarrosa* plants mediate N fluxes in tillers (chapter III), taking advantage of information obtained in chapter II, to better understand N metabolism in the context of the whole plants' physiology. Particularly, emphasis is given to the N dynamics of blades of different ages in mature tissue, which is the primary tissue for photosynthesis, N turnover and the main source of endogenous N for growing tissues. N import for tiller growth is discussed by the analysis of the time course of tracer incorporation in immature tissue (chapter IV). Based on the above results, I try to characterize the framework of sink-source relationships in the N dynamics of a vegetative grass tiller.

3) To illustrate the usefulness of the knowledge of the morphological development of *C. squarrosa* to deliver a time scale for the reconstruction of environmental conditions and ecophysiological responses.

To this end, experiments were conducted in specialized gas exchange and labeling mesocosms with identical and constant growth conditions except for nutrient supply and relative humidity. Effects of N fertilizer supply and water stress (as atmospheric water stress) on phytomer growth were tested by combinations of low (0.63 kPa) or high (1.58 kPa) VPD with low (7.5 mM) or high (22.5 mM) N fertilizer supply during plant vegetative growth. In the treatment combination of low N and low VPD, $^{15}NO_3/^{14}NO_3$ labeling was applied to disentangle net N fluxes into recent N import and N mobilization, thus quantifying N turnover in mature leaves along a tiller in dependence of their ages.

Chapter II

Effects of nitrogen fertilizer supply and vapor pressure deficit on phytomer growth and development in a perennial C_4 grass (*Cleistogenes squarrosa*)

ABSTRACT

Phytomers are basic morphological units of plants. Knowledge of phytomer development is essential for understanding morphological plasticity, functional-structural modeling of plant growth, and the usage of leaf characteristics to indicate growth conditions at the time of production (e.g. stable isotope signals). Yet, systematic analysis on the process of phytomer development is unavailable for wild or perennial C_4 grasses. Also, effects of environmental factors, such as nitrogen nutrition or vapor pressure deficit (VPD), on coordination events of developmental processes of C_4 grasses have not been studied. This study investigates phytomer growth and development in *Cleistogenes squarrosa*, a predominant C_4 grass in the Eurasian steppe, grown at low (0.63 kPa) or high (1.58 kPa) VPD with low (7.5 mM) or high (22.5 mM) nitrogen supply in controlled environments. Elongation of phytomers on marked tillers was measured daily for 13 days. Then lengths of immature and mature phytomer components (blade, sheath and internode) of all phytomers were measured following dissection. Nitrogen nutrition and VPD had no effects on coordination of growth within and between phytomers: phytomer tips emerged when phytomers reached 26% of their final length, coincident with the acceleration phase of its elongation; blade elongation stopped when phytomers reached ~75% of their final length and elongation of the preceding phytomer was confined to the internode. The relationship between fraction of final phytomer length and days after tip emergence for all treatments was well described by a sigmoidal function: $y = 1/\{1 + \exp[(1.82 - x)/1.81]\}$. *Cleistogenes squarrosa* exhibited little morphological plasticity at phytomer-level in response to nitrogen supply and VPD, but a clear increase in tillering under high N supply. Also, the invariant coordination of elongation within and between phytomers was a stable developmental feature, thus the quantitative coordination rules are applicable for

The main part of this chapter has been published as Yang et al. (2016) AoB PLANTS. doi: 0.1093/aobpla/plw075

predicting morphological development of *C. squarrosa* under contrasting levels of nitrogen nutrition or VPD.

The main part of this chapter has been published as Yang et al. (2016) AoB PLANTS. doi: 0.1093/aobpla/plw075

INTRODUCTION

The morphology of almost all grasses can be conceptualized as a hierarchical arrangement of subunits, termed phytomers, which are composed of a leaf blade, leaf sheath, node, internode, and axillary buds in the leaf axil at the node between the leaf and the stem (Moore & Moser, 1995). Phytomer development can be described as the succession of its components' elongation which follows an invariable developmental sequence: the leaf blade starts to elongate first, followed by the sheath and the internode (for some species) (Fournier & Andrieu, 1998). The size, number, and spatial arrangement of phytomers determine the architectural organization of individual tillers (Briske, 1991; Boe *et al.*, 2000). Therefore, knowledge of phytomer growth and development serves as a basis to elucidate the rhythm of grass growth.

It has been repeatedly shown that the growth of phytomer components as well as the growth of successive phytomers is well coordinated and synchronized by certain events (e.g. leaf tip emergence or ligule emergence); namely, the dynamics of phytomer development are repeated in a certain sequence along the axis of a branch or tiller (Moore & Moser, 1995; Boe *et al.*, 2000; Boe & Casler, 2005; Forster *et al.*, 2007). Synchrony between emergence events and the dynamics of organ extension has been observed for species in which the internode does not elongate, such as C_3 grasses in the vegetative stage (Skinner & Nelson, 1995; Fournier *et al.*, 2005), and for species with internode elongation, such as grasses during the generative (or reproductive) stages (Lafarge & Tardieu, 2002; Zhu *et al.*, 2014). The coordination rules underlying phytomer development form an important basis for plant growth models in different cereal crops, e.g. maize (Fournier & Andrieu, 1998; Zhu *et al.*, 2014), wheat (Evers *et al.*, 2005; Vos *et al.*, 2010) and barley (Buck-Sorlin *et al.*, 2005; Buck-Sorlin *et al.*, 2008). The need to quantify the coordination of phytomer elongation, the timing of developmental events, growth duration, phyllochron and final phytomer number is critical for crop modeling (Evers *et al.*, 2005). Furthermore, carbon and oxygen isotope compositions of leaf cellulose are potentially powerful tools for reconstruction of environmental conditions, e.g., oxygen isotope composition of leaf cellulose reflects mainly source water isotopic signal and evaporative demand (Helliker & Ehleringer, 2002). Accordingly, oxygen isotope composition of leaf cellulose of *C. squarrosa* was shown to reflect VPD of the growth environment (Liu *et al.*, 2016). For this type of

studies, the predictability of phytomer development is essential for the dating of isotopic signal imprinted in plant material. In addition, the knowledge of phytomer development provides important insights into environmental influences on plant morphological and phenotypic plasticity (Boe *et al*., 2000). In wild (i.e. non-domesticated) or perennial C_4 grasses phytomer development as well as the potential influence of environmental factors on coordination rules has not been studied, which impairs our understanding on the plasticity and predictability of morphological development.

In principle, environmental influences on plant development can result from changes in component elongation rate or from changes in component elongation duration (Zhu *et al.,* 2014), or from the timing of development events. To explicitly elucidate how plants respond to varying environments, studies performed in the field and in controlled conditions have shown that leaf elongation rate in grasses is very sensitive to water supply (Passioura & Gardner, 1990), vapor pressure deficit (VPD) (Ben Haj Salah & Tardieu, 1996, 1997), and nutrient supply, especially of nitrogen (Volenec & Nelson, 1983; Gastal & Nelson, 1994). Nitrogen (N) deficiency slows leaf blade growth (Kavanová *et al.*, 2008), decreases mature leaf size (Vos & van der Putten, 1998) and reduces leaf appearance rate (Metay *et al.*, 2014), but there is apparently little effect on leaf initiation (Ma *et al.*, 1997). It has been reported that high evaporative demand reduces maize leaf elongation rate due to water deficit (Ben Haj Salah & Tardieu, 1996, 1997). Accordingly, one may propose that phytomer growth and development in a wild grass with internode elongation in the vegetative state also responses to alterations of N and VPD supply. To know this phytomer morphological plasticity in different environments is of importance to broaden our understanding of plant life-history strategies.

Our objectives were to investigate phytomer growth and developmental characteristics of a perennial C_4 grass (*Cleistogenes squarrosa*) and its morphological response to factorial combinations of nitrogen fertilization and VPD treatments. *C. squarrosa* is a perennial C_4 grass and a co-dominant species in Inner Mongolia Grassland, a natural arid and semiarid ecosystem (Wang & Wang, 2001; Bai *et al.*, 2008). *C. squarrosa* has higher relative abundance in warm habitats such as sunny slopes (Gong *et al*., 2008), and it has been noted by authors that moderate to heavy grazing increased its relative abundance (Gong *et al*., 2008; Liang *et al.*, 2002). Due to

the dominance in many grassland types especially degraded grasslands, *C. squarrosa* is considered as a key species for sustainable grassland and livestock management in this area (Liang *et al.*, 2002). In Inner Mongolian grasslands, water and nitrogen are the primary limiting factors for plant growth (Bai *et al.*, 2008); furthermore, interaction effects of N and water strongly influences physiology and morphology of dominant species (Gong *et al.*, 2011). Moreover, soil properties exhibit strong spatial heterogeneity in nitrogen and other resources due to the inattentively managed grazing activities, e.g. grazing influences N turnover via faeces and urine redistribution (Giese *et al.*, 2013). Thus, understanding phytomer development of *C. squarrosa* and its response to VPD and N nutrition, has important implications for improving productivity and forage quality in this grassland. In this work, I hypothesized, first, that phytomer development in *C. squarrosa* exhibits coordination rules similar to those found in other grasses, but with quantitatively different dynamics in phytomer development. Second, I predicted that the growth, characterized by both leaf and internode elongation, and the final length of phytomers are affected by N supply and VPD, mediated by the well-established effects of N and water stress on leaf elongation in other grasses (see above). Third, I predicted the constancy of coordination rules within and between phytomer growths across treatments. Aiming at quantitative descriptions on phytomer development of *C. squarrosa*, I assessed phytomer elongation both for visible growth (i.e. after emergence of the blade tip above the surrounding sheath of preceding phytomers) and invisible growth (i.e. before blade tip emergence), thus covering the whole elongation from (near) initiation to cessation of elongation.

MATERIALS AND METHODS

Plant material and growth conditions

Seeds of *C. squarrosa* were collected in autumn 2010 and 2012 in the Xilin River watershed, China. Four seeds were sown in individual plastic tubes (5 cm diameter, 35 cm high) filled with quartz sand (0.3-0.8 mm diameter). Tubes were placed in free-draining plastic boxes (length: 77 cm, width: 57 cm, depth: 30 cm) with 164 tubes per box. Two boxes were placed in each of four growth chambers (Conviron PGR15, Conviron, Winnipeg, Canada). One week after sowing, plants were thinned to one plant per tube so that final density was 234 plants m^{-2}. Except for nutrient supply and VPD,

growth conditions were the same in all chambers: 16 h light period with a photosynthetic photon flux density of 800 µmol m^{-2} s^{-1} at canopy height during the light period, provided by cool-white fluorescent tubes, and constant air temperature of 25 °C throughout the light-dark cycle. CO_2 concentration in the light period was kept constant between 380 and 390 µmol mol^{-1}. Every eight hours, a modified Hoagland nutrient solution (see below) was supplied by an automatic irrigation system. The nutrient solution was completely renewed after four weeks, i.e. in the middle of experiments.

The study had a factorial design with two treatment factors, nitrogen supply and VPD; and each factor had two levels. Experiments were conducted in two separate runs with a low and high rate of N supply. All four chambers were supplied with a nutrient solution containing 7.5 mM N (N1) in the first run, and 22.5 mM (N2) in the second run, in the form of equimolar concentrations of calcium nitrate and potassium nitrate ($Ca(NO_3)_2$ and KNO_3). In each experimental run, two chambers were operated with a relative humidity of 80% and the other two with 50% relative humidity, yielding a VPD of 0.63 kPa (V1) and 1.58 kPa (V2), respectively. Thus, every combination of N supply and VPD (N1 V1, N1 V2, N2 V1 and N2 V2) was replicated in two growth chambers. The concentration of other nutrients was kept the same in both nutrient solutions: 1.0 mM $MgSO_4$, 0.5 mM KH_2PO_4, 1 mM NaCl, 125 µM Fe-EDTA, 46 µM H_3BO_3, 9 µM $MnSO_4$, 1 µM $ZnSO_4$, 0.3 µM $CuSO_4$, 0.1 µM Na_2MoO_4.

Monitoring and measurements of plant growth and calculation of phytomer elongation

Sixteen plants per treatment (eight plants per growth chamber) were tagged when the first true leaf had emerged. I started to measure phytomer elongation on main tillers on the 24th day after the imbibition of seeds. At the start of elongation measurements, the main tiller had at least ten emerged leaves. Elongation measurements lasted until the 37th day after imbibition. This corresponds to a thermal time of 925 degree days, close to the thermal time of the main vegetation period for *C. squarrosa* in Inner Mongolia (Liang *et al*. 2002). This also ensured that a sufficiently high number of phytomers completed their growth during the experiment. Each day, the distance between the tip of a phytomer and the next older visible ligule, and also the distance between successive visible ligules was measured to the nearest 0.5 mm. Our preliminary data showed that

sheath elongation stopped with the emergence of the ligule (data not shown). Thus, phytomer elongation was calculated as the change of distance from phytomer tip to the next older visible ligule. A phytomer was considered fully expanded when the distance from its tip to the next older visible ligule had ceased to change. After elongation measurements and the following dissection (see below), ranks of phytomers were counted basipetally starting from the tip of the main tiller. In most cases, tips of phytomers 4 and 5 appeared (leaf tips emerged) and terminated elongation during the observation period between 24 and 37 d after imbibition. These data were used to calculate 'visible growth duration' and the visible time course of phytomer elongation. Phytomer tip emergence was defined as the moment a blade tip had grown past the highest visible ligule of the preceding phytomers. However, as elongation measurements were performed only once a day, a phytomer tip could have emerged before our first observation on that phytomer. Therefore, the time lag between tip emergence and our first observation on that phytomer was estimated as the distance between the tip of the phytomer in question and the next older visible ligule divided by the elongation rate measured just following tip emergence; and this time lag was accounted for in the calculation of days after tip emergence. The phyllochron was calculated as the time interval between the appearances of successive phytomers. The number of tillers formed at the base of the shoot was also recorded.

Measurements on length of phytomers and their components

At the end of each experiment, all main tillers (16 main tillers from 16 plants per treatment) on which elongation rate had been measured were sampled and dissected into individual phytomers. On these dissected phytomers, the lengths of blades, sheaths, and internodes were measured to the nearest 0.5 mm, and phytomer length was obtained as the sum of the length of its components. Thus, destructive measurements provided the actual length of blades, sheaths, internodes, and the total length of successive phytomers. Dissected tillers included fully expanded phytomers, emerged (i.e. visibly growing) phytomers, and unemerged (invisibly growing) phytomers whose tips had not yet emerged. A scheme of phytomer arrangement along successive nodes on one tiller is presented in Figure II.1. Within a tiller, all phytomers are arranged along an axis. The basipetal succession of phytomers corresponds to a gradient of increasing phytomer age. Each phytomer is composed of a leaf blade, a leaf sheath, a node and an internode.

Phytomer elongation starts with the (tip of the) blade and successively passes over to elongation of the sheath and internode. The sheath of a given phytomer enclosed the internode of the next younger phytomer and a part of its sheath. In the dissection, only phytomers with a length > 4 mm were taken into consideration excluding the shoot apex with shorter phytomers and primordia.

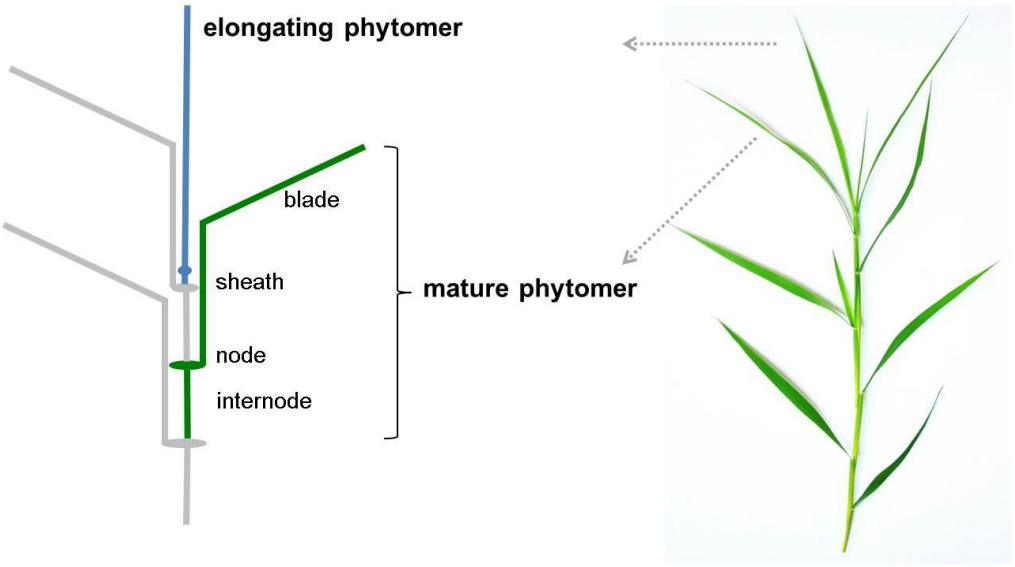

Figure II.1 Schematic of a mature phytomer and its components, and arrangement of phytomers along a tiller of *C. squarrosa*. The ligule (or collar; not shown) marks the blade-sheath junction, and the node forms the site of insertion of the leaf on the stem. Immature, growing phytomers are situated at the tip of the tillers (note: for simplicity, the scheme depicts only two growing phytomers, but up to five concurrently expanding phytomers in different developmental stages are found along the distal part of tiller axis upon dissection).

Assessing coordination within a phytomer and between phytomers

The length of successive, fully expanded phytomers (obtained from destructive measurements) was used to determine ontogenetic changes in the final length of phytomers, i.e. the relationship between final phytomer length and phytomer rank. By extrapolating this relationship, the final length of still growing phytomers (immature ones) was predicted. That prediction was performed for each individual tiller, using the

data from that same tiller. The fraction of final phytomer length (f_L) for immature phytomers was calculated as:

$$f_L = L_a/L_p \qquad \text{Eqn 2.1}$$

where L_a is the actual phytomer length at a given time, L_p is predicted final phytomer length.

Accordingly, the fraction of final phytomer length is 1 for a fully expanded phytomer. In an analogous manner, the fractional contribution of components (blade, sheath, and internode) to final phytomer length was calculated as the ratios of actual blade-, sheath-, and internode-length to predicted final phytomer length.

The coordination of elongation within a phytomer was assessed by plotting the fractional contribution of components (blade or sheath or internode) to final phytomer length against the fractions of final phytomer length. The coordination of elongation between phytomers was assessed by analyzing the relationship between fractions of final phytomer length of successive phytomers. The normalized length of components and phytomers was used to compensate for heterogeneity in plant size, which is higher for wild plants than for genetically much more uniform cultivars.

Constructing the time course of phytomer development

A young phytomer grows within the sheath tube of the preceding phytomer before tip emergence. Therefore, the complete time course of the development of a phytomer includes a visible phase (tip emergence - full expansion) and an invisible phase (initiation - tip emergence). These time courses were all established by plotting the fraction of final phytomer length against their ages (days after tip emergence).

The visible time course of phytomer development was established using the data of phytomers (numbers 4 and 5) on which the elongation rate had been monitored from tip emergence to full expansion. From the dissection of plants, the final length of those phytomers was obtained, and the actual length of those phytomers on each day during expansion was calculated retrospectively using the measured daily elongation rate. Thus, the fraction of final phytomer length of those phytomers was calculated

using Eqn 1 (using the actual measured final length as denominator) for each day from tip emergence to full expansion.

The initial phase of phytomer development was established using the data of younger phytomers which were not fully elongated (immature) at the time of dissection. For these phytomers, their fractions of final phytomer length were determined using Eqn 1. As their ages (the corresponding days after their tip emergence) were not known, these had to be estimated. In each tiller, an immature phytomer was selected that had reached 60 – 80% of its final length (typically the second oldest immature phytomer). Using the visible time course of phytomer development (see previous paragraph) the time after tip emergence of this particular phytomer was estimated. This time minus the respective number of phyllochrons gave the time after tip emergence for each phytomer younger than the selected one on this tiller. I plotted the fraction of final phytomer length against the calculated age of those immature phytomers to obtain the initial phase of phytomer development that included the invisible phase and overlapped with a small range of the visible phase of phytomer development. The construction of the initial phase of phytomer development was done separately for each treatment, using the treatment-specific data. The visible time course and initial phases of phytomer development were then combined to obtain the complete time course (i.e. the fraction of final phytomer length vs. days before/after tip emergence).

Statistical analyses

The effects of N supply (low and high N: N1 and N2), VPD (low and high VPD: V1 and V2) and their interaction on phytomer growth parameters were analyzed by two-way analysis of variance (ANOVA) using R (R Core Team, version 3.1.2, 2012). There were 16 replicates (16 main tillers: eight tillers per growth chamber) in each treatment. For parameters that were measured on several ranks of phytomers of a tiller, i.e. phyllochron, visible growth duration, maximal phytomer elongation rate and final phytomer length, the mean value of all phytomers on that tiller was used in the statistical tests. For repeatedly observed parameters, e.g. the number of visibly growing phytomers, the total number of phytomers, and the number of tillers, the mean values of repeated observations on each tiller were used in the statistical tests. The data were analyzed with a linear model using the generalized least squares method. This was

implemented with the generalized least squares (gls) function by maximizing the restricted log-likelihood (REML) method in the "nlme" package (Pinheiro *et al*., 2014), and the chamber effect was also included in the model. None of the analyses yielded a significant chamber effect. For the developmental pattern of phytomers, 95% confidence bands of regressions were fitted using Sigmaplot (Systat Software, San Jose, CA) and used to test for treatment effects.

RESULTS

Phytomer growth and developmental parameters

Averaged over all experiments (Table II.1), the number of emerged (non-enclosed) phytomers that were growing simultaneously averaged 3.9 per main tiller. The average number of phytomers per main tiller observed during the 24th to 37th day after imbibition was ~14. The phyllochron averaged 2.3 d, and the duration of visible growth (i.e. the time span from tip emergence to cessation of elongation) was about 11 d. Mean number of tillers was 21 and mean phytomer length was 93 mm (Fig. II.2). In all treatments, final phytomer length decreased by about 20% between phytomer number 9 and number 4 (Fig. II.2).

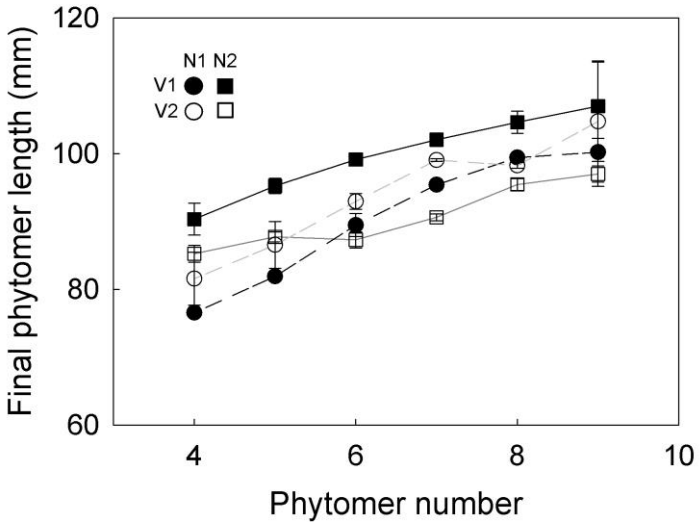

Figure II.2 Final (mature) length of phytomers along the axis of the main tiller of *C. squarrosa* under contrasting nitrogen fertilizer and VPD treatments. Phytomer number was counted from the tip of the tiller. Error bars indicate SE (n = 16).

Effects of VPD and N fertilizer supply or their interactions were relatively small or non-significant, except for the effect of N fertilizer supply where high N increased the number of tillers by 23% relative to low N (averaged over VPD levels) (Table II.1). Also, averaged over VPD levels, high N increased the number of phytomers per tiller by 6%, and shortened visible growth duration by 7%. Averaged over N levels, high VPD increased visible growth duration by 4% relative to low VPD. All other parameters of phytomer growth and development were influenced by the interaction of nitrogen fertilizer supply and VPD. Thus, high N increased the number of visibly growing phytomers per tiller by 17% and phytomer length by 8%, and shortened the phyllochron by 13% at low VPD, but not at high VPD.

Table II.1 Growth and developmental parameters of *C. squarrosa* under contrasting N fertilizer and VPD treatments and the results of two-way ANOVA for each parameter.

Parameter	Treatment				F value			Df
	N1 V1	N1 V2	N2 V1	N2 V2	N	VPD	N × VPD	
Nr of visibly growing phytomers (tiller^{-1})	3.6 ± 0.1	3.8 ± 0.1	4.2 ± 0.1	3.8 ± 0.1	6.083*	2.257	8.276*	58
Nr of phytomers (tiller^{-1})	13.4 ± 0.2	13.3 ± 0.2	14.5 ± 0.2	13.7 ± 0.2	8.073*	4.035	1.938	59
Phyllochron (days leaf^{-1})	2.4 ± 0.1	2.4 ± 0.0	2.1 ± 0.0	2.4 ± 0.1	8.627*	2.663	4.734*	60
Visible growth duration (days)	11.0 ± 0.5	11.8 ± 0.2	10.6 ± 0.2	10.6 ± 0.3	12.131*	4.604*	3.498	57
Nr of tillers	19.7 ± 1.8	17.6 ± 1.0	24.0 ± 1.1	21.7 ± 1.6	7.754*	2.005	0.003	60

A low or high N fertilizer supply (N1 or N2) was combined with low or high VPD (V1 or V2). Values are means ± SE (n = 16). The number of visibly growing phytomers on a tiller, the number of phytomers per main tiller, and the number of tillers at the base of the plant are mean values for the period between 24 and 37 days after imbibition; phyllochron was measured on phytomer ranks 1-10; visible growth duration, the period from tip emergence to the cessation of elongation, was measured on ranks 4-5. Asterisk indicates significant effect ($P < 0.05$). Df is the degree of freedom for the denominator in F and the degree of freedom for the numerator is 1 in all cases.

Coordination within a phytomer

The contributions of phytomer components (blade, sheath and internode) to final phytomer length in expanding phytomers did not show treatment effects (Fig. II.3A – C; see Fig. II.S1 in Appendix 1 for confidence intervals of the different treatments), so data of all treatments were pooled for further analysis. Solid lines in Fig. II.3A – C denote regressions with $y = 0.73/\{1 + \exp[(0.37 - x)/0.17]\}$ ($R^2 = 0.90$; residual standard error = 0.06) for blade (A); $y = 0.46/\{1 + \exp[(0.94 - x)/0.13]\}$ ($R^2 = 0.78$; residual standard error = 0.07) for sheath (B); $y = 0.04*x - 0.0063$ ($R^2=0.06$) for internode (C). The relationship between the contribution of components to final phytomer length and fractional final phytomer length showed a gradual transition between different phytomer ranks (from just after initiation of rapid expansion to near-fully expanded). Hence, the phytomers of different ranks were treated as representing one phytomer in different developmental stages. Within a phytomer, initial expansion was exclusively due to blade elongation (Fig. II.3A). Transition between blade and sheath elongation was a relatively sudden event. Sheathes were first measured when phytomers had reached approx. 50% of their final length (Fig. II.3B); moreover, initial sheath elongation was slow. When blade length had reached 66 ± 1% (SE) of final phytomer length, blades ceased to elongate and rapid sheath elongation began. As the phytomer had attained 75% of its final length by that time, initial sheath elongation must have contributed 9% to final phytomer length. Internode elongation started when the phytomer had reached approx. 80% of its final length (Fig. II.3C). Transition between sheath and internode elongation also appeared to be a relatively sudden event, as internodes significantly contributed to phytomer elongation only when sheath elongation was nearly terminated.

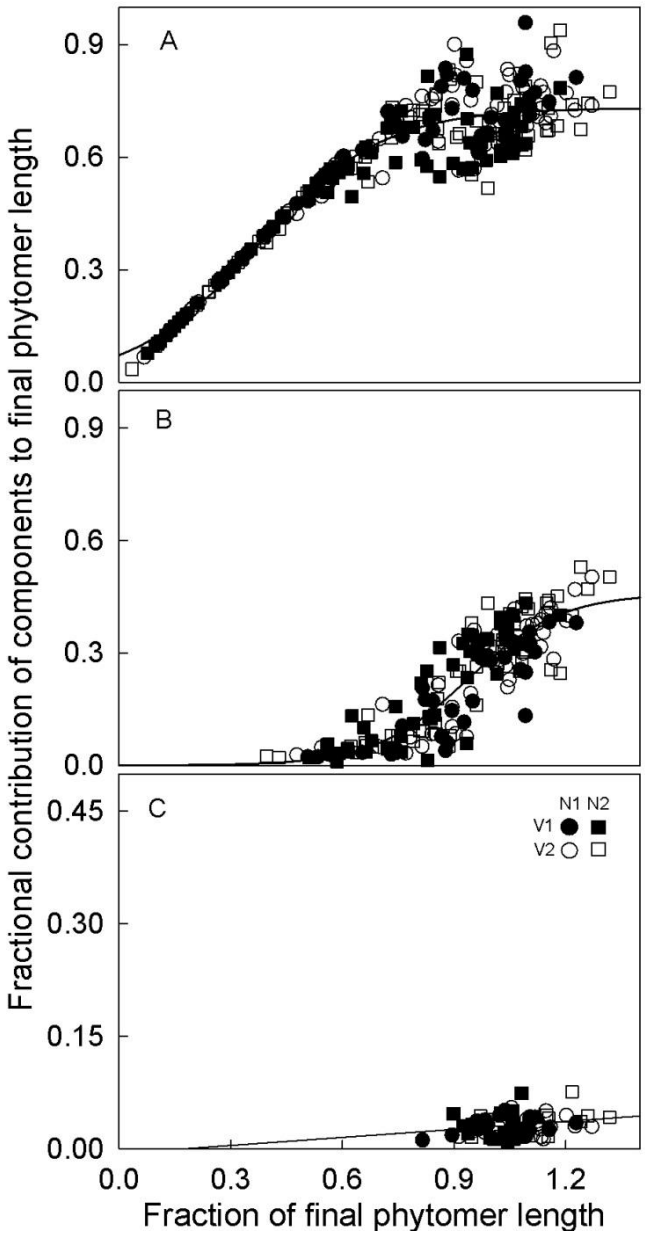

Figure II.3 Fractional contributions of phytomer components to the final length of phytomers at successive stages of phytomer elongation of *C. squarrosa* under contrasting N fertilizer and VPD treatments. Panel A, blade; panel B, sheath; Panel C, internode. The solid lines were fitted to the data of all treatments. Stage of elongation is given by the fraction of final phytomer length, estimated as the ratio of the actual phytomer length to the predicted final phytomer length (see Methods). All data were obtained from destructive measurements. Each point corresponds to a single measurement.

Coordination between successive phytomers

The coordination of development of successive phytomers was investigated by plotting their fractions of final phytomer length (Fig. II.4). At the time of the final sampling, five phytomers, including emerged and unemerged phytomers, were expanding simultaneously on the main tiller. Moreover, the fractions of final phytomer length showed a gradual transition between different phytomer ranks, indicating that these data almost contained all developmental stage phytomers.

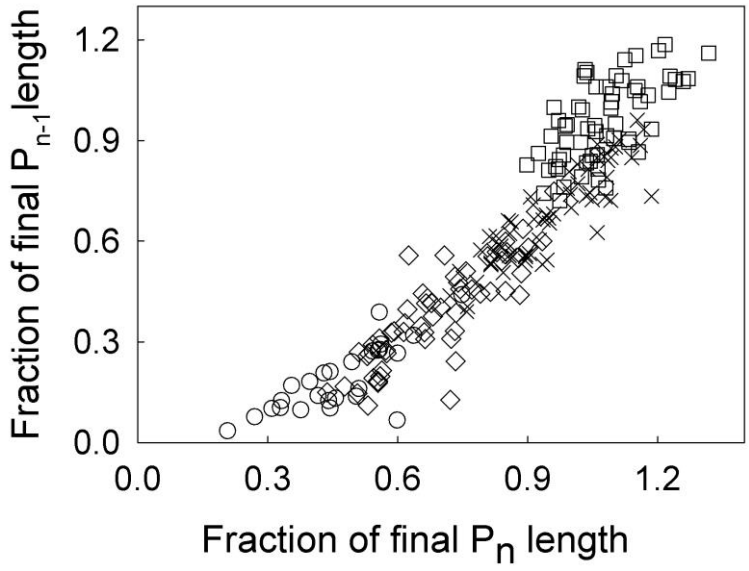

Figure II.4 Relationships between the lengths of two successive immature (non-fully-elongated) phytomers. Different symbols denote different phytomer ranks: open squares, P_{S-1} vs. P_S; crosses, P_{S-2} vs. P_{S-1}; open diamonds, P_{S-3} vs. P_{S-2}; open circles, P_{S-4} vs. P_{S-3}. P_S indicates the phytomer that bore the youngest emerged ligule (youngest near-fully elongated phytomer with ligule visible above the surrounding leaf sheath of the next older phytomer); P_{S-1}, P_{S-2}, P_{S-3} and P_{S-4} refer to progressively younger phytomers. Each point corresponds to a single measurement.

Similar to the relationship within a phytomer, the relationships between phytomers was not affected by treatments (Fig. II.5). A sigmoidal function (solid line) was fitted to the combined data of all treatments ($y = 1.34/\{1 + \exp[(0.91 - x)/0.24]\}$

(R^2 = 0.90; residual standard error = 0.1). A given phytomer (P_{n-1}) did not elongate significantly until the preceding phytomer (P_n) had reached approx. 25% of its final length. Then, P_{n-1} elongated more slowly than P_n until P_n had reached approx. 50% of final phytomer length. When the younger phytomer (P_{n-1}) had elongated to approx. 20% ± 3% (SE) of its final length, both phytomers elongated at nearly the same rate until P_n was near-fully elongated (defined here as 99% of the final length). At that time, P_{n-1} had reached 79 ± 2% (SE) of its final length, which corresponded to the length at which blade growth stopped (see previous paragraph).

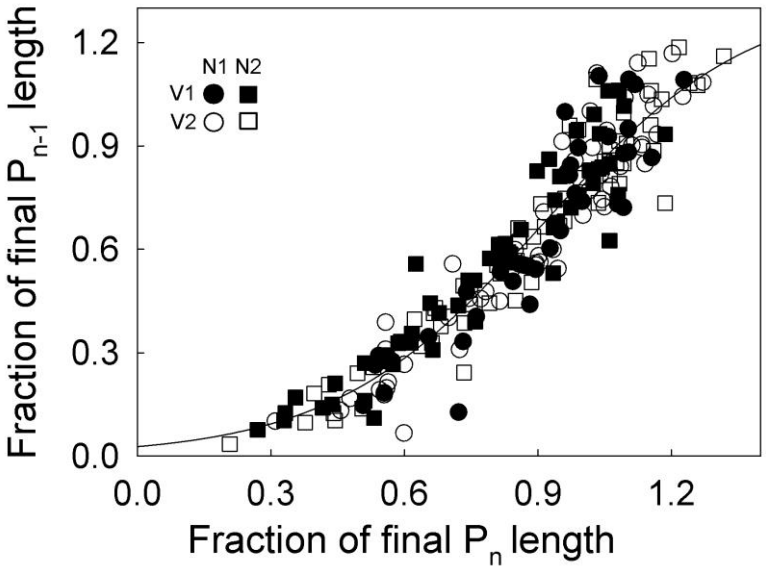

Figure II.5 Relationships between the lengths of two successive immature (non-fully-elongated) phytomers of *C. squarrosa* under contrasting N fertilizer and VPD treatments. A low or high N fertilizer supply (N1 or N2) was combined with high or low VPD (V1 or V2). P_n refers to any given immature phytomer and P_{n-1} to the corresponding next younger phytomer. Symbols differentiate treatments: closed circles, N1 V1; open circles, N1 V2; closed squares, N2 V1; open squares, N2 V2. All data were obtained from destructive measurements. Each point corresponds to a single measurement. Solid line denotes a sigmoidal function fitted to the combined data of all treatments: $y = 1.34/\{1 + \exp[(0.91 - x)/0.24]\}$ (R^2 = 0.90; residual standard error = 0.1).

Kinetics of a phytomer development

For a small number of phytomers (mainly ranks 4 and 5), the observation period of phytomer elongation covered the complete visible phase of phytomer development, which began with the appearance of the leaf tip and ended with the cessation of internode elongation. In all treatments, the visible time course of phytomer elongation followed a sigmoidal pattern (colored symbols in Fig. II.6). The parameters of corresponding sigmoidal functions were shown in Table II.2 with confidence intervals. This relationship was nearly identical for the four treatments (also see Fig. II.S2 in Appendix 1)

Table II.2 Coefficients and confidence intervals of the fitted two-parameter sigmoidal regressions for visible time course of phytomer elongation in four treatments.

Parameter	Coefficients ± 95% confidence interval			
	N1 V1	N1 V2	N2 V1	N2 V2
b	1.73 ± 0.07	1.90 ± 0.08	1.71 ± 0.05	1.82 ± 0.07
X0	1.87 ± 0.07	1.94 ± 0.08	1.69 ± 0.05	1.73 ± 0.07
R^2	0.98	0.97	0.99	0.99

The equation: $y = 1/(1 + \exp(-(x - x_0)/b))$

The curve denotes the two-parameter sigmoidal function for all data: $y = 1/\{1 + \exp[(1.82 - x)/ 1.81]\}$($R^2 = 0.96$; residual standard error = 0.04). At the time of tip emergence, phytomers had attained approx. 26% of their final lengths in all treatments. After tip emergence, phytomer length increased linearly with time until reaching approx. 85% of final length, approx. 5 days after emergence. Thereafter, phytomer elongation decreased, but continued for another 6 days. The visible period of phytomer elongation (defined here as 99% of the final length) terminated at about 11 days after tip emergence.

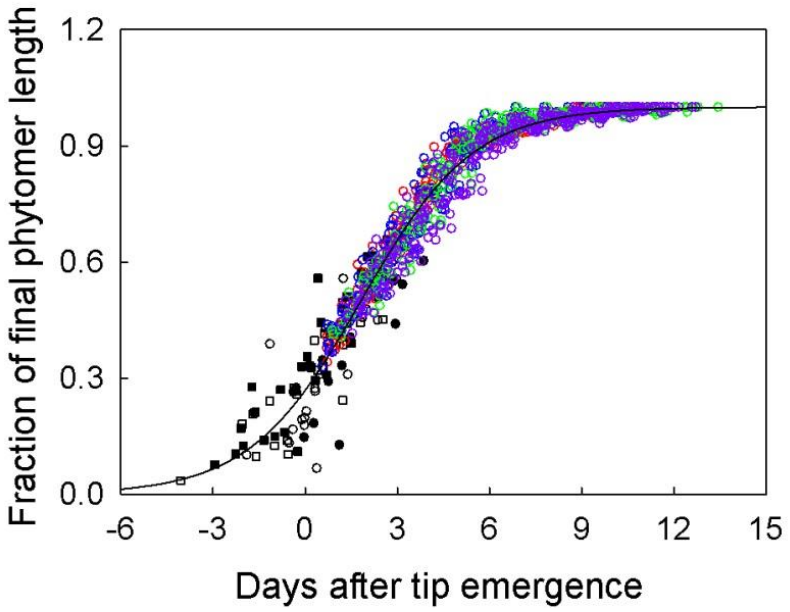

Figure II.6 Time course of the fraction of final phytomer length in *C. squarrosa* under contrasting N fertilizer and VPD treatments. A low or high N fertilizer supply (N1 or N2) was combined with low or high VPD (V1 or V2). Colored circles represent the visible phase of the time course of phytomer development (see Materials and Methods): green circles, N1 V1; purple circles, N1 V2; red circles, N2 V1; blue circles, N2 V2. Black and white symbols represent the initial phase of phytomer development based on predictions of age and the final length: closed circles, N1 V1; open circles, N1 V2; closed squares, N2 V1; open squares, N2 V2. Tip emergence was defined as the moment a leaf blade tip had grown past the highest visible ligule of the preceding phytomers. The curve denoted the two-parameter sigmoidal function for all data: $y = 1/\{1 + \exp[(1.82 - x)/ 1.81]\}$ ($R^2 = 0.96$; residual standard error = 0.04).

The reconstruction of the initial phase of phytomer development using the immature phytomers was based on the notion that the difference in age between successive phytomers corresponds to the phyllochron. Thus, data on immature phytomers and phytomers which finished elongation during the observation period could be combined to establish the complete time course of phytomer elongation from 3.5% of final phytomer length to cessation of elongation (Fig. II.6).

Data of immature phytomers (black and white symbols in Fig. II.6), for which the age had been estimated, and data of phytomers, for which the age had been directly measured (colored symbols in Fig. II.6) fit a two-parameter sigmoidal function: $y = 1/\{1 + \exp[(x_0 - x)/ b]\}$, with y denoting the fraction of final phytomer length, x days after tip emergence, b the slope of the curve, and x_0 the time when phytomer growth rate was maximum. The individual function was fitted to the complete time courses of phytomer elongation for four treatments (Fig. II.S3 in Appendix 1).The comparison of parameters of four functions was shown in Table II.3.

Table II.3 Coefficients and confidence intervals of the fitted two-parameter sigmoidal regressions for the complete time courses of phytomer elongation in four treatments.

Parameter	Coefficients ± 95% confidence interval			
	N1 V1	N1 V2	N2 V1	N2 V2
b	1.69 ± 0.07	1.84 ± 0.07	1.79 ± 0.06	1.82 ± 0.07
X_0	1.97 ± 0.07	2.02 ± 0.07	1.61 ± 0.05	1.75 ± 0.07
R^2	0.96	0.96	0.98	0.97

The equation: $y = 1/(1 + \exp(-(x - x_0)/b))$

There was no significant treatment effect on the complete time course of phytomer expansion. Phytomers reached maximal growth rate at about 2 d after tip emergence in all treatments. Starting from 3.5% of final length, the estimated time until tip emergence was approx. 4 d. The phase of near-linear maximum elongation began at about 1 d before appearance of the leaf tip when the phytomer had reached approx. 20% of final phytomer length, and ended about 4.5 d after tip appearance when the phytomer had reached approx. 85% of final length. These phases corresponded with the phases of blade and sheath elongation (Figs. II.3A&3B). The last elongation phase was associated with internode elongation, which occurred at considerably lower rates (Fig. II.3C).

Relationships between the length of blade and sheath of preceding phytomer

The blade had the length ranging from 35 to 80 mm in four treatments. Correspondingly, the sheath length of preceding phytomer ranged between 15 and 40 mm (Fig. II.7). the blade lengths were correlated with the lengths of previous sheaths. In all treatment, the blade length increased linearly with the length of previous sheath. The relationships were fitted by a linear regression. The slope of regression was 1.86 under low nitrogen and high VPD conditions, and 1.28 under high nitrogen and low VPD conditions. There were two intermediate slopes (1.52 and 1.56) in other two treatments. These slopes were significantly different from zero (Table II.4), indicating blade length strongly responded to the sheath length of preceding phytomer. However, the slope of fitted linear regression was not significantly differed in four treatments.

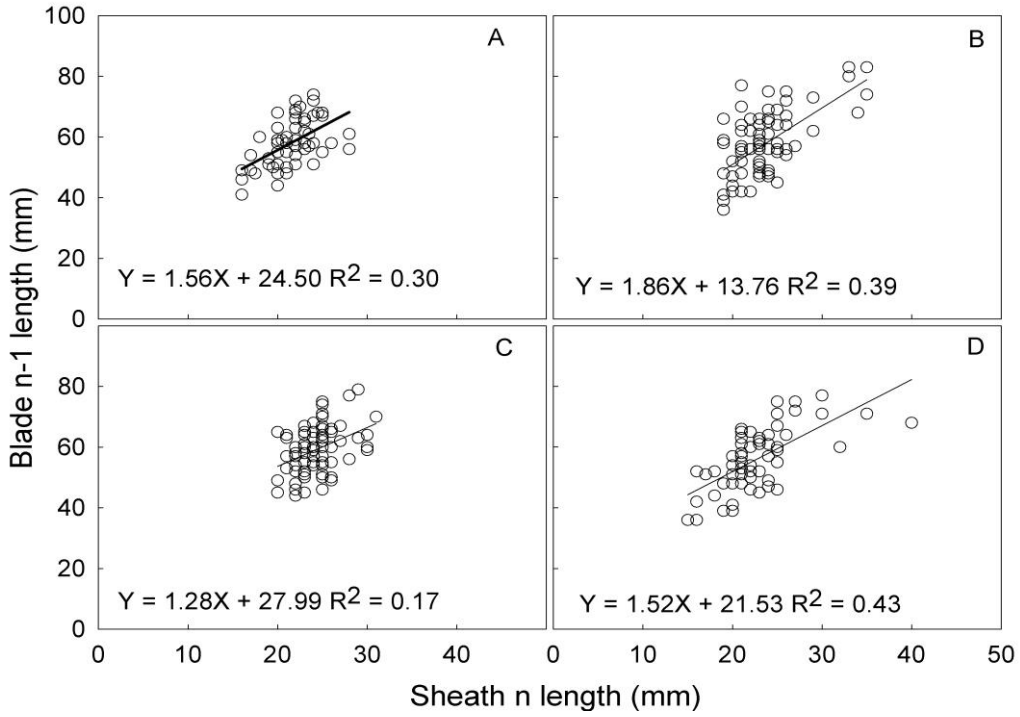

Figure II.7 Relationships between the length of a blade and the length of its preceding sheath (i.e. length of blade Nr. n-1 vs. length of sheath Nr. n) in mature phytomers of *C. squarrosa* under contrasting N fertilizer and VPD treatments. A low or high N fertilizer supply (N1 or N2) was combined with low or high VPD (V1 or V2). Panel A, N1 V1; Panel B, N1 V2; Panel C, N2 V1; Panel D, N2 V2. The solid line indicates the fitted linear regression.

Table II.4 Coefficients and confidence intervals of the fitted linear regressions between the length of a blade and the length of its preceding sheath (i.e. length of blade Nr. n–1 vs. length of sheath Nr. n) of mature phytomers in four treatments in Fig. II.7.

Parameter	Coefficients ± 95% confidence interval			
	N1 V1	N1 V2	N2 V1	N2 V2
a	1.56 ± 0.66	1.86 ± 0.53	1.28 ± 0.65	1.52 ± 0.44
Y_0	24.50 ± 14.29	13.76 ± 12.54	27.99 ± 15.86	21.53 ± 10.05
R^2	0.30	0.39	0.17	0.43

The equation: $y = a*x + y_0$

DISCUSSION

The current study showed little morphological plasticity of *C. squarrosa* at phytomer-level in response to nitrogen supply and VPD, and the main variation in morphology was observed in tillering across N levels. The coordination of growth within a phytomer and between phytomers of *C. squarrosa* was virtually unaffected by N nutrition and VPD. Although plant development is highly sensitive to environmental conditions (Moulia *et al.*, 1999), to the best of our knowledge, growth coordination in *Gramineae* has so far only been studied in relation to temperature (most often expressed as thermal time; e.g. (Lafarge & Tardieu, 2002; Fournier *et al.*, 2005). In field studies, where VPD inevitably varies over the growing period, the timing of key events of phytomer development was fully explained by thermal time, which indicates that VPD had no effect on coordination (Lafarge & Tardieu, 2002; Fournier *et al.*, 2005).

The constancy of coordination across treatments should be related to the regularity of trigger events. The emergence of the blade tip is recognized as one trigger event for coordination, although the exact signaling involved is not clear yet (Fournier *et al.*, 2005; Zhu *et al.*, 2014). Sheath tube length affects the development of a young phytomer (Wilson & Laidlaw, 1985; Casey *et al.*, 1999), as cell production of the blade is thought to be regulated by the light signal received by the emerging blade tip. In this

study, the relationship between blade length and previous sheath length showed no treatment response. Moreover, at the time of tip emergence, phytomers had reached on average 26% of their final length with very little variation between treatments. Hence, if N nutrition and VPD treatment do not affect the relationship of blade and sheath tube length, coordination rules can be generalized for *C. squarrosa* across nitrogen and VPD treatments.

Coordination of phytomer development

The elongation of a phytomer of *C. squarrosa* followed a sigmoidal pattern similar to that found in other grasses like maize (Fournier & Andrieu, 2000), wheat and tall fescue (Fournier *et al.*, 2005). It has been shown that, for wheat and tall fescue (Fournier *et al.*, 2005), the elongation of a leaf can be subdivided into four phases. While in this study, the initial phase of phytomer elongation was not captured, the acceleration phase, the quasi-linear phase and the elongation-decay phase were also apparent in *C. squarrosa*. The transition between the acceleration phase and the quasi-linear phase occurred 1 d before the tip emergence. Thus, the first phase of visible elongation corresponded to the quasi-linear phase of phytomer elongation, when phytomer elongation was still exclusively due to blade elongation. Maximum elongation rates were observed at 2 d after tip emergence, when phytomers had reached 52% of their final length. This corresponded to blade elongation, as final blade length contributed 63% to final phytomer length. Although elongation rates during the visible growth phase were continuous without a significant break, transition between blade and sheath growth must have occurred suddenly, as significant sheaths were only observed when blades were (nearly) fully elongated as revealed also in the destructive harvest. Research on a variety of grass species has shown that significant internode elongation is synchronized with the end of elongation of the associated sheath in maize (Hesketh *et al.*, 1988), in sorghum (Lafarge *et al.*, 1998) and in barley (Kirby *et al.*, 1994). Here, the final gradual fading out of phytomer elongation was mainly associated with internode elongation. Hence, elongation rates for the internode were significantly lower than elongation rates of blade and sheath. This difference is associated with the activity of different meristems responsible for leaf (blade *plus* sheath) and internode growth.

Elongation of successive phytomers was also tightly coordinated: thus, the acceleration phase of the elongation of a young phytomer commenced, when the preceding phytomer had reached approx. 25% of its final length, i.e. when the tip of the preceding phytomer emerged. This may also indicate a signal transduction within a tiller based on tip emergence; as some studies discussed the regulation of shoot development by hormonal signals (Tamas, 1995; Horvath *et al.*, 2003; Schmitz & Theres, 2005). When a phytomer terminated elongation, the blade of the next younger phytomer was fully expanded and its internode started to elongate.

Due to the tight coordination in phytomer growth across N and VPD levels, the time course of phytomer development was describable using one single equation. The duration of elongation from the time when the phytomer had reached 3.5% of final length until the cessation of elongation (99% of final length) was approx. 13 d, which corresponds to 185 degree days - approx. half of the thermal time necessary to complete phytomer elongation in *Sorghum bicolor* (assuming the same base temperature of 10.8 °C, Lafarge & Tardieu, 2002), a C_4 annual grass and crop species. Moreover, the duration of the linear elongation phase was about 6 d, i.e. 85 degree days in this study, which is again approx. half of that reported for *S. bicolor* (Lafarge & Tardieu, 2002).

Effects of VPD and N supply on plant morphology

The overall effects of VPD and N supply on phytomer development were small. N fertilization supply slightly increased the number of visibly growing phytomers and phytomer length, and shortened the phyllochron at low VPD but not at high VPD. Positive effects of nitrogen fertilization and low VPD on leaf elongation are well established (MacAdam *et al.*, 1989; Gastal & Nelson, 1994; Ben Haj Salah & Tardieu, 1996; Vos & van der Putten, 1998; Tardieu *et al.*, 2000; Kavanová *et al.*, 2008). Although high VPD clearly increased the leaf-level transpiration rate and decreased stomatal conductance in the same experiment (Gong *et al.*, 2016), the non-significant VPD effects on phytomer growth parameters may be due to the non-limiting water supply in this experiment, i.e. the supplementation of nutrient solution with a frequency of three times per day. Grass species were shown to be able to adjust root hydraulic conductance in response to VPD (Ocheltree *et al.*, 2014) to maintain a high leaf water potential if water supply is sufficient. The main variation in plant morphology was

observed in tiller development and growth, namely, the number of tillers was significantly increased by 23% by N supply. These results are in line with the findings that whole-plant relative growth rate of *C. squarrosa* increased following N addition but not affected by VPD (Liu *et al.*, 2016). A positive effect of N supply on the tillering of grasses is a common response (Longnecker *et al.*, 1993; Baethgen *et al.*, 1995; McKenzie, 1998), as N fertilizer promotes the outgrowth of axillary meristems to produce more tillers (McSteen, 2009). For barley, it has been shown that wild varieties exhibit a similar affinity to N as crop cultivars (Bloom, 1985). Thus, the low N treatment exerted only a moderate limitation, which did not limit the development of individual phytomers. However, the reduced phyllochron in the high N treatment might be responsible for the positive effect on tillering, as it increases the number of axillary meristems.

CONCLUSIONS

Results revealed a strong coordination of elongation both within a phytomer and between successive phytomers on a tiller of *C. squarrosa*, a wild, perennial C_4 grass. The coordination in phytomer development was virtually unaffected by nitrogen nutrition and VPD, which indicates that tiller development of *C. squarrosa* can be captured using general quantitative coordination rules across VPD or nitrogen nutrient levels. On the other hand, a clear response in tillering to N addition was observed. Similarly, a field study showed that both tiller weight and tiller density responded to N and water supply in this grassland ecosystem (Gong *et al.*, 2015). These results emphasize the importance of understanding tillering kinetics in modeling the whole shoot morphological development of *C. squarrosa*. Tip emergence, a key event, may have a crucial role in signal transduction to coordinate phytomer elongation. Accordingly, the time course of phytomer development was established using observations on visibly growing phytomers, applying a sigmoidal function. This quantitative discription of phytomer development potentially can be used for: functional-structural modeling, analyzing morphological plasticity, and elucidating environmental factors using leaf isotopic signals of *C. squarrosa*.

Chapter III

Nitrogen dynamics in a perennial C_4 grass (*Cleistogenes squarrosa*) at the leaf and tiller level during vegetative growth

ABSTRACT

N dynamics in aerial tissues of plants is crucial for N metabolism of the whole plant, and has been investigated intensively because of its relationship to biomass yield and quality. However, there is little quantitative information on N dynamics of individual tillers in perennial grasses particularly during vegetative growth. This study was performed in controlled environmental conditions and assessed N dynamics of a perennial C_4 grass (*Cleistogenes squarrosa*) at the vegetative stage. N dynamics was investigated in the immature part of major tillers (the totality of immature phytomers that are expanding at the tip of a tiller) and the successive fully developed mature and senescing leaves along major tillers using dynamic ^{15}N-labeling with nitrate. ^{15}N labeling served to separate net fluxes of nitrogen into (labeled) and (non-labeled) fluxes in both mature and immature tissues. Based on published knowledge on the site of N reduction and assimilation, it was assumed that initially labeled N import into leaves (via the xylem) occurred essentially as nitrate, while export (in the phloem) was near exclusively in the form of amino acids. The turnover rate of bulk N in mature blades was 0.36% per hour. N export from the mature tissues of major tillers was approx. 2.5 times higher than N import into the immature part of the same tiller. Net changes of N content would have strongly underestimated N turnover in mature tissue, as N content in the upper 6 to 8 mature blades was nearly constant during the experiment. Remarkably, the growth rate of the whole shoot was about three times higher than that of the major tillers, due to continued tiller production. Evidently, the excess of mobilized and exported amino acid-N was used as a substrate for young tiller growth, indicating that N dynamics at the tiller level is integrated with that of the remainder of the shoot.

INTRODUCTION

Nitrogen (N) is most often the growth-limiting plant nutrient in natural and anthropogenic ecosystems (Aerts & Chapin III, 2000). Most of the N taken up by plants is allocated to the aerial tissues, mainly leaves, to satisfy the high N demand of the photosynthetic apparatus and associated metabolic machinery (Evans, 1989; Hörtensteiner & Feller, 2002; Hikosaka, 2004). While organic N mobilized from seed reserves and inorganic N taken up from the soil (or air in the case of N fixing plants) represent the main N sources for growth in early developmental stages, organic N mobilized from vegetative organs contributes increasingly to the growth of vegetative and reproductive organs during later developmental stages of seed plants (Lemus *et al.*, 2008; Heaton *et al.*, 2009; Strullu *et al.*, 2011; Dohleman *et al.*, 2012; Kering *et al.*, 2012). By way of steady-state $^{15}N/^{14}N$ labeling experiments, investigations of leaf growth and associated $^{15}N/^{14}N$ dynamics in leaf growth zones and in adjacent recently-formed leaf tissue, and compartmental modeling (Lattanzi *et al.*, 2005; Lehmeier *et al.*, 2013) have demonstrated very significant contributions (24-76%) of N mobilization to the N supply of the leaf growth process in C_3 and C_4 grasses in mixed and pure stands. Such analyses, previously performed at the individual leaf level, have not – as yet – been performed at the whole tiller or plant levels. Also, to my knowledge, the concurrent processes of N mobilization in source tissues and use in growing sinks have not been studied jointly in grasses during vegetative growth. The present work addresses this question, by investigating N dynamics of the whole range of growing, mature and senescing leaves on mature tillers of a perennial C_4 grass, *Cleistogenes squarrosa*.

Shoots of grasses in the vegetative state are virtually an assembly of individual tillers. A tiller consists of a linear arrangement of successively produced phytomers, with each phytomer composed of a leaf blade, a leaf sheath, a node (and associated axillary buds), and an (elongated or unelongated) internode. In mature vegetative tillers, the production of new phytomers at the tip of the tiller occurs *in tandem* with the senescence of older phytomers that are situated at the base of the tiller. In dense stands, the vertical arrangement of leaves causes an attenuation of light availability with depth in the canopy (Monsi & Saeki, 2005). Thus, particularly in herbaceous stands, the senescence of leaves is associated with a displacement to progressively more shaded

positions in the canopy. Senescence and shading cause N mobilization in leaves (Hirose & Werger, 1987; Millard, 1988; Diaz *et al.*, 2008) and it is thought that such mobilized N is an important N source for growing tissues. The senescence and shading-driven N mobilization has been recognized as an important mechanism supporting the optimization of canopy photosynthesis and N use efficiency (Field, 1983; Hirose & Werger, 1987; Farquhar, 1989; Grindlay, 1997; Bertheloot *et al.*, 2008; Posada *et al.*, 2009). Unsurprisingly, that mechanism is expected to be more important in dense than open canopies (Hirose & Werger, 1987).

N moving through a plant experiences a sequence of metabolic pathways. While the majority of the N taken up by plant roots is in the form of inorganic N, mainly nitrate (Andrews, 1986; Masclaux-Daubresse *et al.*, 2010), the supply to sink tissues occurs in the form of organic N (Sugiharto & Sugiyama, 1992; Gastal & Nelson, 1994; Baki *et al.*, 2000; Scheurwater *et al.*, 2002). The metabolic pathways linking nitrate to organic N forms include nitrate and nitrite reduction, GS/GOGAT cycle, amino acid synthesis, and protein synthesis and degradation (Lea & Forde, 1994; Hirel & Lea, 2002; Novitskaya *et al.*, 2002; Irving *et al.*, 2010; Dechorgnat *et al.*, 2011; Li *et al.*, 2012; Schluter *et al.*, 2012). Amides and amino acids act as the predominant intermediate which transfers N for growing tissues (Feller *et al.*, 2008; Masclaux-Daubresse *et al.*, 2008; Distelfeld *et al.*, 2014). These organic N forms can be derived from current assimilation of N taken up from the soil, and from N mobilization (Hirel & Lea, 2001; Novitskaya *et al.*, 2002; Stitt *et al.*, 2002; Lalonde *et al.*, 2003; Dechorgnat *et al.*, 2011). N mobilization involves the degradation of leaf proteins into amino acids and other nitrogenous compounds, and the subsequent reallocation of these compounds (Mei & Thimann, 1984; Buchanan-Wollaston, 1997; Gregersen *et al.*, 2008, Avice & Etienne, 2014).

In this study, I employ a new approach to enhance the understanding of the N dynamics linking sinks and sources of N within mature, major tillers and the whole shoot of *C. squarrosa*. In that, the tiller is conceptually divided into phytomers of increasing age, particularly distinguishing between the composite of immature, still growing phytomers (termed 'immature tissue', IMT) and the composite of mature and senescing tissues (MT) (Fig. III.1). As it is growing, continuously producing new phytomers, the IMT is treated as the tiller-scale net sink for N. Conversely, the MT (and its component phytomers) is considered as potential source of organic N. This

conceptualization provides the basic framework for a quantitative analysis of N fluxes in a tiller. In every leaf appearance interval, the IMT 'exports' the equivalent of the youngest mature phytomers' N content (that is net N export rate of the IMT corresponds to the amount of N in the youngest mature phytomer divided by the leaf appearance interval). In a steady-state – that is assumed (and also verified) in this work – the net export of N from the IMT must be balanced by an equivalent net import of N. Dynamic labeling (as in Lattanzi *et al.*, 2005; Lehmeier *et al.*, 2013) is added to this approach in order to study the turnover of N in the different phytomers, particularly in their leaf blades, and to assess – in particular – the incorporation of newly absorbed nitrate-N and export of old, previously assimilate N in mature leaf blades of increasing age.

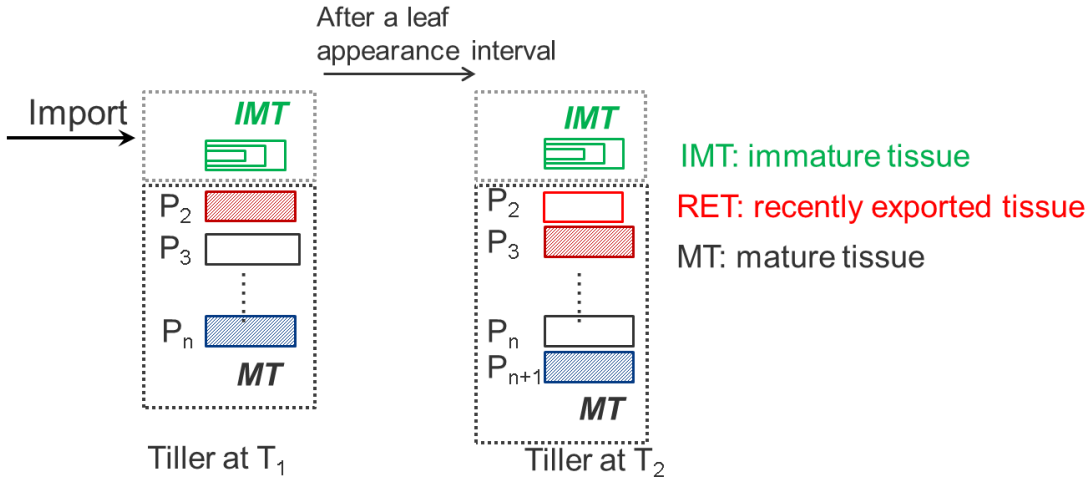

Figure III.1 Schematic representation of growth in a tiller of *C. squarrosa* over one leaf appearance interval. The tiller is divided in two functionally distinct compartments, immature tissue (IMT) and mature tissue (MT), with each composed of a number of phytomers (shown as solid-lined boxes). Mature phytomers are numbered consecutively from the youngest (P_2, the phytomer that bore the youngest emerged ligule) to the oldest (*n*). The grey dash-dotted box denotes the IMT that is composed of immature phytomers. The black dash-dotted box denotes the MT. Two mature phytomers are highlighted by colored boxes. Within one leaf appearance interval, one mature phytomer is added to the MT, and P_2 turns to P_3, and so on. P_2 is exported out of IMT and referred to as "recently exported tissue", i.e. RET.

MATERIALS AND METHODS

Plant material and growth conditions

The experiment was performed in two growth chambers (Conviron PGR15, Conviron, Winnipeg, Canada) that formed part of a modernized version of the controlled environment mesocosm system described by Schnyder *et al.* (2003). Four seeds of *C. squarrosa* were sown in individual plastic tubes (4.5 cm diameter, 35 cm high) filled with quartz sand (0.3-0.8 mm diameter). Tubes were placed in free-draining plastic boxes (length: 77 cm, width: 57 cm, depth: 30 cm) with 164 tubes per box. Two boxes were placed in each growth chamber. One week after sowing, plants were thinned to one plant per tube so that final density was 234 plants m^{-2}. Plants grew under 16/8 h light/dark photoperiod with a photosynthetic flux density of 800 µmol m^{-2} s^{-1} at canopy height. Air temperature was set at 25 °C throughout the light-dark cycle. Relative humidity was controlled at 80%. CO_2 concentration in the light period was kept between 380 and 390 µmol mol^{-1}. Stands in two chambers received a modified Hoagland nutrient solution with 7.5 mM nitrate-N as the sole N source. The N source was in the form of equimolar concentrations of calcium nitrate and potassium nitrate ($Ca(NO_3)_2$ and KNO_3). The nutrient solution also included 1.0 mM $MgSO_4$, 0.5 mM KH_2PO_4, 1 mM NaCl, 125 µM Fe-EDTA, 46 µM H_3BO_3, 9 µM $MnSO_4$, 1 µM $ZnSO_4$, 0.3 µM $CuSO_4$, 0.1 µM Na_2MoO_4. Every eight hours, the nutrient solution was supplied by an automatic irrigation system. The nutrient solution was completely renewed after four weeks, i.e. in the middle of the experiment.

Labeling strategies

The labeling strategy followed the principles outlined by Lehmeier *et al*. (2013). In one chamber, stands grew with a nutrient solution with 0.37 atom% ^{15}N-nitrate [with atom% $^{15}N = {}^{15}N / ({}^{14}N + {}^{15}N) \times 100$] and ^{13}C-enriched CO_2 ($\delta^{13}C$ of -5‰). The other chamber received 1 atom% ^{15}N-nitrate and ^{13}C-depleted CO_2 ($\delta^{13}C$ of -48‰). These treatments were implemented at sowing. Except for the differential ^{15}N- and ^{13}C-labeling, all other conditions were kept identical in the two chambers. Labeling started 47 d after imbibition of seeds, estimated as the date of first watering of pots. $^{15}NO_3/^{14}NO_3$ labeling was performed by swapping randomly selected plants between two growth chambers (i.e. 0.37 atom% ^{15}N-nitrate → 1 atom% ^{15}N-nitrate and *vice versa*) (Fig. III.2). Plants

were labeled for 24, 48, 96 or 168 h. For each labeling duration, four plants (two plants per chamber) were swapped shortly before the beginning of the light period. Thus, all labeled plants experienced one or several full diurnal cycles in the "new" environment. To prevent the uptake of "old" nutrient solution just after transfer to the "new" environment, the pot of each transferred plant was rinsed with the "new" nutrient solution just before placement into the "new" chamber.

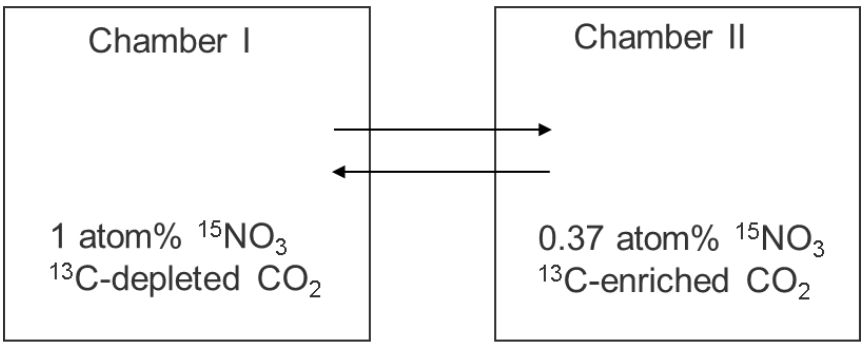

Figure III.2 Experimental scheme. Labeling experiments were performed with plants of *C. squarrosa* grown in two growth chambers. Stands in two chambers received a modified Hoagland nutrient solution with 7.5 mM nitrate-N as the sole N source. Except for the N isotope composition of the nutrient solution and the C isotope composition of the CO_2 all conditions were kept the same in each chamber. Transferred plants were labeled in the new environment for targeted durations. Four plants were sampled in each labeling interval.

Sampling procedures and leaf area measurements

After plants were labeled for target durations, two major tillers of each plant (one main tiller and one secondary tiller, which had approximately the same size as the main tiller) were excised at the base of the shoot. Tillers were dissected by phytomer, starting at the tip. The youngest phytomers that were fully enclosed within the sheath of the youngest mature phytomer were not dissected but collected together and combined in one sample with the partly visible immature phytomers (IMT) (Fig. III.1). For successive phytomers (that is phytomer no. 2 to *n*), the leaf blade, leaf sheath, and the stem section corresponding to these phytomers were collected separately. The rest of the shoot, including all other tillers, was collected as a whole. The entire root system was also

collected following washing with tap water. In phytomer no. 2, the ligule of the leaf had emerged from the surrounding sheath of the next-older leaf, the leaf blade was fully expanded, and the sheath was near-fully elongated (see Chapter II).

In addition to labeled plants, each of the two chambers contained plants that were grown continuously with the same isotope compositions of nitrate-N. These so-called 'labeling controls' were sampled in the same way as labeled plants. The N isotope composition of these control plants served as end members in the two-member mixing model for the assessment of the fraction of tracer in a labeled sample (see below). All samples were quickly frozen in liquid nitrogen, freeze-dried to constant weight (72 h at -80 °C), weighed and ground to fine homogeneous powder with a ball mill, and stored at room temperature before analysis of isotope composition.

Besides samplings in the labeling experiment, from 43 d to 54 d after imbibition of seeds, a series of samplings were conducted regularly in both chambers at three or four day intervals to measure leaf area. On each sampling date, four plants were randomly chosen in each chamber and two major tillers of each plant were dissected in identical manner as labeled plants (see above) to obtain leaf blades. Leaf blades were arranged on white paper (Fig. III.3), and then photographed for measurements of leaf area using the Images J software (National Institutes of Health, Bethesda, Maryland, USA). After taking photographs, these leaf blades were processed in the same way as labeled plants.

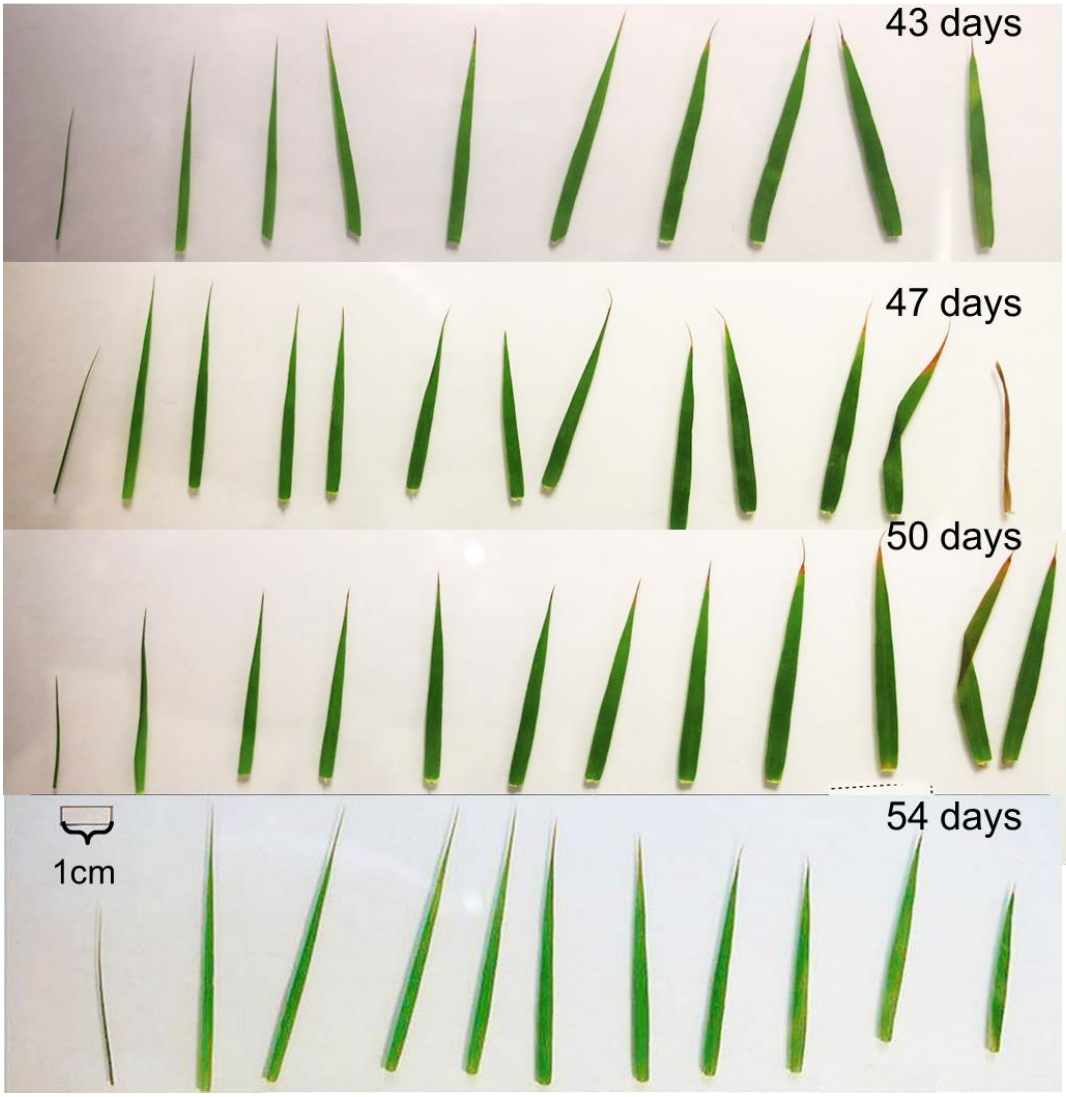

Figure III.3 Representative images of different developmental stage blades in a tiller of *C. squarrosa*. Leaf blades were photographed at 43, 47, 49, and 54 days of age. All plants sampled were in the vegetative growth. Blades were arranged from the left to right on white paper according to their positions in a tiller (i.e. from the tip to the base of the tiller). All blades were fully expanded except for the youngest exposed blade, near the tip of the tiller.

Elemental and isotopic analysis

The N and C content, and the N and C isotope composition of aliquots of sample material (0.7 ± 0.05 mg dry matter) were determined after combustion in an elemental analyzer (NA 1110; Carlo Erba Instruments) interfaced to a continuous-flow isotope

mass ratio spectrometer (Delta Plus; Finnigan MAT). Laboratory standards (wheat powder) were measured after every 10 samples to determine the precision of the isotope analysis and for possible drift correction. All samples and laboratory standards were measured against a reference gas, which was previously calibrated against secondary standards (IAEA-CH6, IAEA-N1, IAEA-N2, Vienna, Austria). The precisions (standard deviation) of laboratory standards for isotope composition was 0.003 atom% (^{15}N) and 0.12‰ (^{13}C), and for element content were 0.02% (N) and 0.37% (C), respectively. For the uncertainty associated with sample preparation, one sample was measured repetitively and exhibited the same precisions as laboratory standards.

Specific leaf N, specific leaf mass, and relative growth rate calculations

Specific leaf N, SLN (g N m^{-2}) and specific leaf mass, SLM (g dry mass m^{-2}) were calculated by dividing the N mass and dry mass of leaf blades by their respective areas. Growth analyses were conducted using the classical approach (Evans, 1972), in which relative growth rate of a plant is calculated as ((ln plant mass) at time 2 − (ln plant mass) at time 1)/time interval between harvest 1 and 2. For tiller growth, RGR was derived from the slope of the fitted linear regression line for tillers collected between 47 and 51 d after imbibition in considering the change of the number of leaves within a tiller in that time span. This time interval of plant age matched that of the plants used in investigations of N dynamics.

The fraction of tracer in a sample

The N in a labeled sample included a fraction that was taken up prior to the transfer between chambers with different atom%^{15}N of the nutrient solution ($f_{unlab\text{-}N}$) and a fraction that was taken up after the transfer ($f_{lab\text{-}N}$; with $f_{unlab\text{-}N} + f_{lab\text{-}N} = 1$). $f_{lab\text{-}N}$ was calculated by isotopic mass balance as:

$$f_{lab\text{-}N} = (\text{atom\%}^{15}N_{spl} - \text{atom\%}^{15}N_{old}) / (\text{atom\%}^{15}N_{new} - \text{atom\%}^{15}N_{old}), \quad \text{Eqn 3.1}$$

with atom%$^{15}N_{spl}$ denoting the N isotope composition of the labeled sample, and atom%$^{15}N_{old}$ and atom%$^{15}N_{new}$ the two end-members of the mixing model that correspond to the N isotope compositions of the labeling control plants that were grown

continuously in the growth chamber of origin ('old') of a plant and the 'new' growth chambers to which the plant was transferred for labeling. For the calculation of the fraction of tracer in a specific sample, I used the tissue- und time-specific atom% ^{15}N as end members in the mixing model. In the present labeling experiments, I did not find an effect of the transfer direction of labeled plants, i.e. from 1.0 atom% ^{15}N to 0.37 atom% ^{15}N or *vice versa*, on $f_{lab\text{-}N}$ (data not shown).

N import and export in immature tissue of a tiller

The analysis of N fluxes in IMT of a tiller followed the principles described by Lattanzi *et al.* (2005) and Lehmeier *et al.* (2013), which studied the N fluxes in leaf growth zones. The net N import into IMT (I_{imt}) was equated with the net N export out of the IMT, assuming a steady-state. Net N export out of IMT (E_{imt}) was taken as the N mass of the youngest (near-)fully expanded phytomer (that corresponded to the 'recently produced tissue' in Lehmeier *et al.* 2013) – approximated by the mass of N in the leaf sheath plus blade of phytomer no. 2 (N_{L2}) – divided by the leaf appearance interval (T_e). In that phytomer, the N content in leaf blade and sheath made up 89% ± 3% of total phytomer N (data not shown). Thus, N import into IMT [I_{imt}: μg h^{-1} $tiller^{-1}$] was estimated as:

$$I_{imt} = E_{imt} = N_{L2}/T_e. \qquad \text{Eqn 3.2}$$

T_e was 57.6 hours, i.e. 2.4 days, as shown in Chapter II. Eqn 3.2 was based on the notion that IMT is in a physiological steady state, where the N content of IMT is constant. Indeed, our data did not indicate a change of the N content of the IMT during the experimental period (see Figure III. 6 in results section).

N import, net change, and export in mature tissue of a tiller

N import into the MT [I_{mt}: μg h^{-1}] was estimated from tracer uptake of the MT measured by short-term (i.e. 24 h) labeling, and calculated as:

$I_{mt} = RI_{mt} \times N_{mt}$, Eqn 3.3

with RI_{mt} [h^{-1}] the relative N import rate, that is the change of the fraction of labeled N in MT over a diurnal circle and N_{mt} the N mass of the MT.

By the same logic, N export out of the MT [E_{mt}; μg h^{-1}] was calculated as RE_{mt} [relative N export rate; h^{-1}] multiplied by N_{mt} (24-h labeled plants), thus:

$E_{mt} = RE_{mt} \times N_{mt}$, Eqn 3.4

with RE_{mt} the difference between RI_{mt} and RN_{mt} ($RE_{mt} = RI_{mt} - RN_{mt}$). RN_{mt}, the relative change rate of the N mass of the MT [h^{-1}], was calculated from the change of the N mass over the experimental period. The detailed steps to derive these parameters are shown in a flowchart (see Fig. III.4).

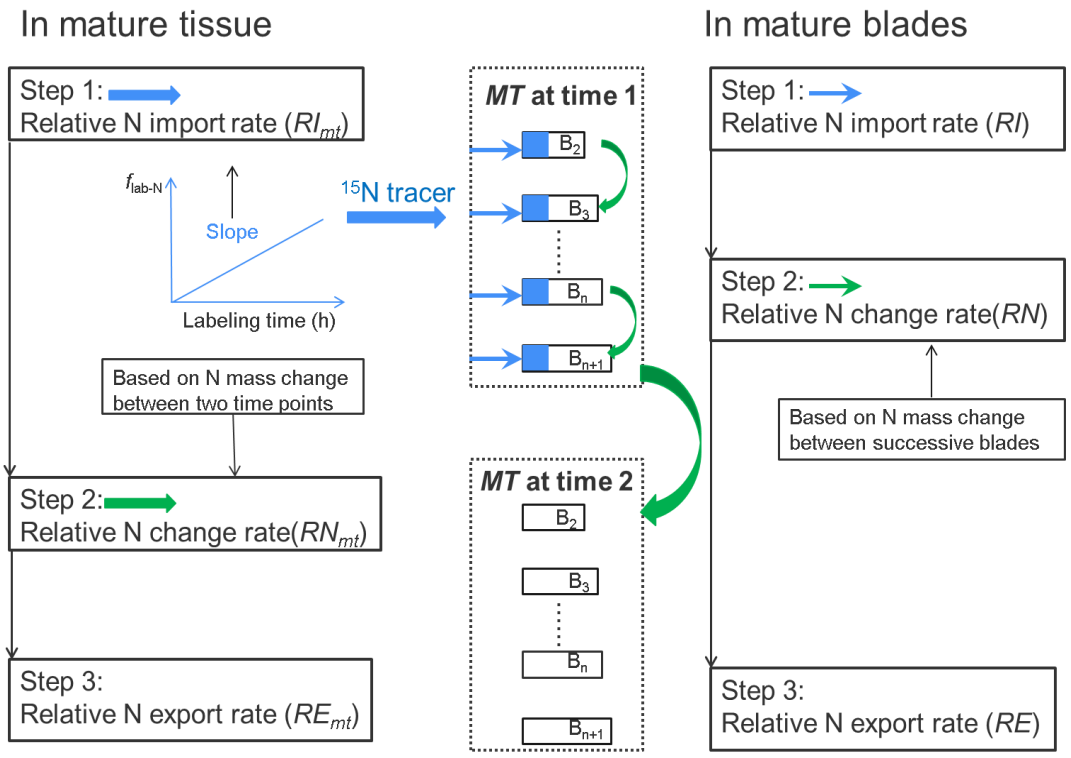

Figure III.4 Flow chart of the individual steps to derive different flux parameters for mature tissue and mature blades in a tiller.

Estimation of N fluxes in individual mature blades

In an analogues manner to the calculation of RI_{mt}, the relative N import rate [*RI*: h^{-1}] of individual mature leaf blades was estimated as the change of the fraction of ^{15}N tracer over 24 hours. As above, that procedure was based on the assumption that all N import occurred in the form of labeled N, and hence import of non-labeled N into mature leaf blades was negligible. This assumption is based on the study of N assimilation in maize with $^{15}NO_3$ labeling, which showed that 93% of newly absorbed nitrogen to the shoot occurs via nitrate (Murphy & Lewis, 1987). The main finding of nitrogen primary-assimilation or mobilization in vegetative tobacco plants also suggested that older senescing leaves import inorganic N and progressively export organic N such as amino acids (Masclaux-Daubresse *et al.*, 2000).

RN, the relative change rate of the N mass of a leaf blade [h^{-1}] was estimated from the change of N mass per unit leaf blade area (SLN) per unit time. The latter was calculated from the change of SLN associated with the passage of a leaf from one leaf age category to the next (i.e. when leaf blade *i* becomes leaf blade *i*+1) divided by the average SLN of the two leaf age categories and the time needed for the passage (the leaf appearance interval):

$$RN = \frac{SLN_{Bi+1} - SLN_{Bi}}{\left(\frac{SLN_{Bi+1} + SLN_{Bi}}{2}\right) \times T_e}, \qquad \text{Eqn 3.5}$$

with SLN_{Bi+1} (g N m^{-2}) and SLN_{Bi} (g N m^{-2}) the SLN of leaf blades *i*+1 and *i*, respectively. These calculations were performed separately for each tiller. The concept of this calculation was based on the notion that the pattern of SLN distribution in a tiller did not vary during the experimental period. Support for that assumption is presented in Tables III.2 & 3 (see results section). These calculations implied that the difference in SLN between two successive leaf blades, leaf blade *i* and leaf blade *i*+1, was entirely due to net accumulation/incorporation or loss associated with the transition from one leaf age category to the next.

Statistics

Data were analysed using R software (R Development Core Team, 2008). Linear mixed models were used to account for random effects and nesting in the data. To assess differences in patterns of N distribution between sampling days (plant age), the SLN was compared using the lme function [nlme package (Pinheiro & Bates, 2014)]. The model included phytomer number, quadratic phytomer number as fixed factors; and chamber, and tiller as hierarchically nested random effects. Since the chamber did not yield a significant effect, this random effect was discarded in the mode. The adequacy and assumption of models were graphically and statistically evaluated. SLN data were tested for linear and quadratic relationships with phytomer number; the 95% confidence intervals of parameters were compared to determine whether slopes were significantly different. If confidence intervals of parameters did not overlap, the relationships

between SLN and phytomer number was considered significantly different between plant ages.

RESULTS

Plant growth

For C, the RGR (RGR_C) of the whole shoot was about 2-fold higher than that of the major tillers (Fig. III.5A). This disparity was even greater for N, as RGR_N of the whole shoot was about 3-fold higher than that of the major tillers (Fig. III.5B). Indeed, during the experiment daughter tillers were continuously produced (Figure III.6), as evidenced by visual observation. However, I did not actually quantify the rate and time course of daughter tiller formation and the RGR of these younger tillers.

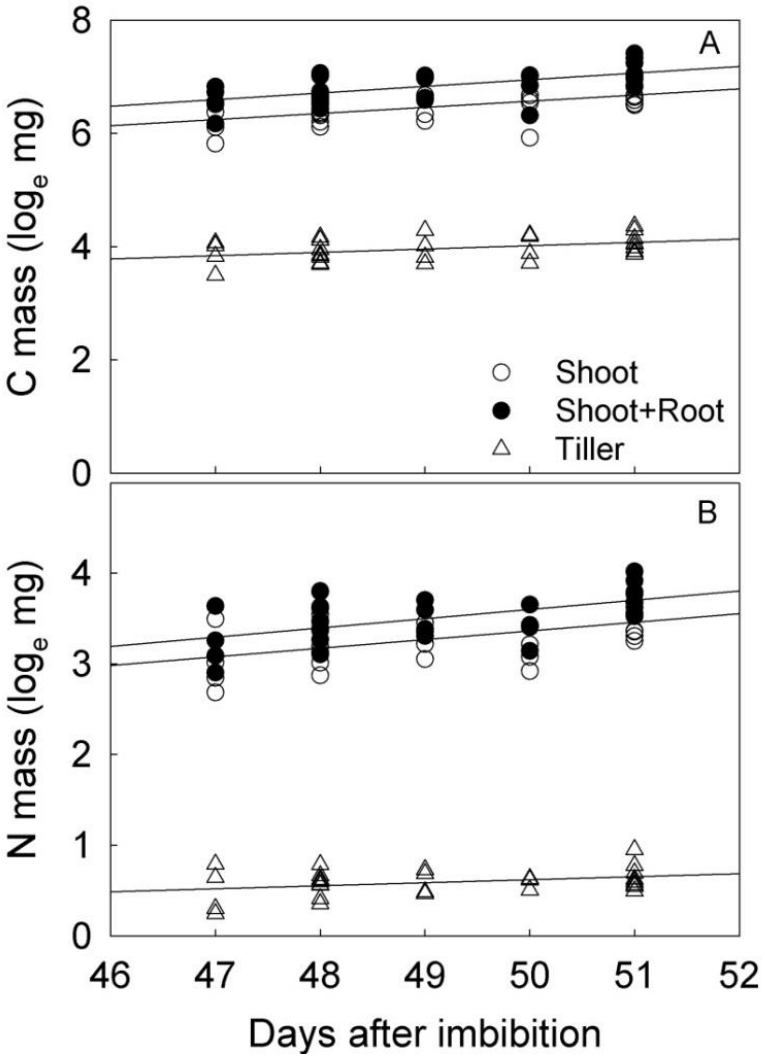

Figure III.5 Natural logarithm of C mass (A) and N mass (B) *versus* time in different plant parts of *C. squarrosa*. Lines indicate linear regressions. Linear regression for whole shoot C: Y = 0.1085*X + 1.153, R^2 = 0.32; for total plant C: Y = 0.117*X + 1.094, R^2 = 0.34; for major tiller C: Y = 0.059*X + 1.089, R^2 = 0.17. Linear regression for whole shoot N: Y = 0.095*X – 1.391, R^2 = 0.24; for total plant N: Y = 0.102*X – 1.491, R^2 = 0.29; for major tiller N: Y = 0.033*X – 1.040, R^2 = 0.10.

Figure III.6 Representative images of a *C. squarrosa* plant at different developmental stages.

Clearly, however, the higher RGR of whole shoots relative to the major tillers was due to continued daughter tiller formation and growth. Including roots in the growth analyses yielded a slightly higher RGR of the total plant than of the whole shoot for both N and C masses. Thus, clearly, N demand of whole shoots or plants was higher than that of the major tillers, which were formed at the beginning of plant development (the main tiller and another tiller of similar size, see above).

Nitrogen in immature tissue and mature tissue of a major tiller

The N mass of IMT (N_{imt}) was 6% of the total N mass of a major tiller (Table III.1). Furthermore, N_{imt} did not change significantly during the labeling experiment (Figure III.7). This result supported the notion that the IMT was in an approximate physiological steady state. As N mass of the IMT did not change, the N import into the IMT must have equaled the N export. Meanwhile, N_{mt} increased slightly by 2.2 µg h^{-1}. Total N import into the MT (estimated from short-term labeling) averaged 8.4 µg h^{-1}, strongly exceeding the N net change (i.e. accumulation) in the MT. N export from the MT was 6.1 µg h^{-1}, approximately 2.5 times the rate of total N import in the IMT.

Table III.1 Nitrogen mass and fluxes in immature tissue, mature tissue of a major tiller during the labeling experiment. Values are means ± SE ($4 \leq n \leq 8$). Values denoted by different letters are significantly different between the immature and mature tissue at $P < 0.05$.

Parameter	Immature tissue	Mature tissue
N mass (μg tiller^{-1})	$118.2^{a} \pm 5.3$	$1881.9^{b} \pm 58.7$
N import (μg h^{-1} tiller^{-1})	$2.5^{a} \pm 0.6$	$8.4^{b} \pm 1.3$
N export (μg h^{-1} tiller^{-1})	$2.5^{a} \pm 0.6$	$6.1^{b} \pm 0.7$
N net change (μg h^{-1} tiller^{-1})	0^{a}	$2.2^{b} \pm 0.2$

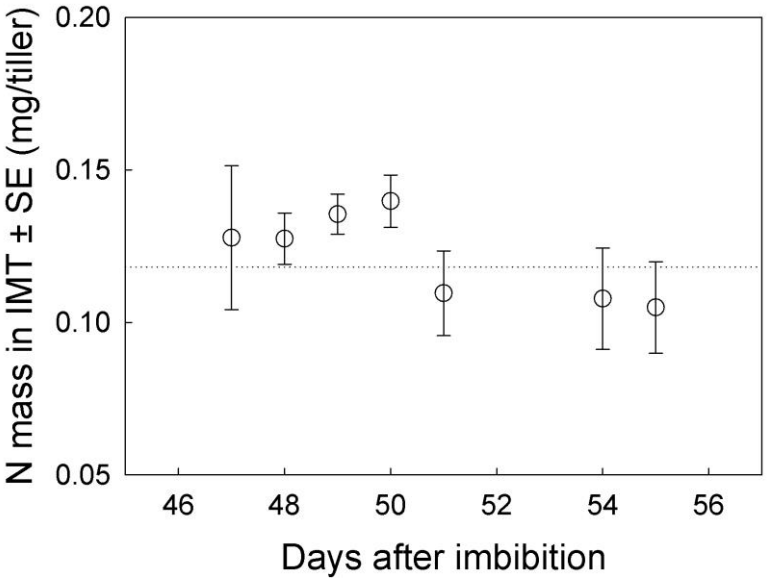

Figure III.7 Changes of N mass in immature tissue of a tiller of *C. squarrosa* over the time. Values are means ± SE ($4 \leq n \leq 8$). The dotted line denotes an average value. A linear function fitted to all individual data: $y = -0.003*x + 0.26$ ($r^2 = 0.04$; $p = 0.15$; $n = 60$).The change of N mass over time was not significant.

Leaf N distribution in mature tissue of a tiller

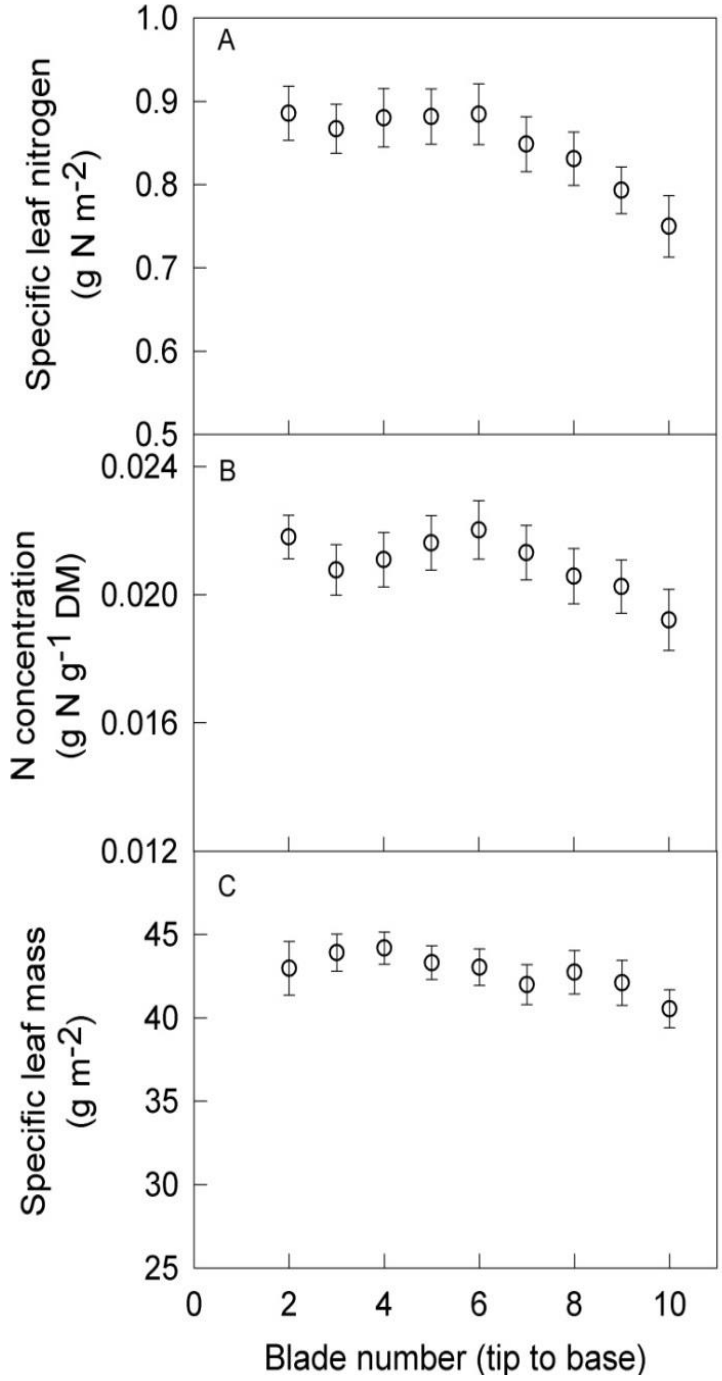

Figure III.8 N mass per unit leaf blade area (specific leaf N; SLN; A), N concentration (B), and dry mass per unit leaf area (specific leaf mass; SLM; C) in mature blades of a major tiller of *C. squarrosa*. Values are means ± SE (n = 32). Leaves were numbered basipetally, that is from the youngest to the oldest, starting at leaf 2, the leaf with the youngest fully expanded leaf blade in a tiller.

In young mature blades of major tillers (Fig. III.8A), there was no significant variation of SLN. In older mature blades, deeper in the canopy, SLN declined clearly from 0.89 to 0.75 g N m^{-2} between blade 7 and blade 10. Overall, SLN declined by approximately 15% from the 2^{nd} to the 10^{th} blade. The pattern of N concentration was rather similar to that of SLN (Fig. III.8B). Within a tiller, the N concentration from blade 2 to blade 7 did not change significantly, but tended to decrease from blade 7 downwards. Thus, N concentration also decreased by 12% from blade 2 to blade 10. Variation of dry mass per unit leaf area (SLM) was very minor and ranged between 41 and 44 g m^{-2} (Fig. III.8C). SLM remained constant in the top three blades, and significantly decreased by 8% from the 4^{th} blade to the 10^{th} blade. The patterns of SLN along major tillers did not change significantly with plant age during the experimental periods, again supporting the conditions/assumptions of the methodological approach taken in the work (Tables III 2 & 3).

Table III.2 Comparison of parameter *a* between plant ages. Parameters were estimated by a quadratic regression of specific leaf nitrogen as a function of phytomer number (y and x, respectively) ($y = a^* x^2 + b^*x + c$).

Plant age	Parameter *a*	Lower CI	Upper CI
43	0.0001a	-0.0002	0.0003
44	-0.0005a	-0.0009	-0.0002
47	-0.0003a	-0.0006	0.0000
48	-0.0001a	-0.0002	0.0001
50	-0.0005a	-0.0008	-0.0001
54	-0.0003a	-0.0004	-0.0002

Columns show the plant age (days after imbibition of seeds), parameter *a* and its confidence interval (95% CI). Different letters indicate statistically significant differences between groups with p-value < 0.05 (for details of the statistic, see "Material and Method" in chapter III).

Table III.3 Comparison of parameter *b* between plant ages. Parameters were estimated by a quadratic regression of specific leaf nitrogen as a function of phytomer number (y and x, respectively) ($y = a^* x^2 + b^* x + c$).

Plant age	Parameter *b*	Lower CI	Upper CI
43	-0.0010a	-0.0043	0.0022
44	0.0057a	0.0005	0.0109
47	0.0024a	-0.0024	0.0073
48	-0.0014a	-0.0059	0.0031
50	0.0040a	-0.0009	0.0089
54	0.0032a	0.0013	0.0051

Columns show the plant age (days after imbibition of seeds), parameter *b* and its confidence interval (95% CI). Different letters indicate statistically significant differences between groups with p-value < 0.05 (for details of the statistic, see "Material and Method" in chapter III).

N fluxes in different age categories of mature leaf blades in a major tiller

24 h-long ^{15}N labeling demonstrated significant incorporation of tracer into the different leaf age categories of mature leaf blades (Fig. III.9). The fraction of labeled N ranged between 0.06 and 0.11, and was higher in the younger leaf age categories (that were positioned in the upper part of the canopy) than in the older mature blades, lower in the canopy. In all age categories of leaf blades, relative import rate [*RI*: h^{-1}] greatly exceeded the net changes of leaf blade N that were associated with the maturation/aging process (Fig. III.10).

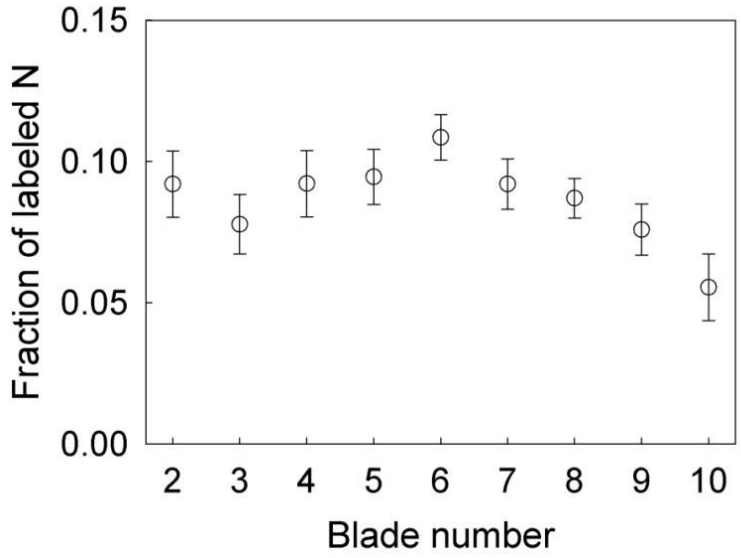

Figure III.9 Fraction of labeled N in mature blades of a tiller of *C. squarrosa* after 24 h-long ^{15}N labeling. The labeling period included a 16-h light period and 8-h dark period. Leaves were numbered basipetally, that is from the youngest to the oldest, starting at leaf 2, the leaf with the youngest fully expanded leaf blade in a tiller. Values are means ± se (n = 4)

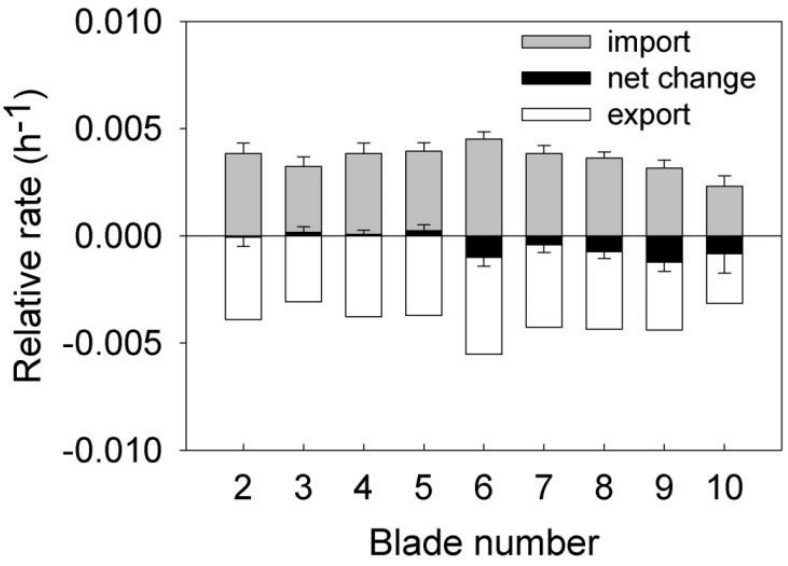

Figure III.10 N fluxes in different leaf age categories of mature blades along major tillers of *C. squarrosa*. Leaves were numbered basipetally, that is from the youngest to the oldest, starting at leaf 2, the leaf with the youngest fully expanded leaf blade in a tiller. Values are means ± se (import: $n = 4$; net change: $n = 32$; export was calculated by the difference between import and net change).

The relative net change of N [*RN*: h^{-1}] in the younger mature leaf blades (2 to 5) was near nil and became only significant and negative (meaning net export) for leaf blades 6 and older. As N import was much higher than the net change in all leaf age categories, all leaf blades exhibited a significant N export in the form on non-labeled N. There was little variation of N export between leaf blades in different position on a tiller except for the oldest leaf blade that exhibited a decreased export rate.

DISCUSSION

This work presents a quantitative analysis of N fluxes in sink and source tissues in major tillers of a perennial C_4 grass. The compartmentalization of IMT (sink tissue) and MT (source tissue) on a tiller led to a better understanding of N fluxes in the two functionally distinct compartments. N export in the form of non-labeled N out of the MT strongly exceeded net N import into IMT, showing that the IMT of the major tiller is not the only sink for the endogenous N mobilized from MT and, accordingly, that N

mobilized in the MT of a tiller may be exported to other plant parts, namely younger daughter tillers or roots. Apparently, N mobilized from all mature leaf blade age categories is an endogenous N source supplying growing tissues and mediates tiller N metabolism. The mobilization of endogenous (non-labeled) N from mature blades started as soon as they were fully expanded and was massive in all mature leaf blade age categories of major tillers. Importantly, the export of non-labeled N, determined via ^{15}N labeling, strongly exceeded the net flux. Again, this feature was largely independent of the age of mature leaf blades.

Tiller growth related to the whole plant growth

There are basically two ways to perform plant growth analyses. In the first, C economy determines the relative growth rate of plants, which has been considered to be driven by biomass deposition. In an analogous way, growth also can be analyzed from the viewpoint of N economy (Garnier, 1991). Plants have to balance the growth of tillers, shoot, and roots in a way to match the prevailing environmental conditions to enable optimal performance by these organs. In this experiment, the RGR_C of the whole shoot was twice as high as the RGR_C of major tillers. Moreover, the RGR_N of the whole shoot was about 3-times higher than the RGR_N of major tillers. This indicates that the ratio of growing to mature tissue (i.e. IMT and MT) on the major tillers, which were sampled in great detail, must have been different in the rest of the whole shoot. The greater disparity of RGR_N than of RGR_C also suggested that the relative N incorporation rate in the younger tillers was much greater than in the major tillers. Indeed, several studies demonstrated that the N concentration of younger tillers was higher than that of old tillers, because the old or major tillers developed and produced progressively more non-assimilating biomass (more old leaves) (Jónsdóttir & Callaghan 1990; Akmal *et al.*, 2010). A high RGR of young plant tissue is associated with a high proportion of metabolically very active tissue with a strong demand for assimilated N (Niemann *et al.*, 1992). In the current study, only 6% of the N mass was allocated to IMT of major tillers. Thus, N mobilization in the MT of the major tillers sustained not only its own IMT but also other sinks within the plant. From the present data it appears that a major sink "outside" the major tillers is branching, i.e. the production of side tillers.

Characteristics of N dynamics in source organs of a tiller

In some way, leaf nitrogen distribution within a tiller reflects the canopy N distribution. The N content was higher in the six uppermost blades than in the older ones, apparently responding to the light gradient within the canopy. Several studies demonstrated that the vertical nitrogen distribution within a canopy is non-uniform and enhances the photosynthetic N use efficiency at plant and canopy scale (Pons *et al.*, 1993; Shiraiwa & Sinclair, 1993; Grindlay, 1997). A study performed under field conditions showed that N content of the three uppermost leaves of *C. squarrosa* was much higher than that of the older leaves within the same tiller (Yang *et al.*, 2011b). Along the tiller of *C. squarrosa* plants grown under field conditions, the N content decreased by 45% among the nine leaf blades at the top of the canopy. However, it only decreased by 11% in the current study. Possibly, this is related to a difference in light extinction between the natural environment conditions and the controlled environment in the present study. Also, the difference could be related to a difference in nutrient and water availability, which would trigger differences in the longevity of leaves.

A significant net change (loss) of N content was only observed for leaf blade 6 and older (Fig. III.10) and might be related to a steeper light gradient in the lower part of the canopy. Without labeling, the invariance of the N content in younger leaves (blade no. 5 and younger) might have been (mis)interpreted as if these leaves did not participate in contributing mobilized N for export. However, tracer incorporation clearly showed that N turnover was active in those leaves that were still exposed to full light. Importantly, turnover was associated with release and export of non-labeled N from the leaf N pool. Clearly this work shows that N mobilization is not limited to senescence and/or shading conditions.

N import into mature blades must have occurred mainly in inorganic form, i.e. as (labeled) nitrate, whereas N export – likely resulting from turnover of leaf proteins – must have occurred mainly in organic form, i.e. predominantly as amino acid-N. It has been reported that 93% of ^{15}N was transported to the shoot as nitrate in ^{15}N-nitrate fed maize plants (Murphy & Lewis, 1987), and tropical legume species assimilated most of their nitrate in the leaves (Andrews, 1986). Moreover, little nitrate is detected in phloem exudates of senescing leaves (Schobert & Komor, 1992) and amino acids deriving from

photosynthetic protein degradation are generally transported to N-demanding tissue *via* the phloem (Feller & Fischer, 1994; Feller *et al.*, 2008).

The significant N turnover in mature blades supporting N mobilization is similar to that found in pigeon pea (*Cajanus cajan*) by Sanetra *et al.* (1998) and Malagoli *et al.* (2005). Here, in these mature blades, N was turned over at a rate of 0.36% h^{-1}, corresponding to nearly 9% per day. N import into mature blades was far greater than the N net change. Since the import of N was in form of labeled N (new N), this must have been balanced by an equivalent export of non-labeled N (old N) that was available for other sink tissues. Possibly the actual rate of N import is even greater than that estimated from the rate of N import, if ^{15}N-nitrate is imported and immediately reduced/assimilated and then exported from tissues within the 24h labeling interval. While the results do not provide evidence for immediate export of newly assimilated N, it can be concluded that these mature leaves act as a temporal storage organ by importing N from uptake and exporting old N (i.e. mainly amino acids produced from leaf protein degradation).

The present study showed that mature blades had similar N turnover rate in the upper part of a tiller (B_2 to B_7) and slightly decreased in low position leaves. Consistent with this, studies with ^{15}N labeling of one leaf of rice plants (*Oryza sativa* L. cv. Notohikari) in a limiting N fertilizer condition showed that both N import and Rubisco synthesis were almost constant for eight days after leaf full expansion (Imai *et al*. 2005) and started decreasing at 16 days after leaf full expansion (Imai *et al*., 2008). Another study compared the turnover of Rubisco in two mature leaves of rice (Suzuki *et al*., 2001), the youngest fully expanded one and a slightly senescent one. The results showed that Rubisco synthesis deceased in slightly senescent leaf. The difference in age of the two leaves corresponded to two leaf appearance intervals. Obviously, *C. squarrosa* kept identical N turnover in more leaves than the rice plants studied by Suzuki *et al*. (2001). Perhaps this is related to the fact that C_4 grasses have a greater number of leaves in given developmental stages: in *C. squarrosa* I found that five leaves were growing simultaneously in a tiller (Table II.1), and mature tillers had more than 10 green leaves (Fig. III.3). Conversely, a rice plant has three to four fully expanded leaves per tiller at nearly all times in the whole life cycle (Suzuki *et al.*, 2009; Dunand & Saichuk, 2014).

Given the absence of protein turnover studies in *C. squarrosa*, some other studies of protein turnover may provide preliminary insight into the correlation between leaf N and protein turnover. Namely, the average turnover rate of total protein was 6% per day in expanded leaves of wheat (Huffaker & Peterson *et al.*, 1974), 12 % per day in barley (Dungey & Davies *et al.*, 1982), and 10% per day in maize (Simpson *et al.*, 1981). These results compare well with the 9% per day N turnover in *C. squarrosa* leaves as observed in this work. Although there may be some species differences in the turnover of leaf proteins, it can be suggested that N turnover in the young mature leaves was generally in conformity with the rhythm of protein synthesis and degradation.

Conclusion

The use of ^{15}N labeling allowed the partitioning of net fluxes of N into (labeled) import and (non-labeled) export fluxes in the leaves that made up the MT of major tillers. The present results illustrate a significant N export out of MT of major tillers, strongly exceeding export assessed from net changes in N mass. The resulting turnover rate for total N in mature blades was 0.36% h^{-1}. Significant mobilization of endogenous (non-labeled) N was observed in all mature blades, including the youngest fully expanded leaf, indicating it started as soon as leaves were fully expanded. N export from the MT of major tillers was approx. 2.5 times higher than N import into the IMT of the same tiller. However, due to continued tiller production in this plant, the growth rate of the whole shoot was about 3 times higher than that of the major tillers. Combing all results, the excess of mobilized and exported amino acid-N means that it is used as a substrate for young tiller growth, showing that N dynamics at tiller level is integrated with that of the remainder of the shoot.

Chapter IV

General and Summarizing Discussion

This study provides detailed information on morphological traits and N dynamics in a perennial C_4 grass – *C. squarrosa* – that is an endemic and co-dominant species in the Central Asia steppe. The work was based on observations of the dynamics of shoot vegetative tissue linear expansion, and of N dynamics in mature (MT) and immature tissues (IMT) of major tillers on the basis of quantitative dynamic ^{15}N labeling. In chapter II, morphological development of grasses subjected to different N fertilization and VPD treatments were compared and summarized. This showed that phytomer development was virtually unaltered by any of the treatments or treatment combinations. Established coordination rules of growth of phytomer components within and between successive phytomers were then used to determine time courses of phytomer and blade development. The further application of phytomer development in the reconstruction of leaf isotopic signals is well illustrated in this chapter. Besides, the findings in chapter II were of fundamental importance in the work of chapter III, as well as in other work that was performed in the frame of the DFG project "*Drivers and mechanisms of ^{13}C discrimination in Cleistogenes squarrosa*" that served as the experimental platform for the present work. The highlight of chapter III is the revelation of N exchange between MT and IMT of a major tiller and the demonstration how the N economy of a mature major tiller is integrated with N processes at the whole shoot or plant level. A significant N mobilization in mature blades of a major tiller was found using ^{15}N labeling. The possible fate of that mobilized N is discussed by exploring relative growth rates of tiller and the whole shoot (chapter III) and N substrate pools for IMT of the same tiller (chapter IV).

To my knowledge, so far the phyllochron has not been employed in the characterization of N fluxes between successively produced organs of a tiller. Other approaches dealt with observations of the export or disappearance of N from source organs over time (Rossato *et al.*, 2001; Yasumura *et al.*, 2007; Schulte auf'm Erley *et al.*, 2010). In this work, knowledge of the phyllochron enabled calculation of N fluxes in successive mature blades of a tiller on the basis of changes of SLN (N content per

leaf area) over a leaf appearance interval. Furthermore, I present an approach for analyzing N export from IMT of a tiller with respect to the phyllochron. Obviously, understanding morphogenetic dynamics is helpful for the analysis of N dynamics in a tiller.

In what follows, I attempt to shed light on the wider implications of the results of the major studies of this work (chapters II and III) and on how they relate to each other. In the context, I also wish to provide a more detailed conceptual framework for the analysis of sink-source relationships in the N dynamics of a vegetative grass tiller. Finally, I show how the works on morphological dynamics have contributed to other works performed on the same experimental platform (in particular the PhD thesis of Haitao Liu, see coauthored manuscripts given in Appendices 3 and 4) and can be helpful in future experimental and (retrospective) ecological or environmental studies (e.g. by use of archived plant material).

Morphological developments under contrasting N supply and VPD conditions: same or different?

Phytomer development was not significantly affected by varying N and VPD supply in this study, as shown by invariant coordination rules and visible growth durations. Numerous studies reported that the length of the leaf blade or sheath is positively associated with the sheath length through which it grows, that is the sheath of the next-older phytomer (Davies *et al.*, 1983; Wilson & Laidlaw, 1985; Skinner & Nelson, 1994a; Casey *et al.*, 1999). This relationship between blade and sheath length of the previous phytomer was found unaltered across treatments in this work, indicating that the invariance of the timing of key events during phytomer development – emergence of the blade tip and of the ligule – was the likely reason for the lack of response of phytomer growth parameters to growth conditions. It also demonstrated that the coordination rules remained the same in different environments. Related parameters, i.e. the duration of phytomer development, the timing of the developmental event (tip emergence), and the extension of phytomer components, have been simulated in architecture models of wheat (Fournier *et al.*, 2003; Evers *et al.*, 2005). Therefore, the resulting coordination rules might be applied to describe the morphological development of C_4 grasses under

contrasting levels of nitrogen nutrition or VPD. This will allow us to evaluate environmental effects on plant morphological plasticity to understand plant life-history strategies.

Notably, the development of whole-plant architecture (e.g. phytomer lengths and tillering rate) significantly responded to varying N fertilization and VPD environments. Besides, a similar effect of N fertilization supply on plant growth was also found (Liu *et al*. 2016 listed in Appendix 3), showing that plant absolute growth rate was increased 45% by high nitrogen fertilizer (relative to low N fertilizer). These results indicated that *C. squarrosa* responded to N supply and VPD in relation to the tillering rate and biomass rather than the developmental process of individual organs (i.e. at the phytomer level). The change in tillering of plants is believed to be a part of the grass domestication process, which influences vegetative architecture (Doust, 2007), and is also an obvious source of morphological plasticity (Boe *et al.*, 2000). The tendency to enhance tiller production in response to high N fertilizer supply thus may act as an adaption of *C. squarrosa* to changing conditions of N stress and supply in the grazed grassland ecosystem of Inner Mongolia.

Light extinction determines spatial N distribution in a vegetative canopy and N dynamics in a tiller

To sustain plant growth, N is required as it plays a key role in canopy photosynthesis. A large investment of N was found in young mature leaves in the upper part of a tiller, which is of benefit to plants as it generates a high "reward" in the form of increased photosynthesis rate. Thus, to allocate more N to leaves which receive high irradiance enables plants to maximize canopy photosynthesis (Field, 1983). Such vertical gradients of leaf N content in a canopy are adjusted in response to light distribution between leaves (Hirose *et al.*, 1988; Hirose *et al.*, 1989; Hirose & Werger, 1994; Anten *et al.*, 1995; Terashima & Hikosaka, 1995; Hikosaka, 1996). Due to the short leaf appearance interval of 2.4 d, plants produced approximately 20 tillers and 14 leaves on the main tiller after 37 days of growth (see Fig. III6). The substantial growth of tillers and leaves generated a dense canopy, which must have caused an appreciable attenuation of light with depth in the canopy. Although I did not measure light extinction in the canopy in

this study, the results of concomitant ^{13}C labeling may be used as a proxy for light distribution, as light availability influences photosynthetic activity. These data demonstrated that relative photosynthesis rate – that is C assimilation rate per unit leaf blade C per hour – decreased with leaf number, i.e. leaf age and depth in the canopy (Figure IV.1A), supporting the idea that light became attenuated from the top to the base of the canopy. Relative N import rate was strongly related to relative photosynthesis rate of the different age classes of fully-expanded leaf blades (Figure IV.1A). The close relationship between relative N import rate and depth in the canopy is probably also related to the fact that light drives both the import of nitrate *via* the xylem through an enhancement of transpiration and N assimilation. However, there was no significant correlation between relative N export rate and relative photosynthesis rate, indicating that relative N export rate was actually independent of relative photosynthesis rate. Thus, N mobilization in these mature blades was apparently not determined by their photosynthetic activity.

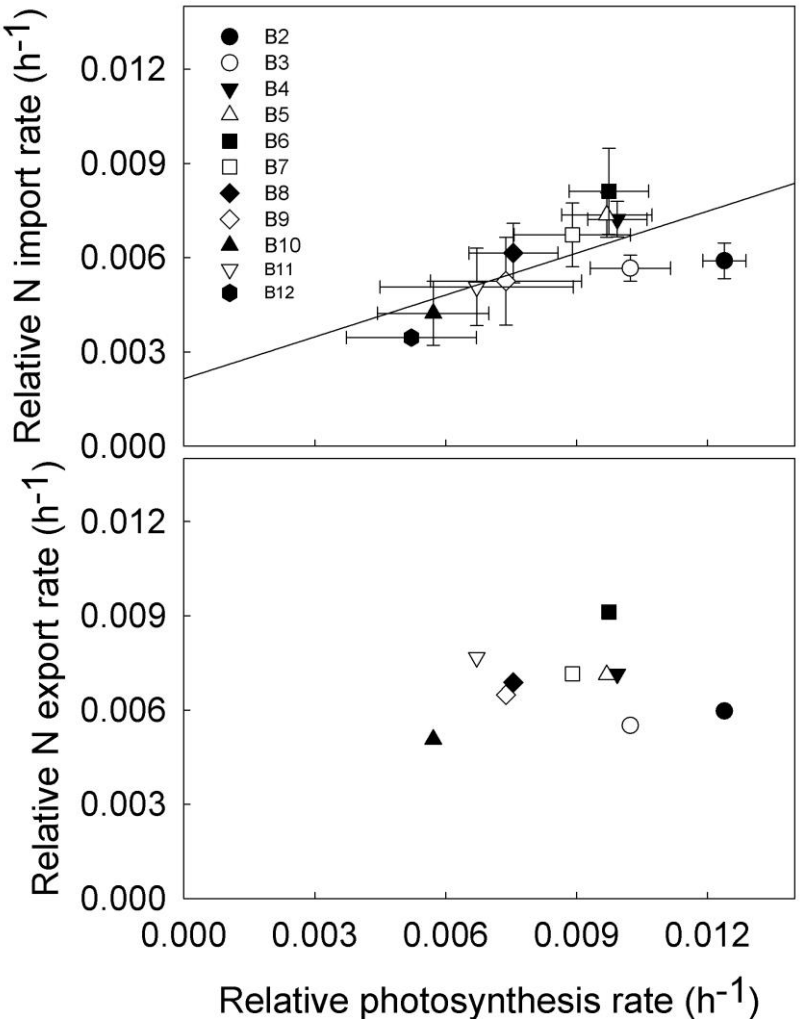

Figure IV.1 Relationships between relative photosynthesis rate (RPR) and relative N import rate (RNIR in panel A), and relative N export rate (RNER in panel B) in mature leaf blades along major tillers of *C. squarrosa*. RPR was determined via concomitant ^{13}C labeling, and different symbols represent different blade age categories. Blades were numbered from the tip to the base of a tiller. The line indicates a linear regression between RNIR and RPR: $y = 0.444*x + 0.002$ ($r^2 = 0.5$; $p = 0.02$). The relationship between RNER and RPR is not significant ($p = 0.79$).

A study of N import in leaf blades of rice from emergence to senescence clearly suggested that N import into a leaf is closely related to the amount of Rubisco synthesized throughout the leaf lifespan (Imai *et al.*, 2005). Thus, N dynamics in a tiller is not only determined by the N requirement of the sink tissue, but also mediated by N turnover of source tissue. As stated by Lattanzi (2004), absorbed N is partly 'stored'

(probably in the photosynthetic apparatus of mature leaves) before being transferred to growing organs, in the form of amino acids. Here, a significant N import and export supports the idea that mature blades act as temporal storage organs that might increase the N sink strength of the whole plant during development. Similar conclusions were previously drawn by Masclaux *et al*. (2000) and Malagoli *et al.* (2005), following the investigations on N fluxes (uptake of exogenous N and N mobilization to other tissues) in source leaves in tobacco and oilseed rape plants, respectively. Importantly, a large discrepancy was found between N export out of MT and N import into IMT of the same tiller in this study. It suggests that the excess of N export could then serve in other parts for balancing the N needs of other sink tissues in the whole plant. This idea is supported by the finding of the higher RGR_N of the whole plant than the RGR_N of major tillers.

Sink-source relationships of N supply in vegetative tillers of grass plants

The analysis of N dynamics presented in chapter III offers detailed quantitative insight into the role of mature leaf tissue in the sink-source system of N in major vegetative tillers of *C. squarrosa*. However, the role of the sink part of the tiller, that is the IMT, could not be evaluated in full detail. There is much evidence, that N supply to expanding tissue of grasses – including leaves – is in the form of amino acids essentially, while N import into MT, e.g. fully expanded leaf blades, occurs mainly (or near-exclusively) in the form of nitrate, if supplied in that form (Figure IV.2). However, the IMT, while only comprising still-developing phytomers, did also contain some fully differentiated tissue. The oldest leaf within the IMT was still growing (as a function of sheath and internode elongation, see Chapter II), in agreement with the definition. But, that same leaf already comprised some fully expanded blade tissue that was directly exposed to light. It is known for growing grass leaves, that leaf tissue emerging into light is fully photosynthetically competent (Wilhelm & Nelson 1978; Allard & Nelson 1991), transpiring (Martre *et al*. 2001), and presumably also able to assimilate N. This would mean that some of the N import into the IMT would have been in the form of nitrate. Accordingly, amino acid-N import would not account for all of N import into the IMT.

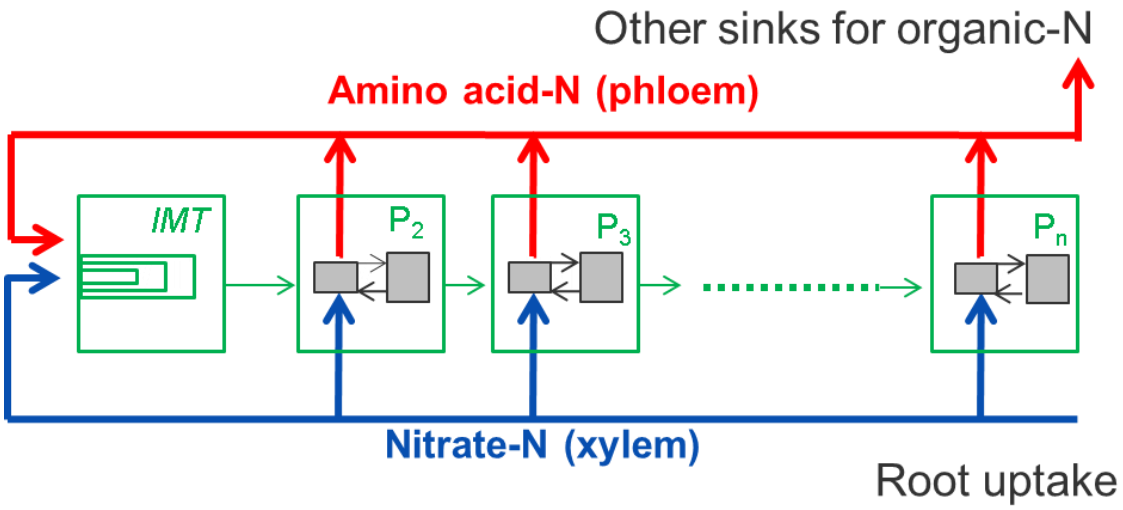

Figure IV.2 Conceptual representation of nitrogen pools (black boxes) and fluxes (blue and red arrows) within a tiller of *C. squarrosa*. The tiller is composed of phytomers of different developmental stages (green): IMT comprises several still-growing phytomers; P_2, the youngest fully differentiated phytomer; P_3 … P_n designate phytomers of increasing developmental age. Nitrogen is taken up by the root system in the form of nitrate and transported to the individual phytomers of the tiller *via* the xylem (blue color). Nitrate is assimilated into amino acids (small black box) within the photosynthetically active tissues of the different phytomers (IMT, P_2, P_3 …. P_n) and used in protein synthesis (large black box). Protein turnover (simultaneous synthesis and degradation) involves exchange with the amino acid pool. N export in the phloem (red) occurs in the form of amino acids. The N supply of growing, heterotrophic tissue in the root and shoot occurs in the form of amino acids exclusively (note: the growth zone of grass leaf blades and sheaths, as well as of the internodes is fully heterotrophic). Green arrows designate 'tissue flux' in the sense that, within one leaf appearance interval, a given phytomer passes from the P_i to P_{i+1} stage.

This issue complicates the interpretation of the labeling kinetics of N in the import flux ($f_{lab\ I}$) of IMT that was observed (but not presented) in the experiment reported in Chapter III (Figure IV.3). That time course showed that $f_{lab\ I}$ increased in two phases: there was a fast increase in the first two days that was followed by a very slow increase during the remainder of the labeling period. Notably, the $f_{lab\ I}$ did not even reach unity ($f_{lab\ I}$ <1) after 7 days of continuous labeling, showing that import of non-

labeled N (which must have been in the form of amino acids) continued to be an important source of N for the IMT for a very long time. This would also indicate the presence of slowly turning over N pools supplying continuously a substantial flux of amino acids to developing sink tissues. Indeed the observed N turnover in fully expanded leaves (0.36% h^{-1}) would mean that after 7 days, the protein pool has been exchanged by only 47% by new N, showing that the mature leaves were a lasting source of mobilized N. That factor is also illustrated by the long leaf lifespan of *C. squarrosa*. Even in blade 10, which had developed more than 24 days before the start of the labeling period, considerable N turnover was evident. Clearly, as long as the leaves were not fully senescent, they acted as a significant source of non-labeled N for growing sink tissues, which likely included the IMT.

Interpretation of the fast initial labeling of the N import flux (i.e. the rapid increase of $f_{\text{lab I}}$) however is more complex, as has been elaborated above, as it may have include (unknown) contributions of nitrate, imported *via* the xylem, and supplying N assimilation in the photosynthetically active part of the IMT, as well as rapidly labeled amino acids imported *via* the phloem, supplying the growing heterotrophic part of the IMT. Clearly, future work characterizing the N supply system of the IMT must address the developmental heterogeneity of that tissue more fully, to test the above prediction/hypothesis.

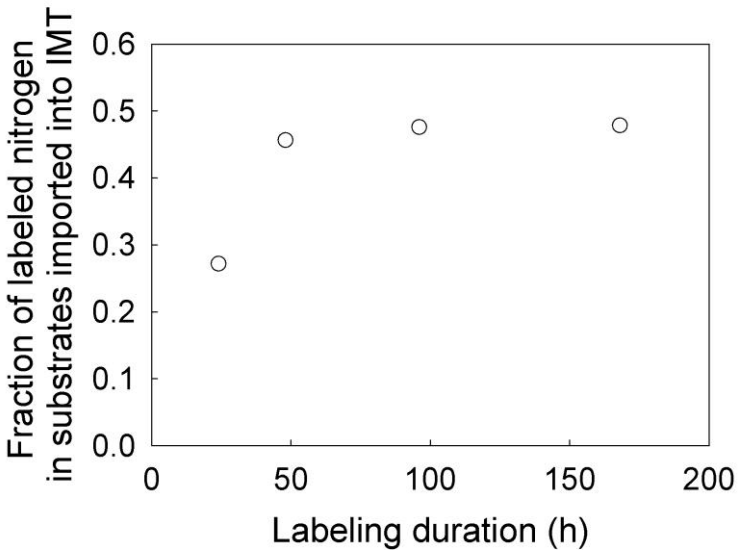

Figure IV.3 Fraction of labeled N in the import flux into immature tissue (IMT) of a tiller of *C. squarrosa* during contentious ^{15}N labeling. The analysis of N substrate supply for IMT followed principles described by Lattanzi *et al.*, 2005 and Lehmeier *et al.*, 2013, which analysed the N fluxes in the growth zones of elongating leaves. Tissue-bound N export out of IMT was estimated as the N mass of the recently exported tissue (L_2) divided by the leaf appearance interval (2.4 d) (see Materials and Methods, Chapter III). Import of tracer-N into IMT was estimated as the sum of tracer-N exported from the IMT and the increase of tracer content within the IMT over one leaf appearance interval (for details of the calculation, see Supplemental Methods in Appendix 2).

Using knowledge from developmental dynamics as a timepiece in ecophysiological studies

The findings in this work formed the basis for evaluating data of a series of other measurements performed on a subset of *C. squarrosa* plants growing in the same experiment. Using knowledge on the phyllochron and on the time course of phytomer development allows the determination of the age and developmental stage of leaves on a tiller in retrospect, i.e. on plants sampled at any time without the necessity of monitoring their growth *before* sampling. This provided a highly-resolved temporal record of ecophysiolgical processes in plants in which oxygen isotope composition of leaf cellulose ($\delta^{18}O_{Cel}$) was investigated. $\delta^{18}O_{Cel}$ is reflective of environmental conditions, namely evaporative demand, which is imprinted in the oxygen isotopic

signature during the process of cellulose synthesis via the evaporative enrichment of leaf water (see Liu *et al.* 2016 for details of the experiment and discussion of the data). One subset of plants (i) grown in constant environment, i.e. growing with the same low or high VPD from imbibition to sampling (Fig. IV.4), was used to determine $\delta^{18}O$ of cellulose ($\delta^{18}O_{Cel}$) in mature leaf blades of different ages. A second subset of plants (2) were grown for 7 days in a new VPD environment by transfering plants from low to high VPD and *vice versa* (Fig. IV.6), and was used to determine the turnover of substrates serving cellulose synthesis in growing leaf blades.

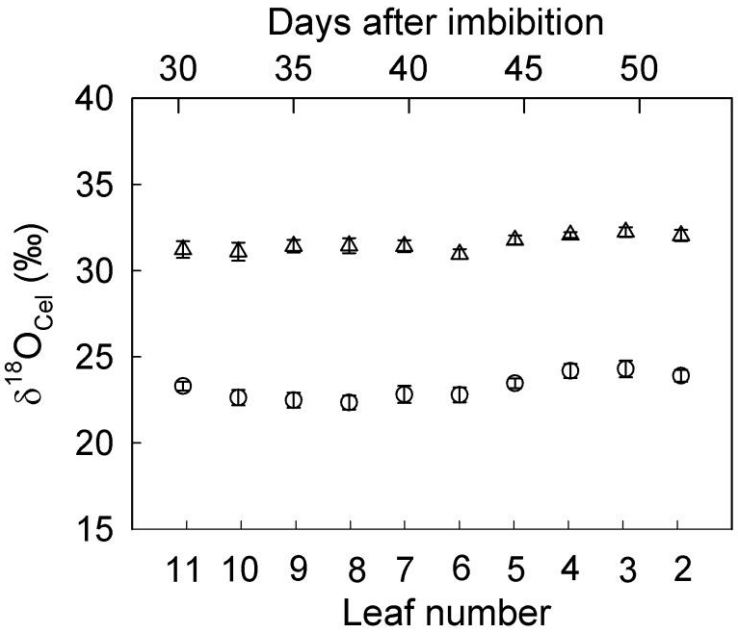

Figure IV.4 $\delta^{18}O$ of cellulose in successively produced mature leaf blades along major tillers of *C. squarrosa* grown under 7.5 mM N fertilizer conditions. Circles: low VPD; triangles: high VPD. Major tillers were harvested on the 53rd day after imbibition of seeds. Values are means ± standard error (n = 6). Leaves were numbered basipetally, that is from the youngest to the oldest, starting at leaf 2, the leaf with the youngest fully expanded leaf blade in a tiller (data from Liu *et al*. 2016 listed in Appendix 3). The $\delta^{18}O_{Cel}$ data were obtained from successively produced leaves, and can also be reported *versus* time by using the knowledge of phyllochron. The youngest leaf 2 was last to appear among these leaves. Accordingly, the age of older leaves was calculated retrospectively, and the leaf number was converted into days after imbibition. These leaf blades are major components of MT shown in Figure III.1.

By calaculating the age of leaves on a tiller, $\delta^{18}O_{Cel}$ data obtained from successively produced mature leaf blades can be analysed as response of leaf cellullose synthesis to enviromental conditions over time (Fig. IV.4). $\delta^{18}O_{Cel}$ of leaves grown in contrasting but constant VPD differed by 9‰, reflecting the difference in evaporative demand. But, in one VPD, $\delta^{18}O_{Cel}$ of leaves produced at different time after imbibition was relatively constant, indicating that environmental conditions in the respective growth chambers were approximately constant over time. For plants which had been transferred to a new environment (i.e. from high to low VPD and *vice versa*), the developmental stage of blades at the time of transfer could be estimated in retrospect (Fig. IV.5). These analyses showed that blades which were already fully elongated at the time of transfer showed no incorporartion of oxgen into cellulose after the transfer (Fig. IV.6). However, incorporation of new oxgen increased linearly with decreasing developmental stage at the time of transfer. In growing leaves of different developmental stages, the fraction of new oxygen ($f_{new\,O}$) in cellulose was not affected by the direction of transfer (for complete presentation of the dataset and discussion see Liu *et al.*, submitted; Appendix 4). This indicates that the incorporation of cellulose is essentially dependent on leaf growth stage and independent of VPD-specific morpho-physiological traits acquired in the original growth environment. Again, this highlights the usefulness of the characterization of phytomer growth and coordination of growth between successive phytomers (Chapter II) (1) for interpretation of isotopic signatures of plant parts in terms of underlying mechanisms and (2) to assist in reconstructions of short-term environmental conditions, here evaporative demand. Clearly, ^{18}O records presented by the successive leaves produced along a tiller can serve as a timepiece in studies of ecopysiological features of *C. squarrosa*. Such a function of timepiece could be helpful for reconstructing past environmental conditions and physiological responses using leaf samples gathered from herbariums (Bonal *et al.* 2011).

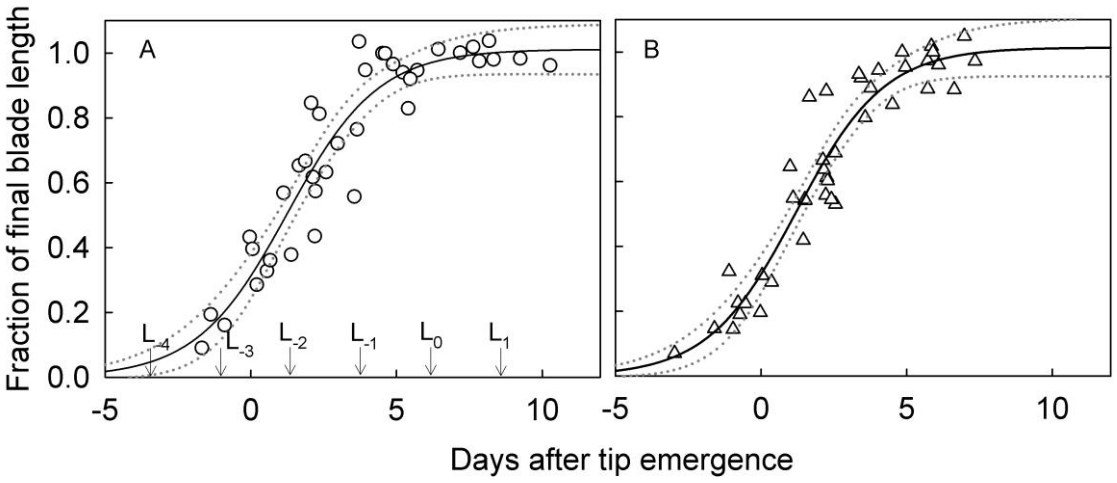

Figure IV.5 Time course of the fraction of final blade length in *C. squarrosa* grown under 7.5 mM N fertilizer conditions (low and high VPD: panel A and B). Leaf blade length was normalized as a fraction of final length. Tip emergence was defined as the moment a leaf blade tip had grown past the highest visible ligule of the preceding leaf. The solid and gray dotted curves denote a 3-parameter sigmoidal function and 95% confidence bands. Panel A (low VPD): $y = 1.01/\{1 + \exp[(1.25 - x)/1.56]\}$($R^2 = 0.88$; residual standard error = 0.1). Panel B (high VPD): $y = 1.01/\{1 + \exp[(1.21 - x)/1.51]\}$($R^2 = 0.90$; residual standard error = 0.1). VPD had no effect on the parameters of the function ($P > 0.05$). Arrows in (A) indicate the ages of leaves at any sampling time estimated from (i) the relationship of successive, growing leaves and (ii) the phyllochron. Leaves were numbered acropetally, starting at the leaf 1 with the youngest exposed blade, near the tip of the tiller. These leaf blades are major components of IMT shown in Figure III.1.

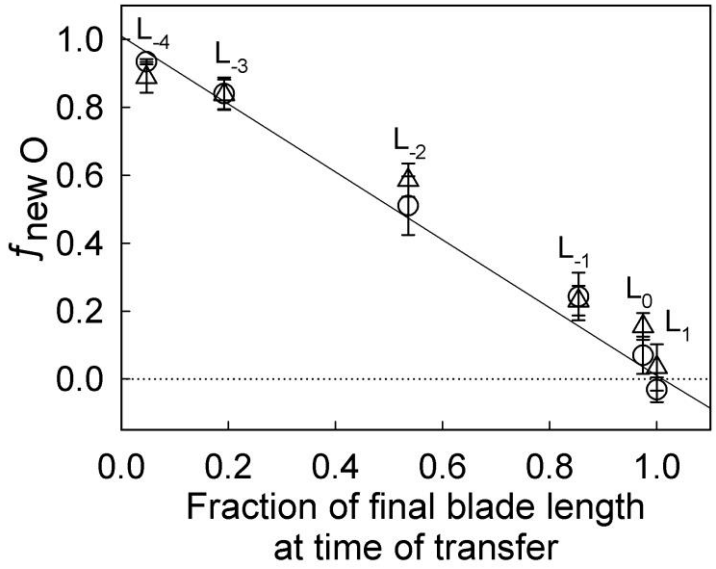

Figure IV.6 Fraction of new oxygen ($f_{new\ O}$) in cellulose of leaf blades of different ages in plants 7 days after transfer to a new VPD environment *versus* fraction of leaf blade length at the time of transfer. Circles: transfer from low to high VPD; triangles: transfer from high to low VPD. The line denotes a linear function fitted to the combined data of two transfer treatments: $y = 1 - x$ ($R^2 = 0.99$). Values are presented as mean ± standard error ($n = 6$). Letters with subscripts refer to leaf age at time of transfer (7 days before sampling) as indicated in Figure IV.5. Data from Liu *et al.*, Appendix 4.

Conclusions and outlooks

Cleistogenes squarrosa exhibited invariant coordination rules during morphological development in response to N fertilization and VPD levels. By using morphological and developmental traits and ^{15}N labeling, it allowed the estimation of the turnover rate of bulk N in mature blades of 9% per day, which is in the range of protein turnover rates observed in other species by other researchers. A very significant and closely similar N export occurred in mature blades of different ages along major tillers. These export rates were much higher than rates of net export assessed from net changes in N mass during aging. The N import into mature blades was obviously associated with light conditions in the canopy. Results also showed that N exported from the MT of major tillers is not only used as a substrate for the growth of IMT in the same tiller but also served other plant parts, probably including younger tillers. Thus, N dynamics at the tiller level is integrated with that of the remainder of the shoot. The present work provided insight into ecopysiological responses of *C. squarrosa* to environmental changes and its increasing abundance in the Inner Mongolia grassland. Furthermore, in retrospective studies, the knowledge of phytomer development (i.e. the time course of leaf elongation and leaf appearance interval) can be applied to provide a temporal record for isotope time series analyses in this grass. It is helpful for the reconstruction of short-term hydrological changes, and the reassessment of environmental changes in the Mongolia grassland. *C. squarrosa* may be particularly suitable for time series analyses, as it exhibits a short leaf appearance interval (phyllochron) and has up to five concurrently growing leaves at different developmental stages during vegetative development.

The developmental heterogeneity of the IMT was a challenge for the understanding of contributions of N assimilation (from exogenous source) and N mobilization (from endogenous source) to N supply of the IMT. Future work should thus focus on solving the developmental heterogeneity of IMT. A combined analysis of N dynamics and C dynamics in leaves on the basis of labeling with higher temporal resolution would form a next step, and should help to understand the underlying mechanisms of the coupling of N and C metabolism.

References

Aerts R, Chapin III FS 2000. The mineral nutrition of wild plants revisited: a re-evaluation of processes and patterns. In: Fitter AH, Raffaelli DG eds. *Advances in Ecological Research*. Colchester, UK: Academic Press, 1-67.

Akmal M, Schellberg J, Khattak R. 2010. Biomass allocation and nitrogen distribution in ryegrass under water and nitrogen supplies. *Journal of Plant Nutrition* 33: 1777-1788.

Allard G, Nelson CJ. 1991. Photosynthate partitioning in basal zones of tall fescue leaf blades. *Plant Physiology* 95: 663-668.

Andrews M. 1986. The partitioning of nitrate assimilation between root and shoot of higher plants. *Plant, Cell & Environment* 9: 511-519.

Anten NPR, Schieving F, Werger MJA. 1995. Patterns of light and nitrogen distribution in relation to whole canopy carbon gain in C_3 and C_4 mono- and dicotyledonous species. *Oecologia* 101: 504-513.

Auerswald K, Wittmer M, Männel T, Bai Y, Schäufele R, Schnyder H. 2009. Large regional-scale variation in C_3/C_4 distribution pattern of Inner Mongolia steppe is revealed by grazer wool carbon isotope composition. *Biogeosciences* 6: 795-805.

Auerswald K, Wittmer M, Bai Y, Yang H, Taube F, Susenbeth A, Schnyder H. 2012. C_4 abundance in an Inner Mongolia grassland system is driven by temperature–moisture interaction, not grazing pressure. *Basic and Applied Ecology* 13: 67-75.

Avice JC, Etienne P. 2014. Leaf senescence and nitrogen remobilization efficiency in oilseed rape (*Brassica napus* L.). *Journal of Experimental Botany* 65: 3813-3824.

Baethgen WE, Christianson CB, Lamothe AG. 1995. Nitrogen fertilizer effects on growth, grain yield, and yield components of malting barley. *Field Crops Research* 43: 87-99.

Bai YF, Wu JG, Clark CM, Naeem S, Pan QM, Huang JH, Zhang LX, Han XG. 2010. Tradeoffs and thresholds in the effects of nitrogen addition on biodiversity and ecosystem functioning: evidence from Inner Mongolia grasslands. *Global Change Biology* 16: 358-372.

Bai YF, Wu JG, Xing Q, Pan QM, Huang JH, Yang DL, Han XG. 2008. Primary production and rain use efficiency across a precipitation gradient on the Mongolia Plateau. *Ecology* 89: 2140-2153.

Baki GKA-E, Siefritz F, Man HM, Weiner H, Kaldenhoff R, Kaiser WM. 2000. Nitrate reductase in *Zea mays* L. under salinity. *Plant, Cell & Environment* 23: 515-521.

Ben Haj Salah H, Tardieu F. 1996. Quantitative analysis of the combined effects of temperature, evaporative demand and light on leaf elongation rate in well-watered field and laboratory-grown maize plants. *Journal of Experimental Botany* 47: 1689-1698.

Ben Haj Salah H, Tardieu F. 1997. Control of leaf expansion rate of droughted maize plants under fluctuating evaporative demand (A superposition of hydraulic and chemical messages?). *Plant Physiology* 114: 893-900.

Bertheloot J, Martre P, Andrieu B. 2008. Dynamics of light and nitrogen distribution during grain filling within wheat Canopy. *Plant Physiology* 148: 1707-1720.

Bloom AJ. 1985. Wild and cultivated barleys show similar affinities for mineral nitrogen. *Oecologia* 65: 555-557.

Boe A, Bortnem R, Kephart KD. 2000. Quantitative description of the phytomers of big bluestem. *Crop Science* 40: 737-741.

Boe A, Casler MD. 2005. Hierarchical analysis of switchgrass morphology. *Crop Science* 45: 2465-2472.

Bonal D, Ponton S, Le Thiec D, Richard B, Ningre N, HÉRault B, OgÉE J, Gonzalez S, Pignal M, Sabatier D *et al.* 2011. Leaf functional response to increasing atmospheric CO2 concentrations over the last century in two northern Amazonian tree species: a historical δ13C and δ18O approach using herbarium samples. *Plant, Cell & Environment* 34: 1332-1344.

Briske DD. 1991. Developmental morphology and physiology of grasses. In: Heitschmidt RK, Stuth JW eds. *Grazing management : an ecological perspective*. Oregon, Portland: Timber Press, 85-108.

Buchanan-Wollaston V. 1997. The molecular biology of leaf senescence. *Journal of Experimental Botany* 48: 181-199.

Buck-Sorlin G, Hemmerling R, Kniemeyer O, Burema B, Kurth W. 2008. A rule-based model of barley morphogenesis, with special respect to shading and gibberellic acid signal transduction. *Annals of Botany* 101: 1109-1123.

Buck-Sorlin GH, Kniemeyer O, Kurth W. 2005. Barley morphology, genetics and hormonal regulation of internode elongation modelled by a relational growth grammar. *New Phytologist* 166: 859-867.

Casey IA, Brereton AJ, Laidlaw AS, McGilloway DA. 1999. Effects of sheath tube length on leaf development in perennial ryegrass (*Lolium perenne* L.). *Annals of Applied Biology* 134: 251-257.

Chapin FS, Schulze E-D, Mooney HA. 1990. The ecology and economics of storage in plants. *Annual review of ecology and systematics* 21: 423-447.

Chen SP, Bai YF, Han XG. 2002. Variation of water-use efficiency of *Leymus chinensis* and *Cleistogenes squarrosa* in different plant communities in Xilin river basin, Nei Mongol. *Acta Botanica Sinica* 44: 1484–1490.

Chen SH, Zhang H, Wang LQ, Zhan BL, Zhao ML. 2001. *Roots of grassland plants in northern China*. Changchun: Jilin University Press.

Comstock JP. 2001. Steady-state isotopic fractionation in branched pathways using plant uptake of NO_3^- as an example. *Planta* 214: 220-234.

Davies A, Evans ME, Exley JK. 1983. Regrowth of perennial ryegrass as affected by simulated leaf sheaths. *The Journal of Agricultural Science* 101: 131-137.

De Visser R, Vianden H, Schnyder H. 1997. Kinetics and relative significance of remobilized and current C and N incorporation in leaf and root growth zones of Lolium perenne after defoliation: assessment by ^{13}C and ^{15}N steady-state labelling. *Plant, Cell & Environment* 20: 37-46.

Dechorgnat J, Nguyen CT, Armengaud P, Jossier M, Diatloff E, Filleur S, Daniel-Vedele F. 2011. From the soil to the seeds: the long journey of nitrate in plants. *Journal of Experimental Botany* 62: 1349-1359.

Diaz C, Lemaître T, Christ A, Azzopardi M, Kato Y, Sato F, Morot-Gaudry J-F, Le Dily F, Masclaux-Daubresse C. 2008. Nitrogen recycling and remobilization are rifferentially controlled by leaf senescence and development stage in Arabidopsis under low nitrogen nutrition. *Plant Physiology* 147: 1437-1449.

Distelfeld A, Avni R, Fischer AM. 2014. Senescence, nutrient remobilization, and yield in wheat and barley. *Journal of Experimental Botany* 65: 3783-3798.

Dohleman FG, Heaton EA, Arundale RA, Long SP. 2012. Seasonal dynamics of above- and below-ground biomass and nitrogen partitioning in

Miscanthus × *giganteus* and *Panicum virgatum* across three growing seasons. *Global Chang Biology Bioenergy* 4: 534-544.

Doust A. 2007. Architectural evolution and its implications for domestication in grasses. *Annals of Botany* 100: 941-950.

Dunand R, Saichuk J 2014. Rice growth and development. *Louisiana Rice Production Handbook.* . Baton Rouge: LA: Louisiana State University AgCenter Publ, 41-53.

Dungey NO, Davies DD. 1982. Protein turnover in the attached leaves of non-stressed and stressed barley seedlings. *Planta* 154: 435-440.

Evans GC. 1972. *The quantitative analysis of plant growth*. Berkeley, CA, USA: University of California Press.

Evans J. 1989. Photosynthesis and nitrogen relationships in leaves of C_3 plants. *Oecologia* 78: 9-19.

Evans RD. 2001. Physiological mechanisms influencing plant nitrogen isotope composition. *Trends in Plant Science* 6: 121-126.

Evers JB, Vos J, Fournier C, Andrieu B, Chelle M, Struik PC. 2005. Towards a generic architectural model of tillering in Gramineae, as exemplified by spring wheat (*Triticum aestivum*). *New Phytologist* 166: 801-812.

Farquhar GD. 1989. Models of integrated photosynthesis of cells and leaves. *Philosophical Transactions of the Royal Society of London B: Biological Sciences* 323: 357-367.

Feller U, Anders I, Mae T. 2008. Rubiscolytics: fate of Rubisco after its enzymatic function in a cell is terminated. *Journal of Experimental Botany* 59: 1615-1624.

Feller U, Fischer A. 1994. Nitrogen metabolism in senescing leaves. *Critical Reviews in Plant Sciences* 13: 241-273.

Field C. 1983. Allocating leaf nitrogen for the maximization of carbon gain: leaf age as a control on the allocation program. *Oecologia* 56: 341-347.

Forster BP, Franckowiak JD, Lundqvist U, Lyon J, Pitkethly I, Thomas WTB. 2007. The barley phytomer. *Annals of Botany* 100: 725-733.

Fournier C, Andrieu B. 1998. A 3D architectural and process-based model of maize development. *Annals of Botany* 81: 233-250.

Fournier C, Andrieu B. 2000. Dynamics of the elongation of internodes in Maize (*Zea mays* L.): analysis of phases of elongation and their relationships to phytomer development. *Annals of Botany* 86: 551-563.

Fournier C, Andrieu B, Ljutovac S, Saint-Jean S 2003. ADEL-wheat: a 3D architectural model of wheat development.In M. IHB-GaJ. *Proceedings PMA03: International symposium on plant growth modeling, simulation, visualization and their applications*. Beijing,China: Tsinghua University Press-Springer. 54-63.

Fournier C, Durand JL, Ljutovac S, Schäufele R, Gastal F, Andrieu B. 2005. A functional–structural model of elongation of the grass leaf and its relationships with the phyllochron. *New Phytologist* 166: 881-894.

Gallais A, Coque M, Quilléré I, Prioul J-L, Hirel B. 2006. Modelling postsilking nitrogen fluxes in maize (*Zea mays*) using 15N-labelling field experiments. *New Phytologist* 172: 696-707.

Gao YZ, Wang SP, Han XG, Chen QS, Zhou ZY, Patton BD. 2007. Defoliation, nitrogen, and competition: effects on plant growth and resource allocation of *Cleistogenes squarrosa* and *Artemisia frigida*. *Journal of Plant Nutrition and Soil Science* 170: 115-122.

Gao YZ, Wang SP, Han XG, Patton BD, Nyren PE. 2005. Competition between *Artemisia frigida* and *Cleistogenes squarrosa* under different clipping intensities in replacement series mixtures at different nitrogen levels. *Grass and Forage Science* 60: 119-127.

Garnier E. 1991. Resource capture, biomass allocation and growth in herbaceous plants. *Trends in Ecology & Evolution* 6: 126-131.

Gastal F, Nelson CJ. 1994. Nitrogen use within the growing leaf blade of tall fescue. *Plant Physiology* 105: 191-197.

Giese M, Brueck H, Gao YZ, Lin S, Steffens M, Kögel-Knabner I, Glindemann T, Susenbeth A, Taube F, Butterbach-Bahl K *et al*. 2013. N balance and cycling of Inner Mongolia typical steppe: a comprehensive case study of grazing effects. *Ecological Monographs* 83: 195-219.

Girondé A, Poret M, Etienne P, Trouverie J, Bouchereau A, Le Cahérec F, Leport L, Orsel M, Niogret MF, Deleu C *et al*. 2015. A profiling approach of the natural variability of foliar N remobilization at the rosette stage gives clues to understand the limiting processes involved in the low N use efficiency of winter oilseed rape. *Journal of Experimental Botany* 66: 2461-2473.

Gong X, Brueck H, Giese K, Zhang L, Sattelmacher B, Lin S. 2008. Slope aspect has effects on productivity and species composition of hilly grassland in the

Xilin River Basin, Inner Mongolia, China. *Journal of arid environments* 72: 483-493.

Gong XY, Chen Q, Lin S, Brueck H, Dittert K, Taube F, Schnyder H. 2011. Tradeoffs between nitrogen- and water-use efficiency in dominant species of the semiarid steppe of Inner Mongolia. *Plant and Soil* 340: 227-238.

Gong XY, Fanselow N, Dittert K, Taube F, Lin S. 2015. Response of primary production and biomass allocation to nitrogen and water supplementation along a grazing intensity gradient in semiarid grassland. *European Journal of Agronomy* 63: 27-35.

Gong XY, Schäufele R, Schnyder H. 2017. Bundle-sheath leakiness and intrinsic water use efficiency of a perennial C_4 grass are increased at high vapour pressure deficit during growth. *Journal of Experimental Botany* 68: 321-333

Gregersen PL, Holm PB, Krupinska K. 2008. Leaf senescence and nutrient remobilisation in barley and wheat. *Plant Biology* 10: 37-49.

Grindlay D. 1997. Towards an explanation of crop nitrogen demand based on the optimization of leaf nitrogen per unit leaf area. *The Journal of Agricultural Science* 128: 377-396.

Heaton EA, Dohleman FG, Long SP. 2009. Seasonal nitrogen dynamics of *Miscanthus×giganteus* and Panicum virgatum. *Global Change Biology Bioenergy* 1: 297-307.

Helliker BR, Ehleringer JR. 2002. Grass blades as tree rings: environmentally induced changes in the oxygen isotope ratio of cellulose along the length of grass blades. *New Phytologist* 155: 417-424.

Hesketh JD, Warrington IJ, Reid JF, Zur B. 1988. The dynamics of corn canopy development: phytomer ontogeny. *Biotronics* 17: 69-77.

Hikosaka K. 1996. Effects of leaf age, nitrogen nutrition and photon flux density on the organization of the photosynthetic apparatus in leaves of a vine (*Ipomoea tricolor* Cav.) grown horizontally to avoid mutual shading of leaves. *Planta* 198: 144-150.

Hikosaka K. 2004. Interspecific difference in the photosynthesis-nitrogen relationship: patterns, physiological causes, and ecological importance. *Journal of Plant Research* 117: 481-494.

Hikosaka K. 2005. Leaf canopy as a dynamic system: ecophysiology and optimality in leaf turnover. *Annals of Botany* 95: 521-533.

Hirel B, Le Gouis J, Ney B, Gallais A. 2007. The challenge of improving nitrogen use efficiency in crop plants: towards a more central role for genetic variability and quantitative genetics within integrated approaches. *Journal of Experimental Botany* 58: 2369-2387.

Hirel B, Lea PJ. 2001. Ammonia assimilation. In: Lea PJ, Morot-Gaudry JF, eds. *Plant nitrogen*. Berlin: Springer, 79–99.

Hirel B, Lea PJ 2002. The biochemistry, molecular biology, and genetic manipulation of primary ammonia assimilation. In: Foyer CH, Noctor G, eds. *Photosynthetic nitrogen assimilation and associated carbon and respiratory metabolism*. Dordrecht: Springer Netherlands, 71-92.

Hirose T, Werger MJA. 1987. Maximizing daily canopy photosynthesis with respect to the leaf nitrogen allocation pattern in the canopy. *Oecologia* 72: 520-526.

Hirose T, Werger MJA. 1994. Photosynthetic capacity and nitrogen partitioning among species in the canopy of a herbaceous plant community. *Oecologia* 100: 203-212.

Hirose T, Werger MJA, Pons TL, Rheenen JWA. 1988. Canopy structure and leaf nitrogen distribution in a stand of *Lysimachia vulgaris* L. as influenced by stand density. *Oecologia* 77: 145-150.

Hirose T, Werger MJA, van Rheenen JW. 1989. Canopy development and leaf nitrogen distribution in a stand of carex acutiformis. *Ecology* 70: 1610-1618.

Hooper DU, Johnson L. 1999. Nitrogen limitation in dryland ecosystems: responses to geographical and temporal variation in precipitation. *Biogeochemistry* 46: 247-293.

Huffaker RC, Peterson LW. 1974. Protein trnover in plants and possible means of its regulation. *Annual Review of Plant Physiology* 25: 363-392.

Hörtensteiner S, Feller U. 2002. Nitrogen metabolism and remobilization during senescence. *Journal of Experimental Botany* 53: 927-937.

Horvath DP, Anderson JV, Chao WS, Foley ME. 2003. Knowing when to grow: signals regulating bud dormancy. *Trends in Plant Science* 8: 534-540.

Imai K, Suzuki Y, Mae T, Makino A. 2008. Changes in the synthesis of rubisco in rice leaves in relation to senescence and N influx. *Annals of Botany* 101: 135-144.

Imai K, Suzuki Y, Makino A, Mae T. 2005. Effects of nitrogen nutrition on the relationships between the levels of rbcS and rbcL mRNAs and the amount of ribulose 1·5-bisphosphate carboxylase/oxygenase synthesized in the eighth leaves of rice from emergence through senescence. *Plant, Cell & Environment* 28: 1589-1600.

Irving LJ, Robinson D. 2006. A dynamic model of Rubisco turnover in cereal leaves. *New Phytologist* 169: 493-504.

Irving LJ, Suzuki Y, Ishida H, Makino A 2010. Protein turnover in grass leaves. In: Jean-Claude K, Michel D, eds. *Advances in botanical research*. Orsay, France: Academic Press, 139-182.

Jigjidsuren S, Johnson DA. 2003. *Forage plants in Mongolia*. Admon, Ulaanbataar.

Jónsdóttir IS, Callaghan TV. 1990. Intraclonal translocation of ammonium and nitrate nitrogen in *carex bigelowii* Torr. ex Schwein. using ^{15}N and nitrate reductase assays. *New Phytologist* 114: 419-428.

Kavanová M, Lattanzi FA, Schnyder H. 2008. Nitrogen deficiency inhibits leaf blade growth in *Lolium perenne* by increasing cell cycle duration and decreasing mitotic and post-mitotic growth rates. *Plant, Cell & Environment* 31: 727-737.

Kering MK, Butler TJ, Biermacher JT, Guretzky JA. 2012. Biomass yield and nutrient removal rates of perennial grasses under nitrogen fertilization. *BioEnergy Research* 5: 61-70.

Kinugasa T, Tsunekawa A, Shinoda M. 2012. Increasing nitrogen deposition enhances post-drought recovery of grassland productivity in the Mongolian steppe. *Oecologia* 170: 857-865.

Kirby EJM, Appleyard M, Simpson NA. 1994. Co-ordination of stem elongation and Zadoks growth stages with leaf emergence in wheat and barley. *The Journal of Agricultural Science* 122: 21-29.

Klepper B, Rickman RW, Peterson CM. 1982. Quantitative characterization of vegetative development in small cereal grains. *Agronomy Journal* 74: 789-792.

Lafarge T, Raïssac M, Tardieu F. 1998. Elongation rate of sorghum leaves has a common response to meristem temperature in diverse African and European environmental conditions. *Field Crops Research* 58: 69-79.

Lafarge T, Tardieu F. 2002. A model co-ordinating the elongation of all leaves of a sorghum cultivar was applied to both mediterranean and sahelian conditions. *Journal of Experimental Botany* 53: 715-725.

Lalonde S, Tegeder M, Throne-Holst M, Frommer W, Patrick J. 2003. Phloem loading and unloading of sugars and amino acids. *Plant, Cell & Environment* 26: 37-56.

Lattanzi FA. 2004. *Sources of carbon and nitrogen for leaf growth in grasses.* PhD thesis, Technical University of Munich, Munich, Germany.

Lattanzi FA, Schnyder H, Thornton B. 2005. The sources of carbon and nitrogen supplying leaf growth: assessment of the role of stores with compartmental models. *Plant Physiology* 137: 383-395.

Lea PJ, Forde BG. 1994. The use of mutants and transgenic plants to study amino acid metabolism. *Plant, Cell & Environment* 17: 541-556.

Lehmeier CA, Wild M, Schnyder H. 2013. Nitrogen stress affects the turnover and size of nitrogen pools supplying leaf growth in a grass. *Plant Physiology* 162: 2095-2105.

Lemus R, Parrish DJ, Abaye O. 2008. Nitrogen-use dynamics in switchgrass grown for biomass. *BioEnergy Research* 1: 153-162.

Li YH. 1989. Impact of grazing on *Aneurolepidium chinense* steppe and *Stipa grandis* steppe. *Acta oecologica*10: 31-46.

Li L, Nelson CJ, Solheim C, Whelan J, Millar AH. 2012. Determining degradation and synthesis rates of Arabidopsis proteins using the kinetics of progressive ^{15}N Labeling of two-dimensional gel-separated protein spots. *Molecular & Cellular Proteomics* 11: 1-16.

Liang C, Michalk DL, Millar GD. 2002. The ecology and growth patterns of *Cleistogenes* species in degraded grasslands of eastern Inner Mongolia, China. *Journal of Applied Ecology* 39: 584-594.

Liu ZL. 1963. An outline of the *Stipa* steppe in Inner Mongolia. *Acta Phytoecologica et Geobotanica Sinica* 1: 156-158.

Liu HT, Gong XY, Schäufele R, Yang F, Hirl RT, Schmidt A, Schnyder H. 2016. Nitrogen fertilization and $\delta^{18}O$ of CO_2 have no effect on ^{18}O-enrichment of leaf water and cellulose in *Cleistogenes squarrosa* (C_4) – is VPD the sole control? *Plant, Cell & Environment* 39: 2701-2712.

Longnecker N, Kirby EJM, Robson A. 1993. Leaf emergence, tiller growth, and apical development of nitrogen-dificient spring wheat. *Crop Science* 33: 154-160.

Ma Q, Longnecker N, Dracup M. 1997. Nitrogen deficiency slows leaf development and delays flowering in narrow-leafed lupin. *Annals of Botany* 79: 403-409.

MacAdam JW. 2009. *Structure and Function of Plants*. Lowa, USA: Wiley-Blackwell.

MacAdam JW, Volenec JJ, Nelson CJ. 1989. Effects of nitrogen on mesophyll cell division and epidermal cell elongation in tall fescue leaf blades. *Plant Physiology* 89: 549-556.

Mae T, Makino A, Ohira K. 1983. Changes in the amounts of ribulose bisphosphate carboxylase synthesized and degraded during the life span of rice leaf (*Oryza sativa* L.). *Plant and Cell Physiology* 24: 1079-1086.

Makino A, Osmond B. 1991. Effects of nitrogen nutrition on nitrogen partitioning between chloroplasts and mitochondria in pea and wheat. *Plant Physiology* 96: 355-362.

Malagoli P, Laine P, Rossato L, Ourry A. 2005. Dynamics of nitrogen uptake and mobilization in field-grown winter oilseed rape (*Brassica napus*) from stem extension to harvest: I. global N flows between vegetative and reproductive tissues in relation to leaf fall and their residual N. *Annals of Botany* 95: 853-861.

Martre P, Cochard H, Durand JL. 2001. Hydraulic architecture and water flow in growing grass tillers (*Festuca arundinacea* Schreb.). *Plant, Cell & Environment* 24: 65-76.

Masclaux-Daubresse C, Daniel-Vedele F, Dechorgnat J, Chardon F, Gaufichon L, Suzuki A. 2010. Nitrogen uptake, assimilation and remobilization in plants: challenges for sustainable and productive agriculture. *Annals of Botany* 105: 1141-1157.

Masclaux-Daubresse C, Reisdorf-Cren M, Orsel M. 2008. Leaf nitrogen remobilisation for plant development and grain filling. *Plant Biology* 10: 23-36.

Masclaux-Daubresse C, Valadier MH, Brugière N, Morot-Gaudry JF, Hirel B. 2000. Characterization of the sink/source transition in tobacco (*Nicotiana tabacum* L.) shoots in relation to nitrogen management and leaf senescence. *Planta* 211: 510-518.

McKenzie FR. 1998. Influence of applied nitrogen on vegetative, reproductive, and aerial tiller densities in *Lolium perenne* L. during the establishment year. *Australian Journal of Agricultural Research* 49: 707-712.

McMaster GS. 2005. Phytomers, phyllochrons, phenology and temperate cereal development. *The Journal of Agricultural Science* 143: 137-150.

McSteen P. 2009. Hormonal regulation of branching in grasses. *Plant Physiology* 149: 46-55.

Mei HS, Thimann KV. 1984. The relation between nitrogen deficiency and leaf senescence. *Physiologia Plantarum* 62: 157-161.

Metay A, Magnier J, Guilpart N, Christophe A. 2015. Nitrogen supply controls vegetative growth, biomass and nitrogen allocation for grapevine (cv. Shiraz) grown in pots. *Functional Plant Biology* 42: 105-114.

Miao H, Chen S, Chen J, Zhang W, Zhang P, Wei L, Han X, Lin G. 2009. Cultivation and grazing altered evapotranspiration and dynamics in Inner Mongolia steppes. *Agricultural and Forest Meteorology* 149: 1810-1819.

Millard P. 1988. The accumulation and storage of nitrogen by herbaceous plants. *Plant, Cell & Environment* 11: 1-8.

Monsi M, Saeki T. 2005. On the factor light in plant communities and its importance for matter production. *Annals of Botany* 95: 549-567.

Moore KJ, Moser LE. 1995. Quantifying developmental morphology of perennial grasses. *Crop Science* 35: 37-43.

Moulia B, Loup C, Chartier M, Allirand JM, Edelin C. 1999. Dynamics of architectural development of isolated plants of maize (*Zea mays* L.), in a non-limiting environment: the branching potential of modern maize. *Annals of Botany* 84: 645-656.

Murphy AT, Lewis OAM. 1987. Effect of nitrogen feeding source on the supply of nitrogen from root to shoot and the site of nitrogen assimilation in maize (*Zea Mays* L. cv. R201). *New Phytologist* 107: 327-333.

Niemann GJ, Pureveen JBM, Eijkel GB, Poorter H, Boon JJ. 1992. Differences in relative growth rate in 11 grasses correlate with differences in chemical composition as determined by pyrolysis mass spectrometry. *Oecologia* 89: 567-573.

Novitskaya L, Trevanion SJ, Driscoll S, Foyer CH, Noctor G. 2002. How does photorespiration modulate leaf amino acid contents? A dual approach through modelling and metabolite analysis. *Plant, Cell & Environment* 25: 821-835.

Ocheltree TW, Nippert JB, Prasad PVV. 2014. Stomatal responses to changes in vapor pressure deficit reflect tissue-specific differences in hydraulic conductance. *Plant, Cell & Environment* 37: 132-139.

Passioura JB, Gardner A. 1990. Control of leaf expansion in wheat seedlings growing in drying soil. *Functional Plant Biology* 17: 149-157.

Pinheiro J, Bates D, Debroy S, Sarkar D, the R Core Team. 2014. nlme: linear and nonlinear mixed effects models. R package version 3.1-118. Available at: http://CRAN.R-project.org/package=nlme.

Pons TL, van Rijnberk H, Scheurwater I, van der Werf A. 1993. Importance of the gradient in photosynthetically active radiation in a vegetation stand for leaf nitrogen allocation in two monocotyledons. *Oecologia* 95: 416-424.

Posada JM, Lechowicz MJ, Kitajima K. 2009. Optimal photosynthetic use of light by tropical tree crowns achieved by adjustment of individual leaf angles and nitrogen content. *Annals of Botany* 103: 795–805.

Pyankov VI, Gunin PD, Tsoog S, Black CC. 2000. C_4 plants in the vegetation of Mongolia: their natural occurrence and geographical distribution in relation to climate. *Oecologia* 123: 15-31.

Robinson D, Handley LL, Scrimgeour CM. 1998. A theory for $^{15}N/^{14}N$ fractionation in nitrate-grown vascular plants. *Planta* 205: 397-406.

Rossato L, Laine P, Ourry A. 2001. Nitrogen storage and remobilization in *Brassica napus* L. during the growth cycle: nitrogen fluxes within the plant and changes in soluble protein patterns. *Journal of Experimental Botany* 52: 1655-1663.

Sanetra CM, Ito O, Virmani SM, Vlek PLG. 1998. Remobilization of nitrogen from senescing leaves of pigeonpea (*Cajanus cajan* (L.) Millsp.): genotypic differences across maturity groups? *Journal of Experimental Botany* 49: 853-862.

Scheurwater I, Koren M, Lambers H, Atkin OK. 2002. The contribution of roots and shoots to whole plant nitrate reduction in fast- and slow-growing grass species. *Journal of Experimental Botany* 53: 1635-1642.

Schluter U, Mascher M, Colmsee C, Scholz U, Brautigam A, Fahnenstich H, Sonnewald U. 2012. Maize source leaf adaptation to nitrogen deficiency affects not only nitrogen and carbon metabolism but also control of phosphate homeostasis. *Plant Physiology* 160: 1384-1406.

Schmitz G, Theres K. 2005. Shoot and inflorescence branching. *Current Opinion in Plant Biology* 8: 506-511.

Schnyder H, Schäufele R, Lötscher M, Gebbing T. 2003. Disentangling CO_2 fluxes: direct measurements of mesocosm-scale natural abundance $^{13}CO_2/^{12}CO_2$ gas

exchange, ^{13}C discrimination, and labelling of CO_2 exchange flux components in controlled environments. *Plant, Cell & Environment* 26: 1863-1874.

Schobert C, Komor E. 1992. Transport of nitrate and ammonium into the phloem and the xylem of ricinus communis seedlings. *Journal of Plant Physiology* 140: 306-309.

Schulte auf'm Erley G, Ambebe TF, Worku M, Bänziger M, Horst W. 2010. Photosynthesis and leaf-nitrogen dynamics during leaf senescence of tropical maize cultivars in hydroponics in relation to N efficiency in the field. *Plant and Soil* 330: 313-328.

Shiraiwa T, Sinclair TR. 1993. Distribution of nitrogen among leaves in soybean canopies. *Crop Science* 33: 804-808.

Simpson E. 1981. Measurement of protein degradation in leaves of *Zea mays* using [^{3}H]acetic anhydride and tritiated water. *Plant Physiology* 67: 1214-1219.

Skinner RH, Moore KJ 2007. Growth and development of forage plants. In: Barnes RF, Nelson CJ, Moore KJ, Collins M, eds. *Forages, the Science of Grassland Agriculture*, 53-66.

Skinner RH, Nelson CJ. 1994. Effect of tiller trimming on phyllochron and tillering regulation during tall fescue development. *Crop Science* 34: 1267-1273.

Skinner RH, Nelson CJ. 1995. Elongation of the grass leaf and its relationship to the phyllochron. *Crop Science* 35: 4-10.

Stitt M, Müller C, Matt P, Gibon Y, Carillo P, Morcuende R, Scheible WR, Krapp A. 2002. Steps towards an integrated view of nitrogen metabolism. *Journal of Experimental Botany* 53: 959-970.

Strullu L, Cadoux S, Preudhomme M, Jeuffroy MH, Beaudoin N. 2011. Biomass production and nitrogen accumulation and remobilisation by *Miscanthus* × *giganteus* as influenced by nitrogen stocks in belowground organs. *Field Crops Research* 121: 381-391.

Su YZ, Li YL, Zhao HL. 2006. Soil properties and their spatial pattern in a degraded sandy grassland under post-grazing restoration, Inner Mongolia, Northern China. *Biogeochemistry* 79: 297-314.

Sugiharto B, Sugiyama T. 1992. Effects of nitrate and ammonium on gene expression of phosphoenolpyruvate carboxylase and nitrogen metabolism in maize leaf tissue during recovery from nitrogen stress. *Plant Physiology* 98: 1403-1408.

Suzuki Y, Makino A, Mae T. 2001. Changes in the turnover of Rubisco and levels of mRNAs of rbcL and rbcS in rice leaves from emergence to senescence. *Plant, Cell & Environment* 24: 1353-1360.

Suzuki Y, Miyamoto T, Yoshizawa R, Mae T, Makino A. 2009. Rubisco content and photosynthesis of leaves at different positions in transgenic rice with an overexpression of RBCS. *Plant, Cell & Environment* 32: 417-427.

Tamas IA 1995. Hormonal regulation of apical dominance. In: Davies PJ, eds. *Plant hormones: physiology, biochemistry and molecular biology*. Dordrecht: Springer Netherlands, 572-597.

Tang H, Liu S. 2001. The list of C_4 plants in Nei Mongol area. *Naturalium Universitatis Nei Mongol* 32.

Tardieu F, Reymond M, Hamard P, Granier C, Muller B. 2000. Spatial distributions of expansion rate, cell division rate and cell size in maize leaves: a synthesis of the effects of soil water status, evaporative demand and temperature. *Journal of Experimental Botany* 51: 1505-1514.

Terashima I, Hikosaka K. 1995. Comparative ecophysiology of leaf and canopy photosynthesis. *Plant, Cell & Environment* 18: 1111-1128.

Volenec JJ, Nelson CJ. 1983. Responses of tall fescue leaf meristems to N fertilization and harvest frequency. *Crop Science* 23: 720-724.

Vos J, Evers JB, Buck-Sorlin GH, Andrieu B, Chelle M, de Visser PHB. 2010. Functional–structural plant modelling: a new versatile tool in crop science. *Journal of Experimental Botany* 61: 2101-2115.

Vos J, van der Putten PEL. 1998. Effect of nitrogen supply on leaf growth, leaf nitrogen economy and photosynthetic capacity in potato. *Field Crops Research* 59: 63-72.

Wang SP, Wang YF. 2001. Study on over-compensation growth of *Cleistogenes squarrosa* population in Inner Mongolia Steppe. *Acta Botanica Sinica* 43: 413-418.

Wang YS. 1992. Vegetation dynamics of grazing succession in the *Stipa baicalensis* steppe in Northeastern China. *Vegetatio* 98: 83-95.

Wilhelm W, Nelson C. 1978. Leaf growth, leaf aging, and photosynthetic rate of tall fescue genotypes. *Crop Science* 18: 769-772.

Wilson RE, Laidlaw AS. 1985. The role of the sheath tube in the development of expanding leaves in perennial ryegrass. *Annals of Applied Biology* 106: 385-391.

Wittmer M, Auerswald K, Bai YF, Schäufele R, Schnyder H. 2010. Changes in the abundance of C_3/C_4 species of Inner Mongolia grassland: evidence from isotopic composition of soil and vegetation. *Global Change Biology* 16: 605-616.

Xiao X, Ojima D, Parton W, Chen Z, Chen D. 1995. Sensitivity of Inner Mongolia grasslands to climate change. *Journal of Biogeography*: 643-648.

Yang F, Gong XY, Liu HT, Schäufele R, Schnyder H. 2016. Effects of nitrogen and vapour pressure deficit on phytomer growth and development in a C_4 grass. *Annals of Botany Plants*. doi:10.1093/aobpla/plw075

Yang H, Auerswald K, Bai YF, Han XG. 2011a. Complementarity in water sources among dominant species in typical steppe ecosystems of Inner Mongolia, China. *Plant and Soil* 340: 303-313.

Yang H, Auerswald K, Bai Y, Wittmer M, Schnyder H. 2011b. Variation in carbon isotope discrimination in *Cleistogenes squarrosa* (Trin.) Keng: patterns and drivers at tiller, local, catchment, and regional scales. *Journal of Experimental Botany* 62: 4143-4152.

Yasumura Y, Hikosaka K, Hirose T. 2007. Nitrogen resorption and protein degradation during leaf senescence in *Chenopodium album* grown in different light and nitrogen conditions. *Functional Plant Biology* 34: 409-417.

Yoneyama T, Takeba G. 1984. Compartment analysis of nitrogen flows through mature leaves. *Plant and Cell Physiology* 25: 39-48.

Zhu J, Andrieu B, Vos J, van der Werf W, Fournier C, Evers JB. 2014. Towards modelling the flexible timing of shoot development: simulation of maize organogenesis based on coordination within and between phytomers. *Annals of Botany* 114: 753-762.

Zhou Z, Sun OJ, Luo ZK, Jin HM, Chen QS, Han XG. 2008. Variation in small-scale spatial heterogeneity of soil properties and vegetation with different land use in semiarid grassland ecosystem. *Plant and Soil* 310: 103-112.

Author contributions to chapter II

Hans Schnyder, Rudi Schäufele, Fang Yang, and Xiao Ying Gong designed and planned the research. Fang Yang performed the measurements, analyzed the data and wrote a first draft. All authors contributed to the discussion of the data, writing and revision.

Author contributions to chapter III

Hans Schnyder Rudi Schäufele, Xiao Ying Gong, and Fang Yang, conceived the project and research plans; Rudi Schäufele and Xiao Ying Gong supervised the experiments; Fang Yang performed most of the experiments; analyzed the data; Fang Yang wrote the article with contributions of all the authors.

Appendix 1

Supplementary figures for chapter II

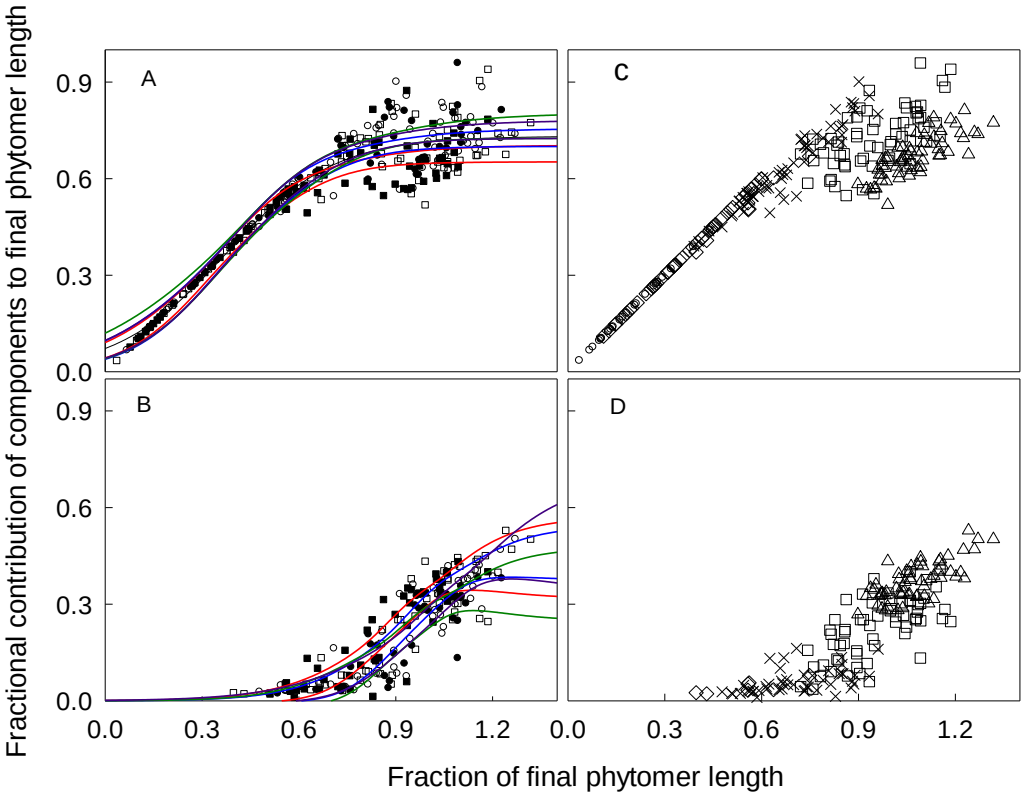

Fig. II.S1 Comparison of fractional contributions of blade (Panle A) or sheath (Panle B) to the total length of phytomers at successive stages of phytomer elongation under contrasting N fertilizer and VPD treatments. A low or high N fertilizer supply (N1 or N2) was combined with low or high VPD (V1 or V2). Panel A and B specify the data according to the treatments: closed circles with green lines, N1 V1; opened circles with purple lines, N1 V2; closed squares with red lines, N2 V1; opened squares with blue lines, N2 V2. Panel C (blade) and D (sheath) show the same data, but depict different phytomer ranks (open triangles, P_S; open squares, P_{S-1}; crosses, P_{S-2}; open diamonds, P_{S-3}; open circles, P_{S-4}). P_S indicates the phytomer that bore the youngest emerged ligule (youngest near-fully expanded phytomer with ligule visible above the surrounding leaf sheath of the next older phytomer); P_{S-1}, $P_{S-2,}$ P_{S-3} and P_{S-4} refer to progressively younger phytomers. All data were obtained from destructive measurements. Each point corresponds to a single measurement on one phytomer. Lines denote the 95% confidence bands of the fitting function.

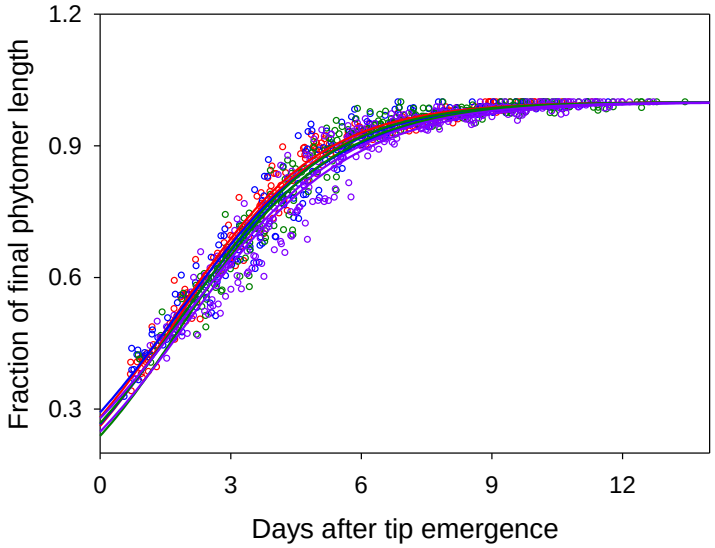

Fig. II.S2 Comparison of visible time courses of the fraction of final phytomer length under contrasting N fertilizer and VPD treatments .A low or high N fertilizer supply (N1 or N2) was combined with low or high VPD (V1 or V2). These visible time courses were established using data of phytomers on which the phytomer elongation has been measured from the time of leaf tip emergence to full elongation. Tip emergence was defined as the moment a leaf blade tip had grown past the highest visible ligule of the preceding phytomers. Sigmoidal regressions were fitted to each treatment. Lines denote the 95% confidence bands of the fitting function. Green circles with green lines, N1 V1, $y = 1/\{1 + \exp[(1.87 - x)/1.73]\}$ ($R^2 = 0.98$, $n = 27$, residual standard error = 0.03); purple circles with purple lines, N1 V2, $y = 1/\{1 + \exp[(1.94 - x)/1.90]\}$ ($R^2 = 0.97$, $n = 31$, residual standard error = 0.03); red squares with red lines, N2 V1, $y = 1/\{1 + \exp[(1.69 - x)/1.71]\}$ ($R^2 = 0.99$, $n = 25$, residual standard error = 0.03); blue squares with blue lines, N2 V2, $y = 1/\{1 + \exp[(1.73 - x)/1.82]\}$ ($R^2 = 0.98$, $n = 26$, residual standard error = 0.03). A sigmoidal regression was fitted for all data: $y = 1/\{1 + \exp[(1.79 - x)/1.81]\}$ ($R^2 = 0.96$, $n = 109$, residual standard error = 0.03).

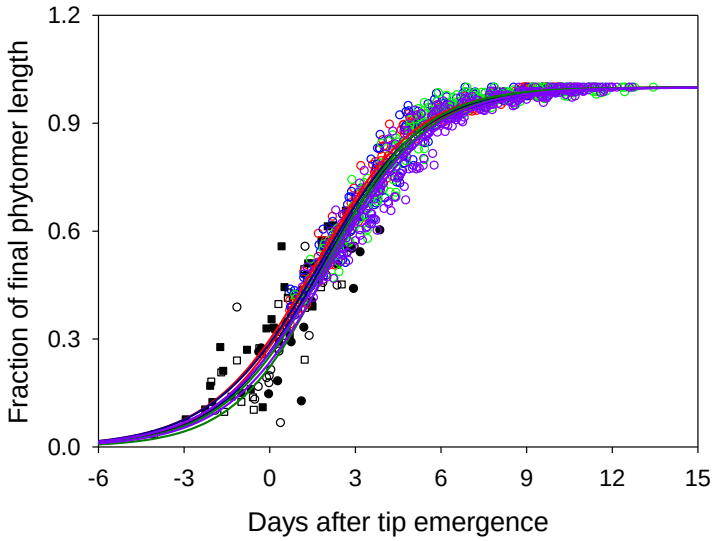

Fig. II.S3 Comparison of the complete time courses of the fraction of final phytomer length *C. squarrosa* under contrasting N fertilizer and VPD treatments. A low or high N fertilizer supply (N1 or N2) was combined with low or high VPD (V1 or V2). Colored circles represent the visible phase of the time course of phytomer development: green circles, N1 V1; purple circles, N1 V2; red circles, N2 V1; blue circles, N2 V2. Black and white symbols represent the initial phase of phytomer development based on predictions of age and the final length: closed circles, N1 V1; open circles, N1 V2; closed squares, N2 V1; open squares, N2 V2. Tip emergence was defined as the moment a leaf blade tip had grown past the highest visible ligule of the preceding phytomers. Sigmoidal functions were fitted to the complete time courses of each treatment. Lines denote the 95% confidence bands of the fitting function. Green circles with green lines, N1 V1, $y = 1/\{1 + \exp[(1.97 - x)/1.69]\}$ ($R^2 = 0.96$, residual standard error = 0.04); purple circles with purple lines, N1 V2, $y = 1/\{1 + \exp[(2.02 - x)/1.84]\}$ ($R^2 = 0.96$, residual standard error = 0.04); red squares with red lines, N2 V1, $y = 1/\{1 + \exp[(1.61 - x)/1.79]\}$ ($R^2 = 0.98$, residual standard error = 0.03); blue squares with blue lines, N2 V2, $y = 1/\{1 + \exp[(1.75 - x)/1.82]\}$ ($R^2 = 0.97$, residual standard error = 0.04).

Appendix 2

Supplementary methods for chapter IV

Fraction of tracer in the N import in immature tissue

The analysis of N supply for IMT elaborated here closely followed the principle described by Lattanzi *et al.* 2005 and Lehmeier *et al.* 2013, which addressed N fluxes in the leaf growth zone. According to N mass balance, the amount of N import into IMT was estimated as the sum of N export out of IMT plus change in IMT N mass. Tissue-bound N export out of IMT was estimated by N mass of the recently exported tissue (RET), which was leaf 2 in a tiller after one leaf appearance interval. Thus, import of N substrates into IMT can be estimated by the sum of N exported out and the variation (negative or positive) in N mass of IMT over one leaf appearance interval. This method was then developed to estimate the labeled N fluxes. This assumes all imported tracer would be present in IMT and RET by the end of the target labeling duration. This was likely true because RET contained the tissue which was produced during the labeling. On the other hand, RET was characterized by a low N turnover rate during the development stage from the IMT to MT (Mae *et al.*, 1983). Therefore, all imported tracer would be firstly deposited in IMT, and any tracer exported out of IMT would still be present in recently exported tissue. The estimation of N import into IMT is based on the condition that IMT is in a physiological steady state, where the N content of IMT is constant. Hence, N import can be equated with N export. During one leaf appearance interval, E_{imt} [μg h^{-1} $tiller^{-1}$] the N export from IMT was estimated by the N content in RET over one leaf appearance interval. Thus, N import into IMT [I_{imt}: μg h^{-1} $tiller^{-1}$] was calculated as

$$I_{imt} = E_{imt} = N_{RET}/T_e, \qquad \text{Eqn S1}$$

with N_{RET} the amount of N mass in RET, T_e the time interval between the emergence of successive leaf blades, here equaling 57.6 hours (2.4 days, Yang *et al.*, 2016).

For the amount of labeled N imported into IMT (I_{lab}) over a certain time interval, it was estimated as the sum of the export of labeled N and the variation in mass of labeled N in IMT over the time interval:

$$<I_{lab}> = <E_{lab}> + \Delta IMT_{lab}/\Delta t, \quad \text{Eqn S2}$$

where < > denotes that values were averaged over a time interval. ΔIMT_{lab} as $IMT_{lab\ \Delta t + t} - IMT_{lab\ t,}$ the mass increment of labeled N in IMT during the given interval ($\Delta t + t$ and t are the end and the beginning of the given labeling interval). E_{lab} denotes the export of labeled N in IMT ($E_{lab} = f_{lab\ E} \times E_{imt}$) over the time interval. Since I_{imt}, E_{imt}, and N_{imt} (the N mass in IMT) are constant for IMT that is in steady state, $I_{imt} = E_{imt}$ and $IMT_t = IMT_{\Delta t + t} = N_{imt}$. Thus, the fraction of tracer in the N import ($f_{lab\ I} = I_{lab} / I_{imt}$) was calculated as:

$$<f_{lab\ I}> = <f_{lab\ E}> + (f_{lab\ IMT\ \Delta t + t} - f_{lab\ IMT\ t}) \times N_{imt} / N_{RET}, \quad \text{Eqn S3}$$

Estimation of $f_{lab\ I}$ over Δt, the time interval required the estimation of (1) $f_{lab\ E}$; (2) $f_{lab\ IMT}$ at the lower (t) and upper ($\Delta t + t$) ends of the time interval. Measured $f_{lab\ E}$ in the recently produced tissue represented the average $f_{lab\ E}$ during the time interval of export from IMT. Since the estimation of N export out of IMT was based on one leaf appearance interval (2.4 d), it determined Δt, the time interval used for the estimation of $f_{lab\ I}$ was also 2.4 d. Two-parameter exponential function was fitted to the time course of $f_{lab\ IMT}$ to estimate values at t and Δt. I_{imt} was calculated by Equation 2, and N_{imt} was N mass of IMT, a measured value. The four specific 2.4–d (57.6–h) intervals over which $f_{lab\ I}$ was estimated by the four harvest dates as follows: hours -33.6 to 24, -9.6 to 48, 38.4 to 96, 110.4 to 168 for 2.4–d interval. As negative hours -33.6 and -9.6 were time when labeling did not commence, the $f_{lab\ IMT}$ was zero at these two time points.

Appendix 3

Plant, Cell & Environment

Plant Cell and Environment (2016) **39**, 2701–2712 doi: 10.1111/pce.12824

Original Article

Nitrogen fertilization and $\delta^{18}O$ of CO_2 have no effect on ^{18}O-enrichment of leaf water and cellulose in *Cleistogenes squarrosa* (C_4) – is VPD the sole control?

Hai Tao Liu, Xiao Ying Gong, Rudi Schäufele, Fang Yang, Regina Theresia Hirl, Anja Schmidt & Hans Schnyder

Lehrstuhl für Grünlandlehre, Technische Universität München, Alte Akademie 12, 85354 Freising, Germany

ABSTRACT

The oxygen isotope composition of cellulose ($\delta^{18}O_{Cel}$) archives hydrological and physiological information. Here, we assess previously unexplored direct and interactive effects of the $\delta^{18}O$ of CO_2 ($\delta^{18}O_{CO2}$), nitrogen (N) fertilizer supply and vapour pressure deficit (VPD) on $\delta^{18}O_{Cel}$, ^{18}O-enrichment of leaf water ($\Delta^{18}O_{LW}$) and cellulose ($\Delta^{18}O_{Cel}$) relative to source water, and $p_{ex}p_x$, the proportion of oxygen in cellulose that exchanged with unenriched water at the site of cellulose synthesis, in a C_4 grass (*Cleistogenes squarrosa*). $\delta^{18}O_{CO2}$ and N supply, and their interactions with VPD, had no effect on $\delta^{18}O_{Cel}$, $\Delta^{18}O_{LW}$, $\Delta^{18}O_{Cel}$ and $p_{ex}p_x$. $\Delta^{18}O_{Cel}$ and $\Delta^{18}O_{LW}$ increased with VPD, while $p_{ex}p_x$ decreased. That VPD-effect on $p_{ex}p_x$ was supported by sensitivity tests to variation of $\Delta^{18}O_{LW}$ and the equilibrium fractionation factor between carbonyl oxygen and water. N supply altered growth and morphological features, but not ^{18}O relations; conversely, VPD had no effect on growth or morphology, but controlled ^{18}O relations. The work implies that reconstructions of VPD from $\Delta^{18}O_{Cel}$ would overestimate amplitudes of VPD variation, at least in this species, if the VPD-effect on $p_{ex}p_x$ is ignored. Progress in understanding the relationship between $\Delta^{18}O_{LW}$ and $\Delta^{18}O_{Cel}$ will require separate investigations of p_{ex} and p_x and of their responses to environmental conditions.

Key-words: growth and morphology; leaf water; nitrogen fertilizer; oxygen isotopes in CO_2 and water; $p_{ex}p_x$; vapour pressure deficit.

INTRODUCTION

The oxygen isotope composition of cellulose ($\delta^{18}O_{Cel}$) is a function of environmental conditions and morpho-physiological plant traits that influence the $\delta^{18}O$ of water in chloroplasts, cellular compartments involved in the synthesis of transport sugars, stores and sink tissues where sugars are metabolized and used in cellulose synthesis (Barbour 2007; Gessler *et al.* 2014). As it contains environmental and physiological information, the $\delta^{18}O$ of cellulose is of great interest to a broad range of scientific disciplines, including palaeoecology, global change science, plant physiology and plant breeding (Roden *et al.* 2000; Barbour 2007; Farquhar *et al.* 2007; Kahmen *et al.* 2011; Xiao *et al.* 2012; Flanagan & Farquhar 2014; Gessler *et al.* 2014). Current knowledge on the relationship between $\delta^{18}O$ of cellulose and $\delta^{18}O$ of source and leaf water has been summarized in a quantitative model by Barbour & Farquhar (2000):

$$\Delta^{18}O_{Cel} = (1 - p_{ex}p_x)\,\Delta^{18}O_{LW} + \varepsilon_o \quad (1)$$

in which $\Delta^{18}O_{Cel}$ is the ^{18}O enrichment of cellulose above source water; $\Delta^{18}O_{LW}$ is the ^{18}O-enrichment of bulk leaf water above source water; $p_{ex}p_x$ is an attenuation factor – reducing the slope of the relationship between $\Delta^{18}O_{Cel}$ and $\Delta^{18}O_{LW}$ – that is determined by p_{ex}, the proportion of oxygen in cellulose that has exchanged with medium water at the site of cellulose synthesis and p_x the proportion of source water (i.e. unenriched by transpiration effects) at that site; and ε_o is the equilibrium fractionation factor between carbonyl oxygen and water. The value of ε_o has been estimated near 27‰ (Sternberg & DeNiro 1983; Sternberg *et al.* 1986), with an – (at least) partly temperature-related (Sternberg & Ellsworth 2011) – uncertainty of a few ‰ (DeNiro & Epstein 1981; Waterhouse *et al.* 2002; Ellsworth & Sternberg 2014). Equation 1 is based on the assumption that oxygen in CO_2 or in metabolic precursors of leaf sucrose – a primary photosynthetic product, common transport sugar and substrate for cellulose synthesis – exchanges with water in such a way that all oxygen in sucrose synthesized by photosynthesis in leaves is in full equilibrium with average leaf water (Cernusak *et al.* 2003a; Barbour 2007, but see also Gessler *et al.* 2013). The exchange of oxygen beween CO_2 and water is greatly accelerated by carbonic anhydrase (Gillon & Yakir 2001a, 2001b; Cousins *et al.* 2006a, 2006b). Together, these conditions imply that $\Delta^{18}O_{Cel}$ is fully independent of the oxygen isotope composition of CO_2 ($\delta^{18}O_{CO2}$). So far, direct empirical support for the absence of a significant $\delta^{18}O_{CO2}$ effect on $\Delta^{18}O_{Cel}$ was provided by a single experiment with wheat (DeNiro & Epstein 1979).

Water uptake by plants occurs with no ^{18}O fractionation, so that source water reflects the $\delta^{18}O$ at the location/soil depth of uptake (White *et al.* 1985; Ehleringer & Dawson 1992; Dawson *et al.* 1993). But leaf water becomes enriched in ^{18}O at the evaporative site in stomatal cavities (Dongmann *et al.*

Correspondence: H. Schnyder and X. Y. Gong. Fax: +49 8161713243; e-mail: schnyder@wzw.tum.de; xgong@wzw.tum.de

1974; Flanagan *et al.* 1991), and this effect propagates through leaves by diffusion of enriched water away from the evaporative sites, against the convective flux of water to the stomata (Farquhar & Lloyd 1993; Farquhar & Gan 2003). Accordingly, evaporative enrichment elevates ^{18}O in leaf water above that of source water ($\Delta^{18}O_{LW} > 0$).

The greatest uncertainty in the relationship between $\Delta^{18}O_{LW}$ and $\Delta^{18}O_{Cel}$ concerns $(1 - p_{ex}p_x)$, the extent to which the enrichment of leaf water propagates to $\Delta^{18}O_{Cel}$. Knowledge of $p_{ex}p_x$, the attenuation of that propagation, is essential for inferring evaporative conditions (which affect $\Delta^{18}O_{LW}$) from $\Delta^{18}O_{Cel}$, particularly in palaeoclimatic and -physiological reconstructions from fossil cellulose samples (e.g. Gessler *et al.* 2009; Ellsworth & Sternberg 2014). Song *et al.* (2014a) expected a potential range for $p_{ex}p_x$ between 0.1 and 0.9, based on empirical estimations of p_x in a number of species including grasses and trees (range 0.5 to 0.9), and theoretical expectations of p_{ex} (range 0.2 to 1). It is thought that p_x is close to 1 in non-transpiring tissue that is spatially separate from photosynthesizing tissue, such as stems of trees (Roden *et al.* 2000; Kahmen *et al.* 2011), while it can be much smaller than 1 inside concurrently expanding and transpiring dicot leaves (Cernusak *et al.* 2003a, 2005; Gessler *et al.* 2007; Kahmen *et al.* 2011; Song *et al.* 2014a). In C_3 and C_4 grass leaves, growth and differentiation, and associated cellulose synthesis, occur in a non-transpiring zone, which is tightly enclosed by the sheaths of the next-older leaves (Sharman 1942; Begg & Wright 1962; MacAdam & Nelson 1987, 2002; Schnyder *et al.* 1987, 1988, 1990; Bernstein *et al.* 1993; Tardieu *et al.* 2000). By using Eqn 1 and measurements of $\Delta^{18}O_{LW}$ and $\Delta^{18}O_{Cel}$, Helliker & Ehleringer (2002a) estimated p_x at 0.5 to 0.62 in 10 different grasses (including five C_3 and C_4 grasses), when p_{ex} was constrained to range between 0.4 and 0.5 and ε_o was set constant at 27‰. Concerning p_{ex}, carbohydrate metabolism along the path from source to sink, during storage/mobilization and cellulose synthesis can all lead to the formation of carbonyl groups in a certain proportion of carbon atoms, leading to exchange with local waters (Barbour & Farquhar 2000; Barbour 2007; Gessler *et al.* 2014). In particular, futile cycling of hexose through triose phosphates or turnover of non-structural carbohydrate pools may affect p_{ex} (Hill *et al.* 1995; Barbour & Farquhar 2000; Song *et al.* 2014a). Yet, in the absence of direct evidence, a value ~0.4 has often been taken as a default (e.g. Cernusak *et al.* 2005; Kahmen *et al.* 2011).

Importantly, the parameters of Eqn 1 may be controlled by different biological and environmental factors. Of all environmental factors, vapour pressure deficit (VPD) has the strongest effect on $\Delta^{18}O_{Cel}$ (Lipp *et al.* 1996; Barbour *et al.* 2002; Kahmen *et al.* 2011). This effect seems to derive virtually entirely from the VPD effect on $\Delta^{18}O_{LW}$ (Flanagan *et al.* 1991; Sheshshayee *et al.* 2005; Farquhar *et al.* 2007), as experiments with different VPDs have not reported variation of the attenuation factor in leaves of dicots and grasses (Barbour & Farquhar 2000; Helliker & Ehleringer 2002a; Song *et al.* 2014a). Temperature and relative humidity (RH) cause changes in $\Delta^{18}O_{LW}$ (Flanagan & Ehleringer 1991; Barbour & Farquhar 2000; Barbour *et al.* 2004; Song *et al.* 2014a), which are largely related to their relationship with VPD (Dongmann *et al.* 1974; Barbour 2007; Ripullone *et al.* 2008; Kahmen *et al.* 2011; Cernusak *et al.* 2016). It has also been suggested that temperature (and perhaps other factors) may affect ε_o (Sternberg & Ellsworth 2011). Different light levels did not lead to differences in $\Delta^{18}O_{LW}$ of *Ricinus communis* when VPD was controlled, but affected $\Delta^{18}O_{Cel}$ *via* the variation of $p_{ex}p_x$ (Song *et al.* 2014a). That variation was related to turnover time of non-structural carbohydrate pools and interpreted as an effect on p_{ex}. Kahmen *et al.* (2011) observed a tight relationship between modelled $p_{ex}p_x$ and specific leaf area (the inverse of leaf mass per area, LMA) of *Metrosideros polymorpha* sampled along climatic gradients. These relationships may be taken to suggest, that one should not expect simple relationships between environmental drivers and morpho-physiological controls on the relationship between $\Delta^{18}O_{LW}$ and $\Delta^{18}O_{Cel}$, and, hence, the attenuation factor.

In that context, it is remarkable that effects of nitrogen (N) nutrition on the relationship between $\Delta^{18}O_{LW}$, $\Delta^{18}O_{Cel}$ and $p_{ex}p_x$ have not been examined to date. N fertilizer supply may affect leaf thickness, leaf mass per area and interveinal distances in C_3 and C_4 grasses and other species (Bolton & Brown 1980; Jinwen *et al.* 2009; Lattanzi *et al.* 2012), parameters that were found to correlate with ^{18}O enrichment of leaf water (Helliker & Ehleringer 2000, 2002a; Farquhar & Gan 2003; Barbour *et al.* 2004) and phloem water and sugars (Barbour *et al.* 2000; Cernusak *et al.* 2003a, 2003b; Gessler *et al.* 2013). Brooks & Mitchell (2011) observed variation of $\delta^{18}O_{Cel}$ that appeared to be related to canopy microclimate effects (associated with temperature and RH) resulting from thinning and N fertilizer treatments. Further, N supply affects plant growth rate, carbohydrate pool sizes and futile cycling of carbohydrates (Stitt & Krapp 1999; Lattanzi *et al.* 2012), which might affect the attenuation factor *via* p_{ex} (Barbour & Farquhar 2000; Song *et al.* 2014a).

Given the lack of knowledge on the effects of N fertilizer supply on $\Delta^{18}O_{LW}$, $\Delta^{18}O_{Cel}$ and $p_{ex}p_x$, and possible interrelationships with VPD, we asked the following questions in experiments with a perennial C_4 grass, *C. squarrosa* (Trin.) Keng.: (1) How do N fertilizer supply and VPD affect – directly or interactively – the $\delta^{18}O_{Cel}$ and $\Delta^{18}O_{Cel}$ of leaf blades, and their relationships with $\Delta^{18}O_{LW}$ and the attenuation factor ($p_{ex}p_x$), as obtained with the Barbour & Farquhar (2000) model (Eqn 1)? (2) Can we confirm with *C. squarrosa* the observation of DeNiro & Epstein (1979) that $\delta^{18}O_{CO2}$ has no effect on the $\delta^{18}O$ of cellulose? *C. squarrosa* is a perennial C_4 grass that is endemic to the Central Asia steppe, distributed over a wide latitudinal and longitudinal (climatic) range (Clayton *et al.* 2006), co-dominant member of the 'typical steppe' of Inner Mongolia (Kang *et al.* 2007) and the most abundant member of the C_4 community that has expanded significantly in the last decades (Wittmer *et al.* 2010; Yang 2010). Question (2) seemed particularly pertinent, as *C. squarrosa* exhibited remarkably high and variable ^{13}C discrimination among leaves of different age in its natural habitats (Yang *et al.* 2011), a trait that might be related to limiting or variable carbonic anhydrase activity (Gillon & Yakir 2001b; Cousins *et al.* 2006a), potentially causing incomplete oxygen exchange between leaf water and CO_2. We also

compared the observed $\Delta^{18}O_{LW}$ of bulk leaf blade water with the Craig–Gordon predicted ^{18}O enrichment at evaporative sites ($\Delta^{18}O_e$), to assess eventual treatment effects on gradients in $\delta^{18}O$ of water at the whole leaf blade level. All experiments were performed in controlled conditions with constant air temperature (25 °C) and constant relative humidities (RH: 50% or 80%) throughout diurnal cycles. These conditions provided constant VPDs of either 1.58 kPa or 0.63 kPa.

MATERIALS AND METHODS

Experimental design

The study had a 2 × 2 factorial design, with VPD and N fertilizer supply as factors, two levels (low and high, see below) for each factor, and four replicates. Combinations of VPD and N levels were termed 'treatments': low N × low VPD (designated N1 V1), low N × high VPD (N1 V2), high N × low VPD (N2 V1) or high N × high VPD (N2 V2). Each replicate consisted of one plant stand of a certain VPD × N combination in a growth chamber. Of the four replicates of these treatments, two received CO_2 that was relatively enriched in ^{18}O, while the other two received CO_2 that was relatively depleted in ^{18}O (Table 1). The CO_2 gases were obtained from CARBO Kohlensäurewerke (Bad Hönningen, Germany) and Linde AG (Unterschleissheim, Germany).

The experiment was performed in plant growth chambers (Conviron PGR15, Conviron, Winnipeg, Canada) that formed part of (a modernized version of) the controlled environment mesocosm system described by Schnyder *et al.* (2003). That system has four chambers; thus, the treatments were distributed between four experimental runs (Table S1), so that pairs of a given treatment were supplied with either high or low $\delta^{18}O_{CO2}$ and run simultaneously. Each run accommodated treatments with high and low VPD, at a given N fertilizer supply level. High N supply treatments were assigned to runs 1 and 4, low N treatments to runs 2 and 3. Besides the treatments factors, all environmental conditions and experimental protocols were kept the same. For details of treatments and growth conditions, including environmental control, see below.

Table 1. Oxygen isotope composition of CO_2 measured at the inlet ($\delta^{18}O_{CO2\ inlet}$) and outlet of the growth chambers ($\delta^{18}O_{CO2\ outlet}$) during light periods. $\delta^{18}O_{CO2\ outlet}$ reflects the $\delta^{18}O$ of CO_2 in the well-mixed atmosphere of the growth chamber. ^{18}O-enriched and ^{18}O-depleted CO_2 were used in the different experimental runs (see experimental plan, Table S1 and Materials and Methods). Data are shown as averages of 10-day-long continuous measurements on two chambers receiving the same source CO_2 (mean ± standard error, $n = 20$). These measurements preceded the sampling of plants for leaf water and cellulose.

Exp. run	$\delta^{18}O_{CO2\ inlet}$ (‰)		$\delta^{18}O_{CO2\ outlet}$ (‰)	
	^{18}O-enriched	^{18}O-depleted	^{18}O-enriched	^{18}O-depleted
1st	−14.18 ± 0.05	−36.80 ± 0.04	−11.25 ± 0.12	−31.30 ± 0.34
2nd	−14.14 ± 0.05	−36.21 ± 0.08	−11.37 ± 0.13	−30.52 ± 0.16
3rd	−1.67 ± 0.08	−16.45 ± 0.13	−0.58 ± 0.12	−13.71 ± 0.11
4th	0.11 ± 0.29	−14.67 ± 0.20	2.21 ± 0.26	−11.69 ± 0.26

Plant material and growth conditions

Seed lots of *C. squarrosa* were collected in 2010 and 2012 in typical steppe grasslands near the Inner Mongolia Grassland Ecosystem Research Station (IMGERS, 43° 38′ N, 116° 42′ E), China. Seed lots were well mixed before seeding.

Four seeds were sown in individual tubes (4.5 cm diameter, 35 cm deep) filled with quartz sand (0.3–0.8 mm diameter). Tubes were placed in free-draining plastic boxes (length: 77 cm, width: 57 cm, depth: 30 cm) with 164 tubes in each box. Two boxes were placed in each growth chamber. The time of first watering was referred to as imbibition of seeds. Before germination, the conditions in all chambers and runs were kept the same with a VPD of 0.63 kPa. About one week after imbibition, plants were thinned to one per tube, and the designated VPD and N treatments were implemented (see below).

Light was supplied by cool white fluorescent tubes with a photosynthetic photon flux density (PPFD) of 800 μmol m^{-2} s^{-1} at canopy height during the 16 h photoperiod. During the development of canopies, irradiance at the top of the canopy was kept constant by periodic measurements with a quantum sensor (LI-190R, Li-Cor, Lincoln, Nebraska, USA) and adjustment of the distance (height) between the fluorescent tubes and the top of the canopy. Air temperature in all chambers was maintained constant at 25 °C throughout the diurnal cycles (Fig. S1).

CO_2-free, dry air (dew point < −70 °C), generated by use of a screw compressor and adsorption dryer system, was mixed with ^{18}O-enriched or ^{18}O-depleted CO_2 and water vapour, and distributed between the four chambers (Schnyder *et al.* 2003). CO_2 and water vapour concentrations in chamber air were measured by an infrared gas analyser (LI-6262, Li-Cor Inc. Lincoln, USA). CO_2 concentration in the chamber was controlled at 390 μmol mol^{-1} during the light period. Water vapour was generated from deionized water using a high-pressure air humidification system (FF4Z, Finestfog, Ottobrunn, Germany). The operation of the humidifier was controlled by humidity sensors in the growth chambers, to keep RH constant throughout the diurnal cycle at either 50% or 80%, thus providing constant VPDs of 1.58 kPa (high VPD) or 0.63 kPa (low VPD), respectively, at 25 °C (Fig. S1).

Nutrient solution was supplied three times per day by an automatic irrigation system throughout the whole experiment similar to Lehmeier *et al.* (2008). The solution contained 7.5 mM N (termed 'low N', as it limited plant growth, see below) or 22.5 mM N (high N) in the form of equimolar concentrations of calcium nitrate and potassium nitrate ($Ca(NO_3)_2$ and KNO_3). The concentration of other nutrients was the same in both nutrient solutions: 1.0 mM $MgSO_4$, 0.5 mM KH_2PO_4, 1 mM NaCl, 125 μM Fe-EDTA, 46 μM H_3BO_3, 9 μM $MnSO_4$, 1 μM $ZnSO_4$, 0.3 μM $CuSO_4$, 0.1 μM Na_2MoO_4.

Plant sampling

Separate sets of plants were sampled at intervals for the assessment of morphological parameters, joint leaf water and cellulose extraction, and determination of developmental gradients (see below). In each experiment sampling activities occurred over a period of three weeks. An average of <3% of all plants were collected from random positions in canopies on any given sampling date. On the whole, <20% of all plants were sampled until the end of an experiment.

Morphological parameters of C. squarrosa

In each experimental run, plants were sampled four or five times at 2 or 3 d intervals after canopy closure (leaf area index, LAI > 2) to determine morphological parameters. On each sampling date, four plants in each chamber were removed from random positions. From each plant, we excised two major tillers (the main tiller and another tiller, which had approximately the same length as the main tiller). Leaf blades were clipped off, counted, photographed (to measure leaf area using the Image J software, National Institutes of Health, Bethesda, Maryland, USA) and combined by position (i.e. leaf age) in one sample (Fig. S2). The remaining shoot material and roots were collected as separate samples. After weighing the fresh mass, all samples were dried in an oven at 60 °C for 48 h and weighed again. For each plant, the following parameters were obtained: number of leaf blades per major tiller, number of tillers per plant (total shoot mass divided by mean major tiller mass), mean leaf area per leaf, leaf thickness estimated as leaf fresh mass per leaf area (Arredondo & Schnyder 2003), leaf blade water content per area, leaf blade dry mass per area (LMA), tiller mass, total shoot mass and LAI (leaf area per plant times number of plants per unit ground surface area, with leaf area per plant = shoot mass × leaf area per tiller/tiller mass). Morphological parameters were calculated from those 2 d of sampling which were closest to the days of sampling for leaf water and cellulose.

Joint sampling of leaf water and cellulose

Samples for leaf blade water and cellulose extraction were collected on the 54th, 55th, 37th or 46th day after imbibition in experimental runs 1 to 4, respectively. Three plants were chosen in each chamber, successively removed from the chambers at approx. 2 h after the beginning of the light period and sampled quickly using a scalpel to minimize changes of the content and $\delta^{18}O$ of leaf water. For each plant, mature (fully expanded) blades in the upper part of the canopy were sampled (including leaf ages 1 to 5 in Fig. S2). In addition we also sampled the lower leaves. For each sample of upper or lower leaves, about 40 blades were pooled and immediately sealed in a 12 mL Exetainer vial (*Labco* Ltd, High Wycombe, UK), capped and then wrapped with Parafilm (PM996, Bemis Company, Wisconsin, USA). All vials were weighed before and after filling with leaf blades. Samples were stored in a freezer at −20 °C until cryogenic extraction of leaf water. Following leaf water extraction, the same samples were used to extract leaf blade cellulose.

Cellulose in leaf blades of different age categories

Additional samples were collected to assess potential developmental gradients, possibly related to changes in canopy microclimate, by sampling separately the different leaf age categories along tillers. These samplings occurred in two experimental runs, on the 53rd day after imbibition in the second experimental run (N1 V1, N1 V2) and the 44th day in the fourth run (N2 V1, N2 V2) (cf. Table S1). For this, eight plants were randomly chosen from each chamber, and five to eight major tillers per plant excised at the base of the shoot. Leaf age categories were numbered from the tip of the tiller (the youngest leaf) to the base (oldest) (cf. Fig. S2). To obtain sufficient material for cellulose extraction, 16 to 20 leaf blades per age category were pooled in one sample. This procedure provided three samples for each plant fraction (individual age categories of leaves) for each growth chamber.

Using knowledge of the leaf appearance interval (time interval between appearance of successive leaves: 2.4 d; Fang Yang *et al.*, unpublished data), the different leaf age categories were assigned to the respective periods of leaf production during stand growth.

Leaf water and cellulose extraction

Leaf water was extracted for 3 h using a custom-built cryogenic vacuum distillation apparatus (see description in Fig. S3). Water extraction was virtually complete, as was confirmed by the absence of weight change of the cryogenically vacuum-extracted samples in a drying oven at 40 °C for 24 h. Water samples were placed in 2 mL Eppendorf tubes and stored at −20 °C until isotope analysis.

α-cellulose was extracted from 50 mg or 25 mg of dry sample material using the procedure of Brendel *et al.* (2000) as modified by Gaudinski *et al.* (2005).

Measurement of $\delta^{18}O$ in CO_2 and vapour

The $\delta^{18}O$ of CO_2 at the inlet and outlet of the well-ventilated growth chambers was measured in a quasi-continuous manner throughout the whole experiment by on-line $^{13}C/^{12}C$- and $^{18}O/^{16}O$-CO_2 mass spectrometry, as in Schnyder *et al.* (2003, 2004).

In experimental runs 1, 3 and 4, the $\delta^{18}O$ of vapour in the growth chambers ($\delta^{18}O_v$) was measured on-line by Cavity Ring-Down Spectroscopy (CRDS, L2120-I, Picarro, California, USA) one day before sampling leaves for leaf water ^{18}O analysis. Measurement started 2 h after the beginning of the light period. Values of measured $\delta^{18}O_v$ were stored when the reading of the vapour concentration measured by the CRDS became stable. In the second experimental run, water vapour in growth chambers was sampled above the canopy by drawing air through a glass trap submerged in a mixture of ethanol and dry ice for 2 h using a pump. Vapour collection started 2 h after the beginning of the light period. $\delta^{18}O_v$ did not differ significantly between growth chambers and treatments, and averaged −13.0‰ (±0.6‰ standard error, $n = 16$). The flux of vapour from transpiration was, under our

experimental conditions, proportionally minor compared to the flux of inlet vapour.

Oxygen isotope analysis of leaf water, nutrient solution and biomass samples

Oxygen isotope composition was expressed in per mil (‰) as

$$\delta^{18}O = \left(\frac{R_{sample}}{R_{standard}} - 1\right) \times 1000 \quad (2)$$

where R_{sample} and $R_{standard}$ are the $^{18}O/^{16}O$ ratios of the sample and the Vienna Standard Mean Ocean Water standard (V-SMOW), respectively.

$\delta^{18}O$ of water samples (leaf water, collected vapour or nutrient solution) was analysed on 300 μL aliquots using the CRDS analyser coupled to an A0211 high precision vaporizer set at 110 °C (Picarro Inc., Sunnyvale, Ca, USA). Each sample was measured repeatedly (five to twelve injections of each 1 μL, depending on memory effects of successive samples differing in isotopic composition) and the results of the last two measurements averaged. Post-processing correction was applied by running the ChemCorrect™ v1.2.0 software (Picarro Inc.) to eliminate the influence of volatiles according to Martín-Gómez *et al.* (2015). However, no sample was flagged as 'possibly contaminated' or 'bad'. After every 20 to 25 samples, two laboratory water standards that spanned the range of the isotopic compositions of samples ($\delta^{18}O$ +13.1‰ and −21.2‰, respectively) were run for possible drift correction and normalizing results to the SMOW-scale. The laboratory standards were previously calibrated against V-SMOW, V-GISP and V-SLAP (from IAEA) using the same analytical procedure as used in sample analysis. Analytical uncertainty (the SD for repeated measurements) for $\delta^{18}O$ was ±0.1‰.

Cellulose samples were re-dried at 40 °C for 24 h, 700 μg aliquots packed in silver cups (size: 3.3 × 5 mm, LüdiSwiss, Flawil, Switzerland) and stored above Silica Gel orange (2–5 mm, ThoMar OHG, Lütau, Germany) in exsiccator vessels. For ^{18}O analysis, samples were pyrolysed at 1400 °C in a pyrolysis oven (HTO, HEKAtech, Wegberg, Germany), equipped with a helium-flushed zero blank auto-sampler (Costech Analytical technologies, Valencia, CA, USA) and interfaced (ConFlo III, Finnigan MAT, Bremen, Germany) to a continuous-flow isotope ratio mass spectrometer (Delta Plus, Finnigan MAT). Solid internal laboratory standards (SILS, cotton powder) were run as a control after every fifth sample. All samples and SILS were measured against a laboratory working standard carbon monoxide gas, which was previously calibrated against a secondary isotope standard (IAEA-601). The long-term precision for the internal laboratory standards was better than 0.3‰ (SD for repeated measurements).

^{18}O enrichment of leaf blade water above source water ($\Delta^{18}O_{LW}$) was calculated as:

$$\Delta^{18}O_{LW} = \frac{\delta^{18}O_{LW} - \delta^{18}O_{SW}}{1 + \delta^{18}O_{SW}/1000}, \quad (3)$$

with $\delta^{18}O_{LW}$, the $\delta^{18}O$ of leaf blade water and $\delta^{18}O_{SW}$ that of the nutrient solution. ^{18}O enrichment of leaf blade cellulose above source water ($\Delta^{18}O_{Cel}$) was calculated accordingly, using $\delta^{18}O_{SW}$ and $\delta^{18}O_{Cel}$ data. The $\delta^{18}O$ of the nutrient solution – the sole source of water for uptake by roots – increased from −8.8 to −8.2‰, at a rate of 0.028‰ d^{-1} ($R^2 = 0.84$) during the experimental period, that is the period of growth and differentiation of all leaves collected in an experimental run. This effect was accounted for in the estimation of source water isotope composition at various times using the regression of the $\delta^{18}O$ of the nutrient solution versus time in the experiment.

The enrichment of evaporative site water above source water ($\Delta^{18}O_e$) was calculated using the precise version of the Craig–Gordon model as provided by Farquhar *et al.* (2007):

$$\Delta^{18}O_e = (1 + \varepsilon^+)[(1 + \varepsilon_k)(1 - w_a/w_i) + w_a/w_i(1 + \Delta_v)] - 1 \quad (4)$$

where w_a/w_i is the ratio of water vapour mole fraction in the air to that in the intercellular air space, ε^+ is the equilibrium ^{18}O fractionation between liquid water and vapour, ε_k is the kinetic ^{18}O fractionation for combined diffusion through the stomata and the boundary layer and Δ_v is the ^{18}O enrichment of vapour (the measurement of $\delta^{18}O_v$ was described above) compared to source water. ε^+ and ε_k were calculated using equations in Cernusak *et al.* (2016). w_a/w_i was calculated from air temperature and RH in the growth chamber and the leaf temperature, measured by six thermocouples placed in the top 10 cm of the canopy evenly distributed across each chamber.

Data analysis

For analysis of variance (ANOVA), we used the general linear model of SAS (SAS 9.1, SAS Institute, USA). Firstly, three-way ANOVA was used to test the effects of $\delta^{18}O_{CO2}$, N supply, VPD and their interactions on $\Delta^{18}O_{Cel}$ of leaf blades in the upper canopy. In those tests means of subsamples from each chamber were used as replicates ($n = 2$). Because of the non-significant effect of $\delta^{18}O_{CO2}$ on $\Delta^{18}O_{Cel}$, we combined replicates with ^{18}O-enriched and ^{18}O-depleted CO_2 by VPD × N treatment for the subsequent statistical analysis by a two-way ANOVA. This tested the effects of N supply, VPD and their interactions on morphological parameters, $\Delta^{18}O_{LW}$, $\Delta^{18}O_e$, $\Delta^{18}O_{Cel}$ and $p_{ex}p_x$. This ANOVA used means of subsamples from the same chamber, meaning that the number of true independent replicates was four. $p_{ex}p_x$ of each treatment was calculated according to Eqn 1, using the $\Delta^{18}O_{LW}$ and $\Delta^{18}O_{Cel}$ data of upper canopy leaves and assuming a ε_o of 27‰ (unless indicated otherwise). Absolute growth rate of *C. squarrosa* was determined as the slope of a linear regression between plant dry mass and days after imbibition. Effects of N supply and VPD on growth rate were assessed by comparing confidence intervals of the slope estimates. In addition, we performed sensitivity tests of N and VPD and interactive effects of N and VPD on the $p_{ex}p_x$ by varying ε_o between 24‰ and 30‰ or $\delta^{18}O_{LW}$ in a range of ±1.3‰ around the measured value. In the latter sensitivity tests, ε_o was fixed at 27‰.

RESULTS

The effect of oxygen isotope composition of CO_2 on $\delta^{18}O$ of cellulose

Mesocosm-scale on-line $C^{18}OO/C^{16}O_2$ gas exchange measurements (performed on established plant stands between 5 and 8 weeks after imbibition of seed) demonstrated that the $\delta^{18}O_{CO2}$ of the ^{18}O-enriched and ^{18}O-depleted CO_2 sources differed consistently in each experimental run (Table 1). That difference in $\delta^{18}O_{CO2}$ amounted to approx. 20‰ in the first and second experimental run and 13‰ in the third and fourth experimental run, when comparing measurements taken at the outlet of the rapidly ventilated chambers (Table 1). When measured at the inlet of the chamber, those differences were even larger (Table 1, also see Materials and Methods), but exchange with (plant or other) water pools in the chambers caused partial convergence of the $\delta^{18}O_{CO2}$ of the ^{18}O-enriched and ^{18}O-depleted CO_2 sources.

Three-way ANOVA of the effects of $\delta^{18}O_{CO2}$, N fertilizer supply, VPD and their interactions revealed no statistically significant direct or interactive effect of $\delta^{18}O_{CO2}$ on $\Delta^{18}O_{Cel}$ of leaf blades (Table 2). Along the same line, the $\delta^{18}O_{Cel}$ in the parallel growth chambers with different $\delta^{18}O_{CO2}$ in the same VPD and N treatment were virtually indistinguishable. There was a mean, but non-significant, offset of +0.37‰ for $\delta^{18}O_{Cel}$ of leaves grown in the presence of the ^{18}O-enriched CO_2 source relative to that of the depleted source, and a mean absolute difference of 0.76‰ for the match of $\delta^{18}O_{Cel}$ produced in the presence of ^{18}O-enriched or ^{18}O-depleted CO_2 (Fig. 1). The offset of +0.37‰ would have meant a 2.4% contribution of the original oxygen in CO_2 to the total oxygen in cellulose, given that the leaf water $\delta^{18}O$ was unchanged by the CO_2. Indeed, $\Delta^{18}O_{LW}$ did not differ significantly between chambers receiving CO_2 with different $\delta^{18}O_{CO2}$ ($\Delta^{18}O_{LW}$ differed by +0.35 ± 1.2‰ SE between chambers receiving ^{18}O-enriched and -depleted CO_2). The absence of a significant divergence of leaf water isotope composition in chambers receiving CO_2 from the different sources was also expected from isotopic mass balances considering oxygen fluxes connected with CO_2 assimilation, transpiration and invasion/retrodiffusion fluxes of CO_2 and water vapour in leaves. So, as $\delta^{18}O_{CO2}$ had no effect on any of the relationships analysed in this work, the replicates of the ^{18}O-enriched and ^{18}O-depleted CO_2 environments were combined by VPD and N treatment for the subsequent analyses.

Table 2. Results of a three-way ANOVA testing the effect of $\delta^{18}O_{CO2}$, N supply, VPD and their interactions on $\Delta^{18}O_{Cel}$ of leaf blades in the upper canopy. Significance levels: ns, not significant ($P > 0.05$); **, $P < 0.01$. For each combination of treatments, the number of replicates was two with each chamber as one replicate. Cellulose was obtained from the same materials as used to extract leaf water.

Treatment	DF	Significance
$\delta^{18}O_{CO2}$	1	ns
N	1	ns
VPD	1	**
$\delta^{18}O_{CO2} \times N$	1	ns
$\delta^{18}O_{CO2} \times VPD$	1	ns
$N \times VPD$	1	ns
$\delta^{18}O_{CO2} \times N \times VPD$	1	ns
Total	18	

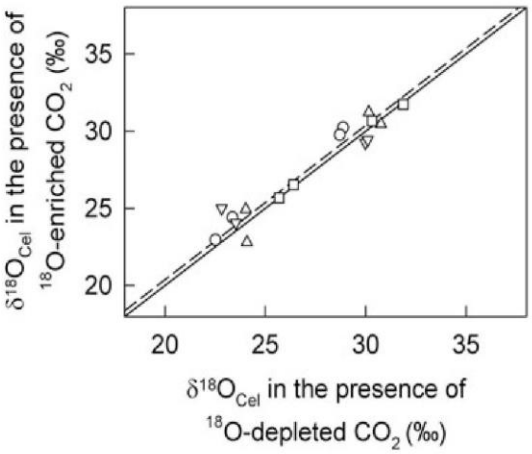

Figure 1. $\delta^{18}O_{Cel}$ of leaf blades grown in the presence of ^{18}O-enriched CO_2 (y-axis) *versus* ^{18}O-depleted CO_2 (x-axis). The two CO_2 sources were used in parallel that is in two growth chambers of the same treatment in the same experimental run (Table S1), with $\delta^{18}O$ of CO_2 as shown in Table 1. The solid line gives the 1:1 relationship; the dashed line is a linear regression line: $\delta^{18}O_{Cel\_E} = \delta^{18}O_{Cel\_D} + 0.37$, with subscript E denoting ^{18}O-enriched and D denoting ^{18}O-depleted CO_2, which did not differ significantly from the 1:1 relationship. The mean absolute difference for the match of $\delta^{18}O_{Cel\_E}$ and $\delta^{18}O_{Cel\_D}$ was 0.76‰ (±0.15‰ standard error) and is based on the comparison of three samples collected both in the upper and lower canopy section in each chamber. Variation of $\delta^{18}O_{Cel}$ was associated with different VPD treatments. Samples from the different runs are designated as: first run, up-pointing triangles; second run, circles; third run, down-pointing triangles, and fourth run, squares.

N fertilizer and VPD effects on plant growth, morphology and $\delta^{18}O$ of leaf blade cellulose

In all treatments, plant dry mass increased near-linearly with time after canopy closure at around 35 d after imbibition (Fig. 2a,b). This indicated that plants exhibited an approx. constant growth rate, in agreement with the 'grand period' of plant growth in a closed canopy (Loomis & Connor 1992).

As expected, N supply had a significant effect on growth, with growth rates of 0.11 (±0.02 confidence interval) g d^{-1} $plant^{-1}$ at low N and 0.16 ± 0.03 g d^{-1} $plant^{-1}$ at high N, demonstrating a clear N limitation for the low N plants. Accordingly, plants grown at high N had higher nitrogen nutrition index (determined from N content and aboveground standing biomass of each stand according to Lemaire *et al.* 2008) of 1.3 ± 0.04 than that of plants grown at low N (0.80 ± 0.02, $n = 8$, averaged over VPD levels). Furthermore, N content of fully expanded young leaves of plants grown at high N (3.0 ± 0.1% DM) was significantly higher than that of low N plants (2.4 ± 0.1% DM), while VPD and its interaction with N supply had no significant effect on leaf N content per DM ($P > 0.05$).

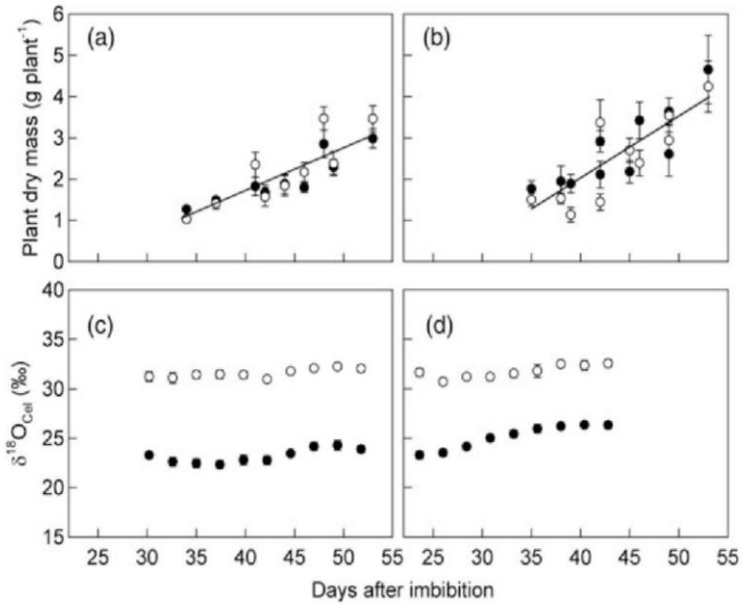

Figure 2. Treatment effects on (a, b) plant growth and (c, d) $\delta^{18}O_{Cel}$ of successively produced leaves in *C. squarrosa*. (a, c), low N; (b, d), high N fertilizer supply. Closed circles: low VPD; open circles: high VPD. Growth rate was determined as the slope of a linear regression in (a) and (b). VPD had no effect on plant growth; therefore, VPD treatments were combined by N supply level for subsequent regression analysis. The linear regression in (a): $y = 0.11\ x - 2.51$, $R^2 = 0.74$; in (b): $y = 0.16\ x - 3.96$, $R^2 = 0.70$. The confidence interval for the slope of the regression line in (a) was 0.11 ± 0.02 (low N), in (b) was 0.16 ± 0.03 g day^{-1} (high N). Each data point and error bar in (a) and (b) represent the mean and standard error of eight plants harvested on the same day. Data in (c) and (d) were obtained from two replicate chambers of each treatment in the second (low N) and fourth experimental run (high N). Major tillers were sampled on the 53rd and 44th day after imbibition of seeds in the second and fourth run, dissected by leaf age category (cf. Materials and Methods, and Fig. S2) and $\delta^{18}O_{Cel}$ determined for each leaf age class. In (c, d), the $\delta^{18}O_{Cel}$ data are reported for the time when the different leaf age categories reached full expansion, using knowledge of leaf appearance interval. Each data point and error bar in (c) and (d) represent the mean ± standard error of six individual plants ($n = 6$).

N content per leaf area was not significantly different between treatments ($P > 0.05$, 1.4 ± 0.1 g m^{-2}, averaged over treatments). High N stimulated plant growth by 45% (relative to low N), increased shoot weight per plant by 42% and enhanced LAI by 53% (Table 3). Greater LAI resulted from greater tiller production (+33%) and, to a lesser extent, individual leaf area (+16%). In addition, high N supply caused a small decrease of LMA (−9%). Apart from these, N supply had no significant effect on morphological parameters: leaf number per tiller, leaf thickness and individual tiller weight. On the other hand, growth rates under low and high VPD did not differ significantly ($P > 0.05$), as indicated by the 95% confidence intervals of the growth rates of the high and low VPD treatments. In addition, VPD (and its interaction

Table 3. Leaf, tiller, plant and canopy parameters of *C. squarrosa* stands grown at low or high N fertilizer supply (N1 or N2) combined with low or high VPD (V1 or V2) in growth chambers. All treatments (N × V combinations) had four true replications and were arranged in four growth chambers in four successive experimental runs (see Table S1). The data of a given replicate is the mean of the data collected in the last two sampling events (see Materials and Methods) of each experimental run: day 49 and 53 after imbibition of seeds in the first (N2 V1 and N2 V2) and second run (N1V1 and N1V2), day 44 and 48 after imbibition in the third run (N1 V1 and N1 V2), and day 45 and 49 after imbibition in the fourth run (N2 V1 and N2 V2). The effects of N and VPD on the different parameters were tested by a two-way ANOVA. Significance levels: ns, not significant; *, $P < 0.05$; **, $P < 0.01$. Values are means ± standard errors ($n = 4$, with each chamber as one replicate).

	Treatment				Significance		
Parameter	N1 V1	N1 V2	N2 V1	N2 V2	N	VPD	N × VPD
Number of leaves tiller^{-1}	11.9 ± 0.4	12.1 ± 0.2	12.0 ± 0.3	12.2 ± 0.2	ns	ns	ns
Number of tillers plant^{-1}	5.8 ± 0.3	7.0 ± 0.3	8.4 ± 0.7	8.6 ± 0.5	**	ns	ns
Individual leaf area (cm^2 leaf^{-1})	2.5 ± 0.1	2.6 ± 0.1	3.1 ± 0.1	2.8 ± 0.1	**	ns	ns
Leaf thickness (μm)	108 ± 3	111 ± 3	110 ± 3	111 ± 1	ns	ns	ns
Leaf blade dry mass per area (LMA, mg cm^{-2})	4.4 ± 0.2	4.2 ± 0.2	3.8 ± 0.2	4.1 ± 0.1	*	ns	ns
Leaf area index (LAI, m^2 m^{-2})	3.6 ± 0.3	4.7 ± 0.2	6.5 ± 0.7	6.2 ± 0.4	**	ns	ns
Tiller dry weight (mg tiller^{-1})	299 ± 9	306 ± 7	317 ± 19	313 ± 13	ns	ns	ns
Shoot dry weight (g plant^{-1})	1.7 ± 0.1	2.1 ± 0.0	2.7 ± 0.2	2.7 ± 0.0	**	ns	ns

with N supply) had no significant effect on any of the morphological variables in Table 3.

The effects of N supply and VPD level on growth and morphology were contrasted by their effects on $\delta^{18}O_{Cel}$ of the successively formed leaf blades: $\delta^{18}O_{Cel}$ was unaffected by N supply, while VPD had a strong effect. Within a treatment, $\delta^{18}O_{Cel}$ of the successively formed leaf blades was nearly constant, except for the low VPD treatment at high N (Fig. 2c,d), for which $\delta^{18}O_{Cel}$ increased somewhat in the period before canopy closure (35 d after imbibition of seed).

The relative constancy of $\delta^{18}O_{Cel}$ after canopy closure was likely related to (1) the near-constant environmental conditions in the growth chambers; (2) the fact that successive leaf growth and associated cellulose synthesis occur at the tip of the grass tiller, at the top of the canopy, where environmental conditions (such as humidity and light) are unaltered by canopy effects; and (3) the substrate for cellulose synthesis is mainly assimilated in the young and (mostly) unshaded leaves at the top of the canopy (Ryle & Powell 1974; Dale 1985, 1988).

The effects of nitrogen supply and VPD on $\Delta^{18}O_{LW}$, $\Delta^{18}O_e$, $\Delta^{18}O_{Cel}$ and $p_{ex}p_x$

In line with the absence of an effect on $\delta^{18}O_{Cel}$, N supply had no effect on $\Delta^{18}O_{LW}$, $\Delta^{18}O_{Cel}$ or $p_{ex}p_x$ (Fig. 3). In the same way, N supply did not affect $\Delta^{18}O_e$ ($P > 0.05$), which was 2.4‰ higher than $\Delta^{18}O_{LW}$ on average of all treatments (see Fig. 4). Meanwhile, high VPD increased $\Delta^{18}O_{LW}$ by 6.5‰ and $\Delta^{18}O_{Cel}$ by 5.8‰ in comparison with low VPD (average of both N treatments) (Fig. 3). Moreover, high VPD increased $\Delta^{18}O_e$ by 10.0‰ in comparison with low VPD ($P < 0.05$), and interaction between VPD and N supply had no effect on $\Delta^{18}O_e$ (Fig. 4). Further, the difference between $\Delta^{18}O_e$ and $\Delta^{18}O_{LW}$ was increased strongly by VPD (+0.6‰ at low VPD and 4.1‰ at high VPD, on average of the N treatments; Fig. 4).

The $p_{ex}p_x$, calculated with Eqn 1 in assuming an ε_o of 27‰, ranged between 0.34 and 0.53 in the different treatments, and was significantly lower at high than at low VPD (Fig. 3c). This VPD effect on $p_{ex}p_x$ was also evident with the cellulose data from the youngest leaves that were growing at the time of leaf water sampling (cf. Fig. 2c,d). Moreover, the significance of the VPD effect on $p_{ex}p_x$ was supported by a sensitivity analysis with ε_o values ranging between 25‰ and 30‰ (Fig. S4), encompassing largely the range of suggested plausible variation of ε_o (Ellsworth & Sternberg 2014; Song *et al.* 2014a). The VPD effect on $p_{ex}p_x$ only became non-significant for $\varepsilon_o \leq 24$‰. Additionally, a sensitivity analysis that varied $\Delta^{18}O_{LW}$ by ±1.3‰ (that is ± 20% of the measured difference between $\Delta^{18}O_{LW}$ at high and low VPD) also generally supported the significance of the VPD effect on $p_{ex}p_x$ (Fig. S5).

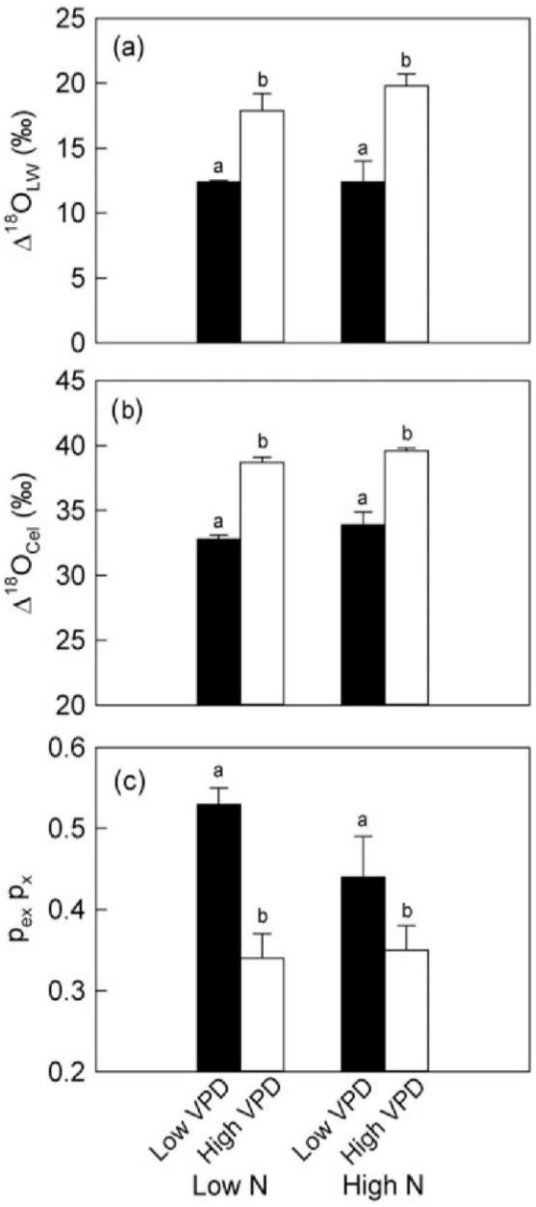

Figure 3. The effects of VPD and nitrogen fertilizer supply (N) on (a) ^{18}O-enrichment of leaf water ($\Delta^{18}O_{LW}$, ‰), (b) ^{18}O-enrichment of leaf blade cellulose ($\Delta^{18}O_{Cel}$, ‰) and (c) $p_{ex}p_x$, estimated using $\varepsilon_o = 27$‰ (cf. Eqn 1) in *C. squarrosa* stands under low VPD (black bars) and high VPD (empty bars) with low and high N supply levels. Samples were collected on the 54th, 55th, 37th and 46th day following imbibition of seeds in the first, second, third and fourth experimental run, respectively. Values are means ± standard error ($n = 4$, with each chamber as one replicate). Letters above bars indicate the results of a two-way ANOVA: effects of VPD on $\Delta^{18}O_{LW}$, $\Delta^{18}O_{Cel}$ and $p_{ex}p_x$ were highly significant ($P < 0.01$); effects of N supply (and of its interaction with VPD) on $\Delta^{18}O_{LW}$, $\Delta^{18}O_{Cel}$ and $p_{ex}p_x$ were not significant ($P > 0.05$).

DISCUSSION

Oxygen isotope composition of CO_2 has no effect on $\delta^{18}O$ of cellulose

The $\delta^{18}O$ of CO_2 had no effect on the $\delta^{18}O_{Cel}$ in this C_4 grass, validating the finding of DeNiro & Epstein (1979) with wheat,

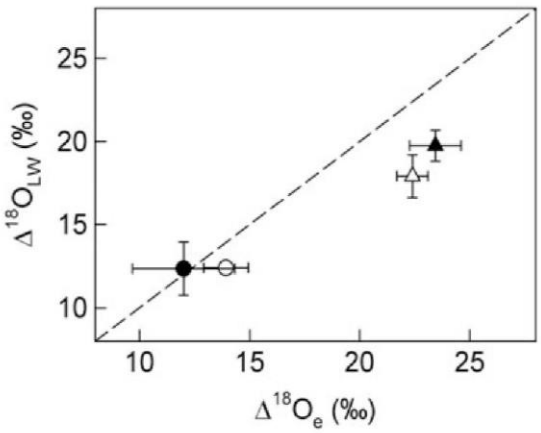

Figure 4. Relationship between observed values of $\Delta^{18}O_{LW}$, measured for bulk leaf blade water, and Craig–Gordon modelled evaporative site ^{18}O-enrichment, $\Delta^{18}O_e$, under low VPD with low nitrogen (empty circle) and high nitrogen supply (filled circle), and under high VPD with low nitrogen (empty triangle) and high nitrogen supply (filled triangle). Each value is presented as the mean ± standard error ($n = 4$). The dashed line represents the 1:1 relationship. Results of two-way ANOVA showed that high VPD significantly increased $\Delta^{18}O_e$ ($P < 0.05$), while N supply and its interaction with VPD had no effect ($P > 0.05$).

a C_3 grass, and providing support for Eqn 1 as a valid mechanistic representation of the factors determining $\Delta^{18}O_{Cel}$. Although biochemical and physiological reasoning has long supported a (near-)complete exchange of oxygen between water and CO_2 or carbonyl oxygen of metabolic intermediates of sugars in leaves, during transport and storage metabolism, and in sink tissue (Sternberg *et al.* 1986; Farquhar *et al.* 1998; Schmidt *et al.* 2001; Song *et al.* 2014b), this is the first experimental assessment of a $\delta^{18}O_{CO2}$ effect on $\delta^{18}O$ of cellulose in a C_4 plant species, and the first verification of the reported absence of such an effect by DeNiro & Epstein (1979). The absence of a significant effect of $\delta^{18}O_{CO2}$ on $\delta^{18}O_{Cel}$ means that carbonic anhydrase activity of *C. squarrosa* was non-limiting or that any limitation in catalysing the exchange of oxygen between leaf water and CO_2/HCO_3^- was overcome by subsequent exchange between water and carbonyl oxygen groups formed during (photosynthetic) reductive pentose phosphate cycle, metabolism of carbohydrates in source leaves, transport and metabolism at the sites of cellulose synthesis (DeNiro & Epstein 1979; Sternberg *et al.* 1986; Hill *et al.* 1995; Farquhar *et al.* 1998; Schmidt *et al.* 2001) in the leaf growth and differentiation zones.

N fertilizer supply had no effect on $\delta^{18}O$ of leaf blade cellulose

N fertilizer supply – and its interaction with VPD – had no significant effect on $\delta^{18}O_{Cel}$, $\Delta^{18}O_{LW}$, $\Delta^{18}O_e$, $\Delta^{18}O_{Cel}$ and $p_{ex}p_x$. This is not a trivial result, given that the effects of N fertilizer supply on the growth and morphology of *C. squarrosa* were typical for effects of N fertilizer supply on growth and development of grass plants and canopies (Cruz & Boval 2000; Gastal & Lemaire 2002), and produced strong effects on plant growth, tillering/branching and LAI. Importantly, however, N fertilizer effects on individual leaf parameters were relatively small (individual leaf area, LMA and N content per DM) or non-existent (leaf thickness, N content per unit area).

A similar analysis of N fertilizer effects on $\Delta^{18}O_{LW}$, $\Delta^{18}O_{Cel}$ and $p_{ex}p_x$ has not been performed previously, restricting somewhat opportunities for discussion of mechanisms. Absence of a significant N supply effect on $\Delta^{18}O_{LW}$ was likely related to weak (or non-existent) effects on leaf morphological parameters and N content per unit area, and lack of a N effect on stomatal conductance and transpiration rates (Xiao Ying Gong *et al.*, unpublished data). Importantly as well, $\Delta^{18}O_e$, estimated by the Craig–Gordon model (Craig & Gordon 1965; Dongmann *et al.* 1974; Flanagan *et al.* 1991; Farquhar & Lloyd 1993; Cernusak *et al.* 2016), did not differ significantly between the N levels and (on average of the two VPDs) was 2.4‰ more enriched than bulk leaf blade water (Fig. 4). Certainly, our finding of the absence of a N effect on $\Delta^{18}O_{LW}$, $\Delta^{18}O_{Cel}$ and $p_{ex}p_x$ should be verified with other species and greater contrasts of N fertilizer supply.

A similar overestimation of $\Delta^{18}O_{LW}$ by $\Delta^{18}O_e$ in C_4 grasses was noted by Webb & Longstaffe (2003) and Gan *et al.* (2003) and in a wide range of (other) taxa (Cernusak *et al.* 2016), but differs from the findings of Helliker & Ehleringer (2000), perhaps because of species differences and variation of transpiration along the leaf (Gan *et al.* 2003). Absence of a N effect on $\Delta^{18}O_{LW}$ and $\Delta^{18}O_e$ is consistent with similar fluxes of xylem water through the (enclosed) sheath towards the exposed leaf blade, similar gradients of leaf water isotope composition between the xylem and evaporative sites (although we did not assess the spatial gradients of leaf $\Delta^{18}O_{LW}$ and $\Delta^{18}O_e$ along the length of the leaf; cf. Helliker & Ehleringer 2000), and analogous turnover of leaf water pools, in plants grown with different supplies of N fertilizer. Assuming the same relationships existed in growing leaves, one would thus expect that these processes bring about a similar p_x in the leaf growth and differentiation zone where cellulose is synthesized, and – as $p_{ex}p_x$ was unaltered by N – a similar p_{ex}, supporting the parsimonious hypothesis.

VPD affected $p_{ex}p_x$, the extent to which the effect of leaf water on $^{18}O_{Cel}$ is attenuated by source water

The VPD effect on $\delta^{18}O_{Cel}$, $\Delta^{18}O_{LW}$ and $\Delta^{18}O_{Cel}$ seen here was comparable with that reported by Helliker & Ehleringer (2002a) with a range of C_3 and C_4 grasses. In addition, in close agreement with a synthesis of previous works in many, mainly woody taxa (Cernusak *et al.* 2016), the proportional difference between $\Delta^{18}O_e$ and $\Delta^{18}O_{LW}$ (i.e. $1 - \Delta^{18}O_{LW}/\Delta^{18}O_e$) averaged 0.09 in our works. VPD affected the proportional difference, which was −0.01 at low VPD and 0.18 at high VPD. Unfortunately, we were unable to measure transpiration of the leaves that we sampled for water extraction, but calculations using transpiration measurements on a smaller set of leaves measured in parallel with a clamp-on leaf chamber (Xiao Ying

Gong *et al.*, unpublished data) and the leaf water isotope data suggested that high VPD elevated the Péclet number (0.38, relative to 0.27 at low VPD; $P < 0.05$), but had no significant impact on effective path length (41 mm on average of all treatments), consistent with observations and reasoning by Loucos *et al.* (2015). The observed effects of VPD on $\Delta^{18}O_{LW}$ and $\Delta^{18}O_{Cel}$ were also similar to those observed in other species and taxonomic groups (Barbour & Farquhar 2000; Helliker & Ehleringer 2002a, 2002b; Song *et al.* 2014a; Cernusak *et al.* 2016) and independent of N fertilizer supply.

Remarkably, we noted a significant effect of VPD on $p_{ex}p_x$. This effect meant that the slope of the relationship between $\Delta^{18}O_{Cel}$ and $\Delta^{18}O_{LW}$ became steeper (that is less attenuated) with increasing VPD, implying that VPD fluctuations estimated from fluctuations of $\Delta^{18}O_{Cel}$ would underestimate the amplitude of the fluctuation if the VPD effect on $p_{ex}p_x$ was not accounted for. To our best knowledge, such an effect has not been discussed previously. However, analysis of the original data of Helliker & Ehleringer (2002a) – who reported on five C_3 and five C_4 grasses exposed to different RHs – also provides some indications for a similar VPD effect on the attenuation factor for the range of RH explored in our work. In their work, the calculated attenuation factor was lower at high VPD (low RH) than at low VPD (medium RH in their study) in 8 out of 10 cases, when the data were evaluated with the Barbour & Farquhar (2000) model using a ε_o of 27‰. If ε_o was set at 28‰, all 10 species had a lower attenuation factor at the high VPD level, similar to our work.

Conclusions and open questions

A certain limitation of this work is that the components of the attenuation factor, the factors p_{ex} and p_x, could not be determined directly. Estimation of p_x, the proportion of unenriched water at the site of cellulose synthesis, requires knowledge of $\Delta^{18}O$ of water in the leaf growth and differentiation zone ($\Delta^{18}O_{LGDZ}$) where primary and secondary cell wall deposition and associated cellulose synthesis occur. During leaf growth and development, that zone (LGDZ) extends between the base of the growing leaf (near the point of attachment to the tiller axis), up to the point where tissue emerges from the surrounding sheath of the next-older, most-recently expanded leaf (Schnyder *et al.* 1990; MacAdam & Nelson 1987, 2002; see also Fig. 5.14 in MacAdam 2009). Such measurements of $\Delta^{18}O_{LGDZ}$ have not been performed to date. Of note, leaf expansion, assimilate import into the LGDZ and structural biomass synthesis within the LGDZ of grass leaves proceed through day–night cycles, and can occur at similar rates in darkness and light (Schnyder & Nelson 1988; Schnyder *et al.* 1988). These relationships are complicated further by (e.g. diurnal) VPD transients, which can provoke strong changes in leaf elongation rate of grasses (Parrish & Wolf 1983), potentially changing the relative rates of daytime versus nighttime cellulose synthesis. These features call for joint analyses of the spatial and temporal dynamics of cellulose synthesis rates and $\Delta^{18}O_{LGDZ}$ during diurnal cycles in scenarios with different VPDs. Execution of such work was not feasible in this experiment.

Conversely, given the absence of VPD effects on plant growth and morphology of *C. squarrosa*, but strong effects on water fluxes in plants, we would expect that VPD-related changes of $p_{ex}p_x$ are mainly determined by the p_x component or by factors emanating from gradients of $\delta^{18}O$ in leaf water on $\delta^{18}O$ of sucrose in source leaves. However, if sucrose was actually in equilibrium with average bulk leaf blade water, then the observation of a mean $p_{ex}p_x$ of 0.48 at low VPD would suggest that p_x should be close to 1 in that scenario, if we accept the notion that p_{ex} is bounded between 0.4 and 0.5 (Helliker & Ehleringer 2002a, 2002b; Cernusak *et al.* 2005; Barbour 2007; Gessler *et al.* 2014).

ACKNOWLEDGMENTS

Brent Helliker is thanked for helpful discussions and comments on an earlier version of this manuscript. W. Feneis and R. Wenzel are thanked for technical assistance with the mesocosm facility. A. Schmidt, M. Michler, A. Ernst-Schwärzli., H. Vogl, L. Li, S. Y. Wang and J. Ciomas provided fine help during sample collection and processing. This research was supported by the Deutsche Forschungsgemeinschaft (DFG SCHN 557/7-1). H. T. L. and F. Y. were supported by the Chinese Scholarship Council (CSC).

REFERENCES

Arredondo J.T. & Schnyder H. (2003) Components of leaf elongation rate and their relationship to specific leaf area in contrasting grasses. *New Phytologist* **158**, 305–314.

Barbour M.M. & Farquhar G. (2000) Relative humidity-and ABA-induced variation in carbon and oxygen isotope ratios of cotton leaves. *Plant, Cell & Environment* **23**, 473–485.

Barbour M.M. (2007) Stable oxygen isotope composition of plant tissue: a review. *Functional Plant Biology* **34**, 83–94.

Barbour M.M., Walcroft A.S. & Farquhar G.D. (2002) Seasonal variation in $\delta^{13}C$ and $\delta^{18}O$ of cellulose from growth rings of *Pinus radiata*. *Plant, Cell & Environment* **25**, 1483–1499.

Barbour M.M., Roden J.S., Farquhar G.D. & Ehleringer J.R. (2004) Expressing leaf water and cellulose oxygen isotope ratios as enrichment above source water reveals evidence of a Péclet effect. *Oecologia* **138**, 426–435.

Barbour M.M., Schurr U., Henry B.K., Wong S.C. & Farquhar G.D. (2000) Variation in the oxygen isotope ratio of phloem sap sucrose from castor bean. Evidence in support of the Péclet effect. *Plant Physiology* **123**, 671–680.

Begg J.E. & Wright M.J. (1962) Growth and development of leaves from intercalary meristems in *Phalaris arundinacea* L. *Nature* **194**, 1097–1098.

Bolton J.K. & Brown R.H. (1980) Photosynthesis of grass species differing in carbon dioxide fixation pathways V. Response of *Panicum maximum*, *Panicum milioides*, and tall fescue (*Festuca arundinacea*) to nitrogen nutrition. *Plant Physiology* **66**, 97–100.

Bernstein N., Silk W.K. & Läuchli A. (1993) Development of *Sorghum* leaves under conditions of NaCl stress—spatial and temporal aspects of leaf growth-inhibition. *Planta* **191**, 433–439.

Brendel O., Iannetta P. & Stewart D. (2000) A rapid and simple method to isolate pure alpha-cellulose. *Phytochemical Analysis* **11**, 7–10.

Brooks J.R. & Mitchell A.K. (2011) Interpreting tree responses to thinning and fertilization using tree-ring stable isotopes. *New Phytologist* **190**, 770–782.

Cernusak L.A., Wong S.C. & Farquhar G.D. (2003a) Oxygen isotope composition of phloem sap in relation to leaf water in *Ricinus communis*. *Functional Plant Biology* **30**, 1059–1070.

Cernusak L.A., Arthur D.J., Pate J.S. & Farquhar G.D. (2003b) Water relations link carbon and oxygen isotope discrimination to phloem sap sugar concentration in *Eucalyptus globulus*. *Plant Physiology* **131**, 1544–1554.

Cernusak L.A., Barbour M.M., Arndt S.K., Cheesman A.W., English N.B., Feild T.S., … Kahmen A. (2016) Stable isotopes in leaf water of terrestrial plants. *Plant, Cell & Environment* **39**, 1087–1102.

Cernusak L.A., Farquhar G.D. & Pate J.S. (2005) Environmental and physiological controls over oxygen and carbon isotope composition of Tasmanian blue gum, *Eucalyptus globulus*. *Tree Physiology* **25**, 129–146.

Clayton W.D., Vorontsova M.S., Harman K.T. & Williamson H. (2006) GrassBase: the online world grass flora.

Cousins A.B., Badger M.R. & Von Caemmerer S. (2006a) Carbonic anhydrase and its influence on carbon isotope discrimination during C_4 photosynthesis. Insights from antisense RNA in *Flaveria bidentis*. *Plant Physiology* **141**, 232–242.

Cousins A.B., Badger M.R. & Von Caemmerer S. (2006b) A transgenic approach to understanding the influence of carbonic anhydrase on $C^{18}OO$ discrimination during C_4 photosynthesis. *Plant Physiology* **142**, 662–672.

Craig H. & Gordon L.I. (1965) *Deuterium and Oxygen 18 Variations in the Ocean and Marine Atmosphere*. Consiglio Nationale Delle Ricerche Laboratorio Di Geologia Nucleare, Pisa, Italy.

Cruz P. & Boval M. (2000) Effect of nitrogen on some morphogenetic traits of temperate and tropical perennial forage grasses. In *Grassland Ecophysiology and Grazing Ecology* (eds Lemaire G., Hodgson J., de Moraes A., Nabinger C. & de F Carvalho P.C.), pp. 151–168. CABI Publishing, Wallingford.

Dale J. (1985) The carbon relations of the developing leaf. In *Control of Leaf Growth* (eds Baker N.R., Davies W.J. & Ong C.K.), pp. 135–153. Cambridge University Press, New York.

Dale J. (1988) The control of leaf expansion. *Annual Review of Plant Physiology and Plant Molecular Biology* **39**, 267–295.

Dawson T.E., Ehleringer J.R., Hall A.E. & Farquhar G.D. (1993) Water sources of plants as determined from xylem–water isotopic composition: perspectives on plant competition, distribution, and water relations. In *Stable Isotopes and Plant Carbon–Water Relations* (eds Saugier B., Ehleringer J.R., Hall A.E. & Farquhar G.D.), pp. 465–496. Academic Press Inc., San Diego.

DeNiro M.J. & Epstein S. (1979) Relationship between the oxygen isotope ratios of terrestrial plant cellulose, carbon dioxide, and water. *Science* **204**, 51–53.

DeNiro M.J. & Epstein S. (1981) Isotopic composition of cellulose from aquatic organisms. *Geochimica et Cosmochimica Acta* **45**, 1885–1894.

Dongmann G., Nürnberg H., Förstel H. & Wagener K. (1974) On the enrichment of $H_2^{18}O$ in the leaves of transpiring plants. *Radiation and Environmental Biophysics* **11**, 41–52.

Ehleringer J.R. & Dawson T.E. (1992) Water uptake by plants: perspectives from stable isotope composition. *Plant, Cell & Environment* **15**, 1073–1082.

Ellsworth P.V. & Sternberg L.S.L. (2014) Biochemical effects of salinity on oxygen isotope fractionation during cellulose synthesis. *New Phytologist* **202**, 784–789.

Farquhar G.D., Barbour M.M. & Henry B. (1998) Interpretation of oxygen isotope composition of leaf material. In *Stable Isotopes: Integration of Biological, Ecological, and Geochemical Processes* (eds Robinson D., Van Gardingen P. & Griffiths H.), pp. 27–74. Environmental Plant Biology series, BIOS Scientific Publishers Ltd, Oxford.

Farquhar G.D. & Gan K.S. (2003) On the progressive enrichment of the oxygen isotopic composition of water along a leaf. *Plant, Cell & Environment* **26**, 1579–1597.

Farquhar G.D. & Lloyd J. (1993) Carbon and oxygen isotope effects in the exchange of carbon dioxide between terrestrial plants and the atmosphere. In *Stable Isotopes and Plant Carbon–Water Relations* (eds Saugier B., Ehleringer J. R., Hall A.E. & Farquhar G.D.), pp. 47–70. Academic Press Inc., San Diego.

Farquhar G.D., Cernusak L.A. & Barnes B. (2007) Heavy water fractionation during transpiration. *Plant Physiology* **143**, 11–18.

Flanagan L.B., Comstock J.P. & Ehleringer J.R. (1991) Comparison of modeled and observed environmental influences on the stable oxygen and hydrogen isotope composition of leaf water in *Phaseolus vulgaris* L. *Plant Physiology* **96**, 588–596.

Flanagan L.B. & Farquhar G.D. (2014) Variation in the carbon and oxygen isotope composition of plant biomass and its relationship to water-use efficiency at the leaf- and ecosystem-scales in a northern Great Plains grassland. *Plant, Cell & Environment* **37**, 425–438.

Flanagan L.B. & Ehleringer J.R. (1991) Effects of mild water stress and diurnal changes in temperature and humidity on the stable oxygen and hydrogen isotopic composition of leaf water in *Cornus stolonifera* L. *Plant Physiology* **97**, 298–305.

Gan K.S., Wong S.C., Yong J.W.H. & Farquhar G.D. (2003) Evaluation of models of leaf water ^{18}O enrichment using measurements of spatial patterns of vein xylem water, leaf water and dry matter in maize leaves. *Plant, Cell & Environment* **26**, 1479–1495.

Gastal F. & Lemaire G. (2002) N uptake and distribution in crops: an agronomical and ecophysiological perspective. *Journal of Experimental Botany* **53**, 789–99.

Gaudinski J.B., Dawson T.E., Quideau S., Schuur E.A., Roden J.S., Trumbore S.E., … Wasylishen R.E. (2005) Comparative analysis of cellulose preparation techniques for use with ^{13}C, ^{14}C, and ^{18}O isotopic measurements. *Analytical Chemistry* **77**, 7212–7224.

Gessler A., Brandes E., Keitel C., Boda S., Kayler Z.E., Granier A., … Treydte K. (2013) The oxygen isotope enrichment of leaf-exported assimilates—does it always reflect lamina leaf water enrichment? *New Phytologist* **200**, 144–157.

Gessler A., Peuke A.D., Keitel C. & Farquhar G.D. (2007) Oxygen isotope enrichment of organic matter in *Ricinus communis* during the diel course and as affected by assimilate transport. *New Phytologist* **174**, 600–613.

Gessler A., Brandes E., Buchmann N., Helle G., Rennenberg H. & Barnard R.L. (2009) Tracing carbon and oxygen isotope signals from newly assimilated sugars in the leaves to the tree-ring archive. *Plant, Cell & Environment* **32**, 780–795.

Gessler A., Ferrio J.P., Hommel R., Treydte K., Werner R.A. & Monson R.K. (2014) Stable isotopes in tree rings: towards a mechanistic understanding of isotope fractionation and mixing processes from the leaves to the wood. *Tree Physiology* **34**, 796–818.

Gillon J. & Yakir D. (2001a) Influence of carbonic anhydrase activity in terrestrial vegetation on the ^{18}O content of atmospheric CO_2. *Science* **291**, 2584–2587.

Gillon J. & Yakir D. (2001b) Naturally low carbonic anhydrase activity in C_4 and C_3 plants limits discrimination against $C^{18}OO$ during photosynthesis. *Plant, Cell & Environment* **23**, 903–915.

Helliker B.R. & Ehleringer J.R. (2000) Establishing a grassland signature in veins: ^{18}O in the leaf water of C_3 and C_4 grasses. *Proceedings of the National Academy of Sciences* **97**, 7894–7898.

Helliker B.R. & Ehleringer J.R. (2002a) Differential ^{18}O enrichment of leaf cellulose in C_3 versus C_4 grasses. *Functional Plant Biology* **29**, 435–442.

Helliker B.R. & Ehleringer J.R. (2002b) Grass blades as tree rings: environmentally induced changes in the oxygen isotope ratio of cellulose along the length of grass blades. *New Phytologist* **155**, 417–424.

Hill S., Waterhouse J., Field E., Switsur V. & Ap R.T. (1995) Rapid recycling of triose phosphates in oak stem tissue. *Plant, Cell & Environment* **18**, 931–936.

Jinwen L., Jingping Y., Pinpin F., Junlan S., Dongsheng L., Changshui G. & Wenyue C. (2009) Responses of rice leaf thickness, SPAD readings and chlorophyll a/b ratios to different nitrogen supply rates in paddy field. *Field Crops Research* **114**, 426–432.

Kahmen A., Sachse D., Arndt S.K., Tu K.P., Farrington H., Vitousek P.M. & Dawson T.E. (2011) Cellulose $\delta^{18}O$ is an index of leaf-to-air vapor pressure difference (VPD) in tropical plants. *Proceedings of the National Academy of Sciences* **108**, 1981–1986.

Kang L., Han X.G., Zhang Z.B. & Sun O.J. (2007) Grassland ecosystems in China: review of current knowledge and research advancement. *Philosophical Transactions of the Royal Society of London B: Biological Sciences* **362**, 997–1008.

Lattanzi F.A., Ostler U., Wild M., Morvan-Bertrand A., Decau M.L., Lehmeier C.A., … Schnyder H. (2012) Fluxes in central carbohydrate metabolism of source leaves in a fructan-storing C_3 grass: rapid turnover and futile cycling of sucrose in continuous light under contrasted nitrogen nutrition status. *Journal of Experimental Botany* **63**, 2363–2375.

Lemaire G., Jeuffroy M.H. & Gastal F. (2008) Diagnosis tool for plant and crop N status in vegetative stage theory and practices for crop N management. *European Journal of Agronomy* **28**, 614–624.

Lehmeier C.A., Lattanzi F.A., Schäufele R., Wild M. & Schnyder H. (2008) Root and shoot respiration of perennial ryegrass are supplied by the same substrate pools: assessment by dynamic ^{13}C labeling and compartmental analysis of tracer kinetics. *Plant Physiology* **148**, 1148–1158.

Lipp J., Trimborn P., Edwards T., Waisel Y. & Yakir D. (1996) Climatic effects on the $\delta^{18}O$ and $\delta^{13}C$ of cellulose in the desert tree *Tamarix jordanis*. *Geochimica et Cosmochimica Acta* **60**, 3305–3309.

Loomis R.S. & Connor D.J. (1992) *Crop Ecology: Productivity and Management in Agricultural Systems*. Cambridge University Press, Cambridge.

Loucos K.E., Simonin K.A., Song X. & Barbour M.M. (2015) Observed relationships between leaf $H_2^{18}O$ Péclet effective length and leaf hydraulic conductance reflect assumptions in Craig–Gordon model calculations. *Tree Physiology* **35**, 16–26.

MacAdam J.W. (2009) *Structure and Function of Plants*. Wiley-Blackwell, Ames.

MacAdam J.W. & Nelson C.J. (1987) Specific leaf weight in zones of cell division, elongation and maturation in tall fescue leaf blades. *Annals of Botany* **59**, 369–376.

MacAdam J.W. & Nelson C.J. (2002) Secondary cell wall deposition causes radial growth of fibre cells in the maturation zone of elongating tall fescue leaf blades. *Annals of Botany* **89**, 89–96.

Martín-Gómez P., Barbeta A. & Voltas J. (2015) Isotope-ratio infrared spectroscopy: a reliable tool for the investigation of plant-water sources? *New Phytologist* **207**, 914–927.

Parrish D.J. & Wolf D.D. (1983) Kinetics of tall fescue leaf elongation—responses to changes in illumination and vapor-pressure. *Crop Science* **23**, 659–663.

Ripullone F., Matsuo N., Stuart-Williams H., Wong S.C., Borghetti M., Tani M. & Farquhar G.D. (2008) Environmental effects on oxygen isotope enrichment of leaf water in cotton leaves. *Plant Physiology* **146**, 729–736.

Roden J.S., Lin G. & Ehleringer J.R. (2000) A mechanistic model for interpretation of hydrogen and oxygen isotope ratios in tree-ring cellulose. *Geochimica et Cosmochimica Acta* **64**, 21–35.

Ryle G. & Powell C. (1974) The utilization of recently assimilated carbon in graminaceous plants. *Annals of Applied Biology* **77**, 145–158.

Schmidt H.L., Werner R.A. & Roßmann A. (2001) ^{18}O pattern and biosynthesis of natural plant products. *Phytochemistry* **58**, 9–32.

Schnyder H., Nelson C.J. & Coutts J.H. (1987) Assessment of spatial distribution of growth in the elongation zone of grass leaf blades. *Plant Physiology* **85**, 290–293.

Schnyder H. & Nelson C.J. (1988) Diurnal growth of tall fescue leaf blades. I. Spatial ditribution of growth, deposition of water, and assimilate import in the elongation zone. *Plant Physiology* **86**, 1070–1076.

Schnyder H., Nelson C.J. & Spollen W.G. (1988) Diurnal growth of tall fescue leaf blades. II. Dry matter deposition and carbohydrate metabolism in the elongation zone and adjacent expanded tissue. *Plant Physiology* **86**, 1070–1076.

Schnyder H., Seo S., Rademacher I.F. & Kühbauch W. (1990) Spatial distribution of growth rates and of epidermal cell lengths in the elongation zone during leaf development in *Lolium perenne* L. *Planta* **181**, 423–431.

Schnyder H., Schäufele R., Lötscher M. & Gebbing T. (2003) Disentangling CO_2 fluxes: direct measurements of mesocosm-scale natural abundance $^{13}CO_2/^{12}CO_2$ gas exchange, ^{13}C discrimination, and labelling of CO_2 exchange flux components in controlled environments. *Plant, Cell & Environment* **26**, 1863–1874.

Schnyder H., Schäufele R. & Wenzel R. (2004) Mobile, outdoor continuous-flow isotope-ratio mass spectrometer system for automated high-frequency ^{13}C- and ^{18}O-CO_2 analysis for Keeling plot applications. *Rapid Communications in Mass Spectrometry* **18**, 3068–3074.

Sharman B. (1942) Developmental anatomy of the shoot of *Zea mays* L. *Annals of Botany* **6**, 245–282.

Sheshshayee M., Bindumadhava H., Ramesh R., Prasad T., Lakshminarayana M. & Udayakumar M. (2005) Oxygen isotope enrichment ($\Delta^{18}O$) as a measure of time-averaged transpiration rate. *Journal of Experimental Botany* **56**, 3033–3039.

Song X., Farquhar G.D., Gessler A. & Barbour M.M. (2014a) Turnover time of the non-structural carbohydrate pool influences $\delta^{18}O$ of leaf cellulose. *Plant, Cell & Environment* **37**, 2500–2507.

Song X., Clark K.S. & Helliker B.R. (2014b) Interpreting species-specific variation in tree-ring oxygen isotope ratios among three temperate forest trees. *Plant, Cell & Environment* **37**, 2169–2182.

Sternberg L. & DeNiro M.J. (1983) Biogeochemical implications of the isotopic equilibrium fractionation factor between the oxygen atoms of acetone and water. *Geochimica et Cosmochimica Acta* **47**, 2271–2274.

Sternberg L. & Ellsworth P.F.V. (2011) Divergent biochemical fractionation, not convergent temperature, explains cellulose oxygen isotope enrichment across latitudes. *PLoS ONE* **6**e28040.

Sternberg L.D.S.L., Deniro M.J. & Savidge R.A. (1986) Oxygen isotope exchange between metabolites and water during biochemical reactions leading to cellulose synthesis. *Plant Physiology* **82**, 423.

Stitt M. & Krapp A. (1999) The interaction between elevated carbon dioxide and nitrogen nutrition: the physiological and molecular background. *Plant, Cell & Environment* **22**, 583–621.

Tardieu F., Reymond M., Hamard P., Granier C. & Muller B. (2000) Spatial distributions of expansion rate, cell division rate and cell size in maize leaves: a synthesis of the effects of soil water status, evaporative demand and temperature. *Journal of Experimental Botany* **51**, 1505–1514.

Waterhouse J.S., Switsur V., Barker A., Carter A. & Robertson I. (2002) Oxygen and hydrogen isotope ratios in tree rings: how well do models predict observed values? *Earth and Planetary Science Letters* **201**, 421–430.

Webb E.A. & Longstaffe F.J. (2003) The relationship between phytolith- and plant-water $\delta^{18}O$ values in grasses. *Geochimica et Cosmochimica Acta* **67**, 1437–1449.

White J.W., Cook E.R. & Lawrence J.R. (1985) The D/H ratios of sap in trees: implications for water sources and tree ring D/H ratios. *Geochimica et Cosmochimica Acta* **49**, 237–246.

Wittmer M.H.O.M., Auerswald K., Bai Y., Schäufele R. & Schnyder H. (2010) Changes in the abundance of C_3/C_4 species of Inner Mongolia grassland: evidence from isotopic composition of soil and vegetation. *Global Change Biology* **16**, 605–616.

Xiao W., Lee X., Wen X., Sun X. & Zhang S. (2012) Modeling biophysical controls on canopy foliage water ^{18}O enrichment in wheat and corn. *Global Change Biology* **18**, 1769–1780.

Yang H. (2010) Water use, discrimination, and temporal change of life forms among C_4 plants of Inner Monogolia grassland (*Doctoral dissertation, Technische Universität München*).

Yang H., Auerswald K., Bai Y.F., Wittmer M.H.O.M. & Schnyder H. (2011) Variation in carbon isotope discrimination in *Cleistogenes squarrosa* (Trin.) Keng: patterns and drivers at tiller, local, catchment, and regional scales. *Journal of Experimental Botany* **62**, 4143–4152.

Received 24 May 2016; received in revised form 23 August 2016; accepted for publication 24 August 2016

SUPPORTING INFORMATION

Additional Supporting Information may be found in the online version of this article at the publisher's web-site:

Figure S1. Typical diurnal time course for (a) air temperature and (b) relative humidity.
Figure S2. A photograph of a major tiller of *Cleistogenes squarrosa*.
Figure S3. Cryogenic vacuum distillation unit with a) overview of the vacuum generating and distributing parts and b) zoom view of the cold trap unit.
Figure S4. Sensitivity analysis showing the effect of uncertainty in ε_o on calculated $p_{ex}p_x$ for leaf blade cellulose of upper leaves at low (circles) and high VPD (triangles).
Figure S5. Sensitivity analysis testing the effect of varying oxygen isotope enrichment of leaf water ($\Delta^{18}O_{LW}$) on the significance of the VPD effect on $p_{ex}p_x$ of upper canopy leaves.
Table S1. Experimental plan that gives the assignment of treatments to the different growth chambers (no. 1 – 4) in the successive experimental runs (first to fourth).

Appendix 4

This manuscript has been submitted to Plant, Cell and Environment as a research paper.

An oxygen isotope chronometer for cellulose synthesis: the successive leaves formed by tillers of a C_4 perennial grass

Running title: Oxygen incorporation in grass leaf cellulose

Hai Tao Liu, Fang Yang, Xiao Ying Gong, Rudi Schäufele, Hans Schnyder

Lehrstuhl für Grünlandlehre, Technische Universität München, Alte Akademie 12, 85354 Freising, Germany.

Corresponding authors:

Hans Schnyder

Tel.: +49 8161713242, Fax: +49 8161713243, Email: schnyder@wzw.tum.de

Xiao Ying Gong

Tel.: +49 8161713722, Fax: +49 8161713243, Email: xgong@wzw.tum.de

An oxygen isotope chronometer for cellulose synthesis:

the successive leaves formed by tillers of a C_4 perennial grass

ABSTRACT

Multiannual time series of (palaeo)hydrological information can be reconstructed from the oxygen isotope composition of cellulose ($\delta^{18}O_{Cel}$) in biological archives, e.g. tree-rings, but our ability to temporally resolve information at subannual scale is limited. We capitalized on the short and predictable leaf appearance interval (2.4 d) of a perennial C_4 grass (*Cleistogenes squarrosa*), to assess its potential for providing highly time-resolved $\delta^{18}O_{Cel}$ records of vapor pressure deficit (VPD). Plants grown at low (0.63 kPa) or high (1.58 kPa) VPD, were swapped between VPD environments, and exposed to the new environment for 7 d with simultaneous $^{13}CO_2$ labeling. Then, leaves were sampled by age/position along individual tillers. Five leaves at different developmental stages were growing simultaneously. The period of most-active leaf elongation, from 10% to 90% of final length, lasted 6.6 d and ~80% of all carbon and oxygen incorporation in whole-leaf cellulose occurred within 7 d. Cellulose synthesis stopped at (or shortly after) full leaf expansion. The direction of change, from low to high or high to low VPD, had no differential effect on new oxygen and carbon incorporation in cellulose. Successive leaves produced by tillers of *C. squarrosa* provide a $\delta^{18}O_{Cel}$ record useful for reconstructions of short-term hydrological dynamics.

BRIEF SUMMARY STATEMENT

- Successive leaves formed by tillers of *C. squarrosa* provide a highly-resolved temporal record of oxygen isotope composition of cellulose
- Cellulose synthesis in leaf blades stops at or shortly after full expansion.
- VPD-driven changes in oxygen isotope composition of leaf cellulose are independent of VPD in the original growth environment

Key words: *Cleistogenes squarrosa*; carbon-13; isotopic record, leaf (blade) growth; oxygen-18; time resolution, tracer; vapor pressure deficit.

INTRODUCTION

The oxygen isotope composition of cellulose ($\delta^{18}O_{Cel}$) is determined by environmental conditions, mainly temperature and relative humidity – which determine evaporative demand – and morpho-physiological plant traits which affect the evaporative enrichment of ^{18}O in leaf water, and the $\delta^{18}O$ of water in plant compartments that are involved in the metabolism of sugars leading up to cellulose synthesis (Barbour 2007, Sternberg 2009, Gessler *et al.* 2014). As they store environmental information, chronologies of $\delta^{18}O_{Cel}$ are powerful tools for (paleo-)climate reconstructions (Libby *et al.* 1976, Hong *et al.* 2000, Roden *et al.* 2000, Anderson *et al.* 2002, Treydte *et al.* 2007, Sternberg 2009, Kahmen *et al.* 2011). In addition, as stomatal conductance is thought to modify the $\delta^{18}O$ of leaf water and hence that of cellulose (Farquhar *et al.* 1998, Scheidegger *et al.* 2000), it is also expected that retrospective analyses of $\delta^{18}O_{Cel}$ archives can shed light on physiological responses of plants' gas exchange to past climate changes. Annually resolved tree-ring series have spanned periods of centuries up to more than 10 000 years in some regions (Pilcher *et al.* 1984, Briffa *et al.* 1990, Esper *et al.* 2002, Treydte *et al.* 2006). At the subannual time scale, state-of-the-art methodologies attain a intra-ring sampling resolution equivalent to average tree-ring increments of <1 d to a few weeks (Helle & Schleser 2004, Schulze *et al.* 2004, Schollaen *et al.* 2014). However, exact position-time relationships for within-ring signals are not evident (Schleser *et al.* 1999, Kagawa *et al.* 2005) and require indirect approximations, such as matching of drought periods and maxima of $\delta^{13}C$ within tree-rings (Schleser *et al.* 1999) or extrapolation from dendrometer measurements (Barbour *et al.* 2002, Gessler *et al.* 2009).

Other morphological units of plants offer a specific potential for resolving subannual isotopic records with precisely dated chronologies of tissue formation. For instance, Helle & Schleser (2004) monitored leaf and bud sprouting, and dated tree-ring sections by comparison of the carbon isotope composition of cellulose ($\delta^{13}C_{Cel}$) in the sprouting leaves and in highly spatially-resolved tree-ring sections. Helliker & Ehleringer (2002) demonstrated that segments of grass leaves provide a record of $\delta^{18}O_{Cel}$ variation that results from effects of changed atmospheric vapor pressure deficit (VPD) on the ^{18}O composition of leaf water and assimilates that were produced during the respective periods of leaf segement growth. Grass-tissue-based isotopic indicators are of interest in grassland ecosytem studies, e.g. in the semiarid steppes in North China

where drought stress is common (Gong *et al.* 2011) but exhibits high spatio-temporal variability (Wittmer *et al.* 2008). Vegetative tillers of grasses – and some other taxa (Schleip *et al.* 2013) – exhibit a repetitive pattern of leaf production throughout the vegetation period. C_4 grasses may be particularly suitable for dynamic isotope time series analyses, as they exhibit short and predictable leaf appearance intervals (phyllochrons) and have several leaves at different developmental stages of the leaf growth process during vegetative development (Yang *et al.* 2016). But that potential has not been explored to date.

A specific challenge in the evaluation of highly spatially-resolved ^{18}O records is their unknown temporal integration (Kagawa *et al.* 2005). In other words, it is generally not known what time period of assimilation is actually reflected in the $\delta^{18}O_{Cel}$ of a given sample. The integration is primarily a function of the turnover time of substrate pools in source and sink tissue (including storage/mobilization processes of sugars that may participate in cellulose synthesis), and the diversity of cell types, developmental stages and characteristic cellulose deposition dynamics of the different cell types in the sample (Hemming *et al.* 2001, Damesin & Lelarge 2003, Gessler *et al.* 2009, 2014). To our best knowledge, there have been no explicit, quantitative investigations of the temporal integration in short-term ^{18}O records in plant tissues. However, in 1 day-long $^{13}CO_2$ pulse labelling experiments with *Cryptomeria japonica* (Japanese cedar) performed in spring and fall, Kagawa *et al.* (2005) observed a half-width of the labeling peak – which comprizes ~80% of the label within the peak (given a Gaussian distribution) – equivalent to 9 to 28 days of earlywood and 33 to 42 days of latewood formation. However, whether or not carbohydrate stores contributed to cellulose synthesis in these periods could not be resolved with that approach. In principle, one may expect a similar or higher temporal resolution of the ^{18}O record of successively formed leaves in grasses as rates of successive leaf appearance and elongation are rapid in grasses (Skinner & Nelson 1995) and growth substrate pools for leaf growth have a high turnover (Lattanzi *et al.* (2005).

The objective of this work was to characterize the temporal resolution of the ^{18}O record that is generated by the successive leaves formed by tillers of *C. squarrosa* following a change of VPD, and hence to evaluate its potential as a quantitative high-resolution biological chronometer of ^{18}O signals. In the same experiment, we performed a detailed analysis of the development of successive phytomers, and of their blade,

sheath and internode parts, for plants grown in contrasting VPDs (Yang *et al.* 2016). Plants were grown at high and low VPD, swapped between VPD environments and exposed to the new environment for 7 days while simultaneously labeling them with $^{13}CO_2/^{12}CO_2$ mixtures of known constant composition at near-ambient CO_2 concentration. After 7 days-long labeling, the incorporation of new oxygen (derived from assimilation in the new VPD environment) and labelled carbon were evaluated in leaves of different developmental stages.

MATERIALS AND METHODS

Plant material and growth conditions

This experiment used the same plant material and growth conditions as the studies of Liu *et al.* (2016) and Yang *et al.* (2016). The work was performed in four growth chambers that were operated as controlled environment $^{13}CO_2/^{12}CO_2$ mesocosms, similar to the system described by Schnyder *et al.* (2003). That system permitted continuous measurements and control of air temperature, relative humidity, and concentration and ^{13}C composition of CO_2 ($\delta^{13}C_{CO2}$) in each chamber.

Plants were established from seed. Four seeds of *C. squarrosa*, were sown in individual tubes (4.5 cm diameter, 35 cm deep) filled with quartz sand. Tubes were arranged in free-draining plastic containers (length: 77 cm, width: 57 cm, depth: 30 cm) with 164 tubes per container. Two containers were placed in each growth chamber. Before germination, the conditions in all chambers were kept the same with a relative humidity (RH) of 80% at a constant growth temperature of 25 ^{o}C, thus yielding a vapor pressure deficit (VPD) of 0.63 kPa. The day of first watering (i.e. imbibition of seeds) is designated as day 1, the start of the experiment. One week after first watering, the germinated plantlets were thinned to one per tube, and RH adjusted to 50% (providing a VPD of 1.58 kPa) in two chambers, while maintaining the VPD of 0.63 kPa in the other chambers. The two chambers of a given VPD regime were supplied with CO_2 of different $\delta^{13}C$: a (relatively) ^{13}C-enriched CO_2 with a $\delta^{13}C_{CO2}$ of −6.2 ± 0.1‰ (mean ± SD, n = 20) was supplied to one chamber and a ^{13}C-depleted CO_2 with a $\delta^{13}C_{CO2}$ of −48.8 ± 0.1‰ (mean ± SD, n = 20) to the other (cf. Fig. S1). Due to carbon isotope discrimination during gas exchange of plants, the $\delta^{13}C_{CO2}$ was −5.3 ± 0.2‰ (mean ± SD) inside the growth chambers with the ^{13}C-enriched CO_2 and −47.7 ± 0.1‰ inside the

chambers with the ^{13}C-depleted CO_2 (cf. Gong *et al*. 2016). Except for the VPD and CO_2 sources, all other environmental parameters were kept the same.

Light was supplied by cool white fluorescent tubes with a photosynthetic photon flux density (PPFD) of 800 μmol m^{-2} s^{-1} at canopy height during the 16 h photoperiod. Irradiance was kept constant by periodic adjustments of the distance between the fluorescent tubes and the top of the canopy following measurements with a quantum sensor (LI-190R, LI-COR, Lincoln, Nebraska, USA). Air temperature was kept constant at 25 °C during dark and light periods. CO_2 concentration was controlled at 390 μmol mol^{-1} during the light period. CO_2 and water vapor concentration in chamber air were measured by an infrared gas analyzer (LI-6262, LI-COR Inc. Lincoln, USA). A modified Hoagland nutrient solution, with 7.5 mM nitrate, was supplied three times per day by an automatic irrigation system as described by Liu *et al.* (2016).

Treatments and sampling

The experiment was run in duplicate (Fig. S1). Each experimental run had two transfer treatments (high-to-low VPD, and low-to-high VPD) and constant VPD 'controls' with plants grown continuously at low or high VPD. Some of the $\delta^{18}O_{Cel}$ data from the constant VPD treatments were already reported by Liu *et al.* (2016). In transfer treatments, eight plants each were swapped with plants growing in contrasting conditions of VPD and $\delta^{13}C_{CO2}$. For example, plants grown at low VPD in the presence of the ^{13}C-enriched CO_2 were exchanged with plants grown at high VPD in the presence of the ^{13}C-depleted CO_2.

Transfers occurred at 1 h before the start of the light period on the 44th day (see Fig. S1). Plants were harvested 7 d later at the same daytime. Harvests also included plants that had remained in the same environment throughout the experiment (controls, see above). Leaves on major tillers (i.e. tillers that had >10 fully developed leaves) were sampled by position, i.e. age category (Fig. 1). Except for the youngest exposed leaf, all other leaf blades were sampled integrally, by cutting at the ligule. Daughter tillers that developed in the leaf axils of older leaves (DT in Fig. 1) were discarded. Same age leaves from 15 to 20 tillers were combined in one sample, and three separate samples of each age category collected in every treatment in every chamber. The youngest sampled leaf (no. 1, Fig. 1) was cut at the point of emergence from the surrounding older leaf. Enrolled within that leaf, there was generally an additional tiny leaf tip (the tip of the

next younger leaf). That tip was not eliminated from the sample of leaf no. 1. All samples were oven-dried for 48 hours at 60 ˚C, and then stored in an exsiccator until milling and cellulose extraction.

Estimation of leaf blade developmental and growth stage

Leaf blade samples collected along tillers were numbered consecutively from the tip of the tiller, starting with the youngest sampled leaf age category (Fig. 1). For every category (1 to *n*), the stage of blade development and growth (as a fraction of final blade length, f_{FBL}) at the times of transfer and harvest was estimated from knowledge of the leaf appearance interval, development of individual phytomers, and the contribution of the leaf blade component to phytomer development in the same study (Yang *et al.* 2016). Fig. 2 illustrates the time course of leaf blade elongation, as calculated from phytomer elongation and the fractional contribution of leaf blades to phytomer elongation for the constant low and high VPD treatments in plants grown at 'low N' (cf. Figs. 3a and 5 in Yang *et al*. 2016), the 'control' treatments presented here. The tip of leaf blades emerged from the enclosing sheath of the next older leaf when the blade had reached 31% of its final length. The period of maximum leaf elongation rate – taken as the time for expansion from 10% to 90% of final length – was 6.6 d, and lasted from 2.1 d before tip emergence to 4.5 d after emergence (Fig. 2). Importantly, the leaf appearance interval (2.4 d) and final leaf blade length were the same in plants grown constantly in the same low or high VPD environment (Yang *et al.* 2016). Also, transfer of plants from one VPD environment to the other did not affect the leaf appearance interval (data not shown).

Cellulose extraction

Aliquots of 50 mg or 25 mg of ball-milled, dry sample material were used to extract α-cellulose using the procedure of Brendel *et al.* (2000) as modified by Gaudinski *et al.* (2005).

Measurements of carbon and oxygen isotope composition

Carbon or oxygen isotope composition was expressed in per mil (‰) as

$$\delta^{13}\mathrm{C} \text{ or } \delta^{18}\mathrm{O} = \left(\frac{\mathrm{R_{sample}}}{\mathrm{R_{standard}}} - 1\right) \times 1000 \quad (1)$$

where, R_{sample} is the $^{13}C/^{12}C$ or $^{18}O/^{16}O$ ratios of the sample, and $R_{standard}$ is $^{13}C/^{12}C$ ratio in the international V-PDB standard or $^{18}O/^{16}O$ ratios in the Vienna Standard Mean Ocean Water standard (V-SMOW).

Carbon isotope discrimination as expressed in leaf blade cellulose ($\Delta^{13}C_{Cel}$) of plants kept continuously in a given growth chamber was calculated as:

$$\Delta^{13}C_{Cel} = \frac{\delta^{13}C_{chamber\ CO2} - \delta^{13}C_{Cel}}{1 + \delta^{13}C_{chamber\ CO2}/1000}, \quad (2)$$

with $\delta^{13}C_{chamber\ CO2}$ referring to the $\delta^{13}C$ of CO_2 in the atmosphere of the respective growth chamber.

Oxygen isotope enrichment of leaf blade cellulose relative to source water ($\Delta^{18}O_{Cel}$) was obtained as:

$$\Delta^{18}O_{Cel} = \frac{\delta^{18}O_{Cel} - \delta^{18}O_{SW}}{1 + \delta^{18}O_{SW}/1000}, \quad (3)$$

with $\delta^{18}O_{SW}$ the oxygen isotope composition of the nutrient solution (Liu *et al.* 2016).

Cellulose samples were redried at 40 °C for 24 h, and 700 µg aliquots were packed in tin cups for carbon and silver cups for oxygen isotope (size: 3.3 × 5 mm, LüdiSwiss, Flawil, Switzerland) and stored above Silica Gel orange (2-5mm, ThoMar OHG, Lütau, Germany) in exsiccator vessels. For measurements of $\delta^{18}O_{Cel}$, samples were pyrolysed at 1400 °C in a pyrolysis oven (HTO, HEKAtech, Wegberg, Germany), equipped with a helium-flushed zero blank auto-sampler (Costech Analytical technologies, Valencia, CA, USA) and interfaced (ConFlo III, Finnigan MAT, Bremen, Germany) to a continuous-flow isotope ratio mass spectrometer (Delta Plus, Finnigan MAT). Solid internal lab standards (SILS, cotton powder) were run as a control after every fifth sample. All samples and SILS were measured against a laboratory working standard carbon monoxide gas, which was previously calibrated against a secondary isotope standard (IAEA-601). For $\delta^{13}C_{Cel}$ measurements, each sample was measured against a laboratory working standard gas, which was previously calibrated against a secondary isotope standard (IAEA-CH6 for $\delta^{13}C$, accuracy of calibration ± 0.06% SD). A laboratory standard (a fine ground wheat flour) was run after every tenth samples. The long-term precision for the SILS was <0.2‰ for $\delta^{13}C$ and <0.3‰ for $\delta^{18}O$.

Fraction of new carbon or oxygen in leaf blade cellulose

The fraction of new carbon or oxygen (f_{new}) in cellulose of a given leaf age category of transferred plants was calculated as

$f_{new} = (\delta_{sample} - \delta_{old})/(\delta_{new} - \delta_{old})$, (4)

with δ_{sample}, δ_{old} and δ_{new} designating the $\delta^{13}C_{Cel}$ or $\delta^{18}O_{Cel}$ (as appropriate) of that same leaf age category in transferred plants, plants kept in the chamber of origin (old) or in the new chamber throughout the experiment, following the rationale in Schnyder (1992). As an exception, for calculation of the fraction of new oxygen ($f_{new\ oxygen}$) in plants transferred from low to high VPD in the 2nd experiment, we used the mean value of repeated measurements from blade 7 to 10 of labeled/transferred plants as the estimate of δ_{old}. With that procedure we accounted (and corrected) for a deviation of the $\delta^{18}O_{Cel}$ of older leaves (leaves no. 7 to 10) from the transfer treatment in the same experimental run, and both the control and transfer treatments in the other experimental run (see Results).

Statistical analysis

The effect of leaf age class (i.e. leaf number) on $\delta^{13}C_{cel}$ or $\delta^{18}O_{cel}$ of controlled plants was tested using one-way ANOVA. For each leaf age class, $\delta^{13}C_{cel}$ or $\delta^{18}O_{cel}$ of controlled plants and transferred plants were compared using paired t-tests. Also, the difference between $f_{new\ C}$ and $f_{new\ O}$ in each leaf age category was tested using a paired t-test. A 3-parameter sigmoidal function was used to fit the relationship between fraction of final blade length and days after tip emergence, and non-lineal regression was performed using SigmaPlot (Ver. 12.5, Systat Software, Inc.).

RESULTS

Leaf development and growth stages

Based on the time course of leaf blade elongation in relation to the time of leaf tip emergence (Fig. 1) and the observations at sampling we estimated that the tip of leaf no. 1 had emerged 3.6 d before sampling (cf. also Fig. 2) on average of all sampled leaves in this age category (leaf no. 1) in every treatment. Therefore, leaf no. 1 had reached 84% of its final blade length at the time of sampling (Figs. 1 and 2, Table 1). At the time of transfer from one VPD environment to the other, 7 d prior to sampling, this leaf had possessed only 5% of its final length. As the leaf appearance interval (2.4 d) was constant and the same for the different treatments, times of leaf tip emergence of successively older leaf numbers (n) were obtained as ((n – 1) × 2.4 d) + 3.6 d and used together with the equation in Fig. 2, to estimate the fraction of final blade length of older leaf categories (i.e. leaf no. 2 to <6) at transfer and harvest. Accordingly, only the

five youngest leaf age categories experienced some leaf blade elongation following the transfer; but within that group, elongation stopped at progressively earlier times for leaves at more advanced developmental stages. For instance in leaf no. 3 the blade had reached 54% of its final length at the time of transfer, it continued to elongate for 5.1 d after the transfer, and hence blade elongation stopped at 1.9 d before sampling. In leaf no. 5, blade elongation stopped very shortly after the transfer. In leaf no. 6 and older, blade elongation had ceased already at the time of transfer. Overall, only leaf no. 1 and 2 experienced blade elongation throughout the 7 d long period following transfer.

Carbon isotope composition

When plants were kept in constant conditions of VPD, the $\delta^{13}C_{Cel}$ of leaf blades did not exhibit any significant variation with leaf age ($P > 0.05$). That is the $\delta^{13}C_{Cel}$ of the successively produced leaves was virtually constant (Fig. 3a, b). As expected, $\delta^{13}C_{Cel}$ was strongly influenced by $\delta^{13}C_{CO2}$. The contrast in $\delta^{13}C_{Cel}$ of plants kept in the presence of the ^{13}C-enriched and ^{13}C-depleted CO_2 source was 41.0‰ (± 0.1‰ SD) in the 1st experiment (Fig. 3a) and 42.2‰ (± 0.2‰ SD) in the 2nd (Fig. 3b). This contrast was virtually independent of VPD as $\Delta^{13}C_{Cel}$ differed little between VPD treatments ($\Delta^{13}C_{Cel}$ was 0.9 ± 0.1‰ SD higher at high VPD, than at low VPD, similar to the VPD effect on photosynthetic discrimination reported in Gong *et al*. 2016).

Where plants were transferred between environments with contrasting $\delta^{13}C_{CO2}$ (and VPD), and kept in the new environment for 7 d, the $\delta^{13}C_{Cel}$ depended strongly on developmental stage/age of the leaf at the time of transfer. When leaves had stopped expanding prior to the transfer (mature leaves; no. 6 to 11; Fig. 2 and Table 1), their $\delta^{13}C_{Cel}$ was virtually the same as that in plants kept in the old/original environment (Fig. 3). But, within the class of still growing (immature) leaves, the younger the leaf at the time of transfer the nearer was its $\delta^{13}C_{Cel}$ to that of the plants grown continuously in the new environment. For leaf no. 1 of transferred plants, the $\delta^{13}C_{Cel}$ was almost the same as that of the corresponding leaves of plants kept constantly in the respective environment.

Oxygen isotope composition

As expected, continuous growth of plants at low and high VPD led to a different $\delta^{18}O_{Cel}$ of leaf blades. On average of all age classes, the $\delta^{18}O_{Cel}$ was 22.9‰ (± 1.2‰ SD) at low

VPD and 31.9‰ (± 1.1‰ SD) at high VPD (Fig. 3c and d). At high VPD, the $\delta^{18}O_{Cel}$ was very similar in the two experiments. However, at low VPD, the $\delta^{18}O_{Cel}$ was lower in the 1st (Fig. 3c) than in the 2nd experiment (Fig. 3d), mainly due to the lower $\delta^{18}O_{Cel}$ of the older leaf blades (blades no. 6 to 11). In addition, $\delta^{18}O_{Cel}$ exhibited some apparently systematic age-related variation among the younger leaf age classes. Again, that effect was particularly evident at low VPD where the $\delta^{18}O_{Cel}$ of leaf blade no. 3 was 1.9‰ higher than that of the other leaves. That (unexplained) deviation was important as it corresponded to 21% of the (average) $\delta^{18}O_{Cel}$-difference between low and high VPD.

Similar to $\delta^{13}C_{Cel}$, the $\delta^{18}O_{Cel}$ in leaf blades of transferred plants depended on developmental stage at transfer. Thus, within the class of still growing leaves, the younger the leaf the closer was its $\delta^{18}O_{Cel}$ to that of plants grown continuously in the respective environment. With older leaves that had stopped expanding before the transfer (that is leaves no. 6 through 11), $\delta^{18}O_{Cel}$ did not vary systematically as a function of age class. Also, the $\delta^{18}O_{Cel}$ of these leaves did not differ significantly from that of plants kept in the original environment throughout the experiment. This was true except for the $\delta^{18}O_{Cel}$ of the older leaves (no. 6 and older) in the low to high VPD transfer treatment in the 1st experiment, which was 2.7‰ higher than that of same age leaves in the constant low VPD treatment in the same experimental run. We had already noted the particularly low $\delta^{18}O_{Cel}$ of leaves no. 6 to 11 in the constant low VPD treatment in the 2nd experiment.

The fractions of new carbon and oxygen in cellulose of transferred plants

The developmental stage-dependent variations of $\delta^{13}C_{Cel}$ and $\delta^{18}O_{Cel}$ observed in plants transferred to a different (new) VPD and altered $\delta^{13}C_{CO2}$ were evaluated in terms of 'labeling kinetics', that is fractions of carbon ($f_{new\ C}$) and oxygen ($f_{new\ O}$) assimilated in the new environments and incorporated into leaf blade cellulose (Fig. 4).

The fractions of new carbon and oxygen revealed near-identical relationships with leaf age in the low-to-high and the high-to-low VPD transfer treatments (Fig. 4 and Fig. S2). In leaves no. 6 and older, both $f_{new\ C}$ and $f_{new\ O}$ were not significantly different from 0. With leaf no. 5 and younger, both the $f_{new\ C}$ and $f_{new\ O}$ increased in a sigmoidal fashion with decreasing leaf age. In leaf no. 1, the leaf blade was near-fully labeled with new carbon (i.e. $f_{new\ C}$ = 0.97 ±0.01 SE), while the estimated $f_{new\ O}$ averaged 0.91 (±0.02 SE).

In general, these relationships corresponded with the fraction of final leaf blade length that was already present at the time of the transfer (Fig. 5) and, hence, time since emergence of the leaf. Thus, the $f_{new\ C}$ and $f_{new\ O}$ decreased near-linearly with the fraction of final blade length that was already present at the time of the transfer.

Although the general relationships of $f_{new\ C}$ and $f_{new\ O}$ with leaf age/developmental stage were similar, in the case of leaf no. 4 the $f_{new\ O}$ was much higher (1.9 times) than $f_{new\ C}$ ($P < 0.05$) (Fig. 6 and Fig. S3).

DISCUSSION

The short-term VPD effect on cellulose-^{18}O of growing leaves is independent of VPD in the original growth environment

The transfer treatments – low to high and high to low VPD – did not differ in their labeling kinetics, that is their effects on $f_{new\ O}$ (or $f_{new\ C}$) of the different age classes of growing leaves. This indicates that the $\delta^{18}O_{Cel}$ of cellulose synthesized after the transfer was determined chiefly by the VPD in the new environment and, hence, was essentially independent of VPD-specific morpho-physiological traits acquired in the original growth environment. Thus the original growth environment seemed to have no significant after- or memory effects on ^{18}O-enrichment of leaf water and (consequently) carbohydrates in the new VPD environment and the propagation of the ^{18}O signal of carbohydrates to that of the newly synthesized cellulose. Principally, a memory effect may be expected if the original growth environment has some constitutive effect on stomatal conductance that would influence the posterior ^{18}O-enrichment of leaf water and hence carbohydrates when plant are exposed to a new VPD regime. However, in modeling the separate effects of VPD and stomatal conductance on $\delta^{18}O_{Cel}$, Barbour *et al.* (2002) found only a very minor effect of stomatal conductance when compared with that of VPD. Stomatal conductance was 20% less in plants of *C. squarrosa* when grown (and measured) with a low VPD in the same experiment (Gong *et al.* 2016), but that effect probably resulted mostly from the VPD-environment during the measurement of stomatal conductance (Schulze 1986, Monteith 1995). Except for transpiration (+27% at high relative to low VPD), measurements of other morpho-physiological parameters indicated no or little effect of VPD (Gong *et al.* 2016, Liu *et al.* 2016): leaf area index of the canopies, plant growth rate and mass, leaf mass and dimensions (individual leaf area and thickness), and nitrogen per unit leaf area or mass were not affected by VPD in

the original growth environment, while net photosynthesis was increased by 11% at low relative to high VPD. Additionally, the absence of aftereffects of prior growth conditions on the ^{13}C-labeling of cellulose ($f_{\text{new C}}$) in growing leaves supports the view that the two VPD transfer treatments had no differential effect on allocation of newly synthesized carbohydrates to leaf growth, the turnover rate and size of the relevant carbohydrate pools and carbohydrate metabolism associated with cellulose synthesis.

The temporal resolution of short-term VPD effects on whole-leaf cellulose-^{18}O

The temporal resolution of the oxygen isotope record represented by whole-leaf cellulose of successively formed leaf blades is influenced by (i) the participation of stores (which dampen and broaden the isotopic signal in the carbohydrate supply to cellulose synthesis), (ii) the leaf appearance interval (which dictates the rate of formation of the individual morphological units that resolve the temporal record), (iii) the duration of leaf expansion (that delimits the integration time of the isotopic signal of cellulose in primary cell walls at the whole-leaf level) and (iv) the duration of post-expansion cell wall synthesis (that is related to post-expansion, continued secondary cell wall synthesis).

In general, one should expect that carbohydrate stores can supply substrate to cellulose synthesis during leaf growth. In the present work, a contribution of carbohydrate stores to cellulose synthesis was potentially detectable in transferred plants based on an increased ratio of $f_{\text{new O}}$ to $f_{\text{new C}}$. In the theoretical situation, that metabolism of storage-derived substrate involves no carbonyl oxygen formation, which is unlikely (Hill *et al.* 1995, Barbour 2007, Gessler *et al.* 2014, Song *et al.* 2014), or that such formation occurs only in unenriched medium water, the oxygen isotope composition of storage-derived metabolites should not be affected by a VPD change. However, if storage-derived metabolites exchange carbonyl oxygen with evaporatively enriched water (e.g. in source leaves), such exchange would generate an ‘oxygen tag’ or label in the new VPD environment, while the carbon isotope composition of the metabolite would remain unchanged, elevating the ratio of $f_{\text{new O}}$ to $f_{\text{new C}}$. In particular, one should expect to see such an effect in leaves that terminate cellulose synthesis shortly after the VPD transition, when stored carbon still reflects the carbon isotope composition of the original growth environment. In agreement with such an expectation, we observed a significant divergence of the $f_{\text{new O}}$ to $f_{\text{new C}}$ ratio, supporting some role of stores in

cellulose synthesis of leaf no. 4. In leaf no. 5, that effect was not statistically significant. Notably, however, such an effect was not evident in the younger leaves (the $f_{new\ O}$ to $f_{new\ C}$ ratio for leaves no. 1 to 3 was 1.01 ± 0.04 SE), indicating that stores supplying leaf growth must be turned over very rapidly by assimilates produced in the new environment. This conclusion is supported by findings with *Paspalum dilatatum*, where stored carbon contributed only 7% to the total carbon incorporation in leaf growth zones during undisturbed growth (Lattanzi *et al.* 2005).

Cellulose synthesis ceased at or very shortly after termination of leaf blade expansion. That finding is consistent with studies of MacAdam and Nelson (2002) in *Festuca arundinacea* (Schreb.) that indicated a termination of secondary cell wall synthesis in leaf blade tissue near the time of its emergence from the surrounding sheath of the next-older leaf. Thus, virtually all cellulose synthesis in leaf tissue occurs while that part of tissue is fully enclosed within the surrounding sheath of the older leaf and non-transpiring.

The dominant factor determining the temporal integration of the ^{18}O-signal in whole-leaf cellulose ($\delta^{18}O_{Cel}$) was the duration of leaf expansion, as we have shown (above) that stores likely contributed little to cellulose synthesis and cellulose synthesis was mainly associated with the expansion phase. This interpretation is in line with that of Helliker & Ehleringer (2002) and is also consistent with the observation that the $\delta^{18}O_{Cel}$ of leaf no. 1 was essentially determined by assimilate produced concurrently with its growth during the 7 d-long exposure to an altered VPD. Leaves at more advanced growth stages at the time of transfer experienced divergent VPD conditions during the different phases of leaf growth, which must have led to divergent $\delta^{18}O_{Cel}$ in the leaf sections formed in the different phases as in Helliker & Ehleringer (2002).

The phase of most-active leaf blade elongation lasted 6.6 d, with – on average – 2.8 leaves at different developmental stages present in that phase simultaneously. At the same time, our data indicate that $f_{new\ O}$ increased from 0.1 to 0.9 over a leaf number-interval of 3.4 (growing) leaves, which corresponds to a 8.2 d-long period (obtained by multiplying the leaf number-interval by the 2.4 d-long leaf appearance interval). The same calculation indicated a period of 5.8 d for $f_{new\ C}$. These relationships all support the idea that similar to 80% of all oxygen and carbon incorporation into a leaf blade derived from current assimilation over a period of approx. 7 d, again supporting the view that

leaf expansion duration was the single most important parameter determining the temporal resolution of the whole-leaf blade based $\delta^{18}O_{Cel}$ record presented by the sequential leaves produced by a tiller of *C. squarrosa*. That interpretation coincides with that of Wright and Leavitt (2006) who noted a fair correspondence between the duration of needle growth and the duration of cellulose synthesis in needles of *Pinus aizonica*.

Remarkably, the leaf appearance interval and leaf growth duration of grass species (and species of other taxa with continuous or 'succeeding' leaf production; e.g. Kikuzawa 1984; Schleip *et al*. 2013) can be predicted/modeled relatively well, as they are determined by growth-effective temperature, expressed in degree days above a certain base temperature GDD (the sum of daily average temperature above a certain base temperature), or other, more complex, functional relationships with (soil or air) temperature and other environemntal factors such as day length (Cao & Moss 1994, Fournier & Andrieu 1998, Fournier *et al.* 2005). Also, these parameters can be verified by simple means including visual inspection (e.g. Yang *et al.* 2016). These findings all suggest that the ^{18}O record presented by the successive leaves formed along tillers of *C. squarrosa* (and probably other C_3 and C_4 grasses and dicotyledonous taxa) can be exploited as short-term isotopic chronologies. Such chronologies could be combined with analyses of ^{18}O in phytoliths (Webb & Longstaffe 2006) and ^{13}C in biomass or cellulose of the same tissue (Köhler *et al.* 2016) for comprehensive reconstructions of environmental conditions and physiological adaptations (Barbour 2007, Franks *et al.* 2013) using plant tissue from herbaria (e.g. Peñuelas & Azcón-Bieto 1992, Bonal *et al.* 2011) or other artificial (e.g. Silvertown *et al.* 2006) and natural archives such as bogs (Ménot-Combes *et al.* 2002).

ACKNOWLEDGEMENTS

Wolfgang Feneis and Richard Wenzel are thanked for technical assistance with the mesocosm facility. Anja Schmidt, Monika Michler, Angelika Ernst-Schwärzli, Hans Vogl, L. Li, S. Y. Wang, and Jennifer Ciomas provided valuable assistance during sample collection and processing. This research was supported by the Deutsche Forschungsgemeinschaft (DFG SCHN 557/7-1). H. T. L. and F. Y. were supported by the Chinese Scholarship Council (CSC). The authors have no conflict of interest.

REFERENCES

Anderson W., Bernasconi S., McKenzie J., Saurer M. & Schweingruber F. (2002) Model evaluation for reconstructing the oxygen isotopic composition in precipitation from tree ring cellulose over the last century. *Chemical Geology*, **182**, 121-137.

Barbour M.M., Walcroft A. & Farquhar G.D. (2002) Seasonal variation in $\delta^{13}C$ and $\delta^{18}O$ of cellulose from growth rings of *Pinus radiata*. *Plant, Cell & Environment*, **25**, 1483-1499.

Barbour M.M. (2007) Stable oxygen isotope composition of plant tissue: a review. *Functional Plant Biology*, **34**, 83-94.

Bonal D., Ponton S., Le Thiec D., Richard B., Ningre N., Hérault B., ..., Sabatier D. (2011) Leaf functional response to increasing atmospheric CO_2 concentrations over the last century in two northern Amazonian tree species: a historical $\delta^{13}C$ and $\delta^{18}O$ approach using herbarium samples. *Plant, Cell & Environment*, **34**, 1332-1344.

Brendel O., Iannetta P.M. & Stewart D. (2000) A Rapid and Simple Method to Isolate Pure Alpha-Cellulose. *Phytochemical Analysis*, **11**, 7-10.

Briffa K.R., Bartholin T.S., Eckstein D., Jones P.D., Karlén W., Schweingruber F.H. & Zetterberg P. (1990) A 1,400-year tree-ring record of summer temperatures in Fennoscandia. *Nature*, **346**, 434-439.

Cao W.X. & Moss D.N. (1994) Sensitivity of winter-wheat phyllochron to environmental-changes. *Agronomy Journal*, **86**, 63-66.

Damesin C. & Lelarge C. (2003) Carbon isotope composition of current-year shoots from *Fagus sylvatica* in relation to growth, respiration and use of reserves. *Plant, Cell & Environment*, **26**, 207-219.

Esper J., Cook E.R. & Schweingruber F.H. (2002) Low-frequency signals in long tree-ring chronologies for reconstructing past temperature variability. *science*, **295**, 2250-2253.

Farquhar G.D., Barbour M.M. & Henry B.K. (1998) Interpretation of oxygen isotope composition of leaf material. In *Stable Isotopes: Integration of Biological, Ecological, and Geochemical Processes* (eds D. Robinson, P. Van Gardingen, H. Griffiths), pp. 27-74. Environmental Plant Biology series, BIOS Scientific Publishers Ltd., Oxford.

Fournier C. & Andrieu B. (1998) A 3D architectural and process-based model of maize development. *Annals of Botany*, **81**, 233-250.

Fournier C., Durand J.L., Ljutovac S., Schäufele R., Gastal F. & Andrieu B. (2005) A functional–structural model of elongation of the grass leaf and its relationships with the phyllochron. *New Phytologist*, **166**, 881-894.

Franks P.J., Adams M.A., Amthor J.S., Barbour M.M., Berry J.A., Ellsworth D.S., …, McDowell N. (2013) Sensitivity of plants to changing atmospheric CO_2 concentration: from the geological past to the next century. *New Phytologist*, **197**, 1077-1094.

Gaudinski J.B., Dawson T.E., Quideau S., Schuur E.A., Roden J.S., Trumbore S.E., …, Wasylishen R.E. (2005) Comparative analysis of cellulose preparation techniques for use with ^{13}C, ^{14}C, and ^{18}O isotopic measurements. *Analytical Chemistry*, **77**, 7212-7224.

Gessler A., Brandes E., Buchmann N., Helle G., Rennenberg H. & Barnard R.L. (2009) Tracing carbon and oxygen isotope signals from newly assimilated sugars in the leaves to the tree-ring archive. *Plant, cell & environment*, **32**, 780-795.

Gessler A., Ferrio J.P., Hommel R., Treydte K., Werner R.A. & Monson R.K. (2014) Stable isotopes in tree rings: towards a mechanistic understanding of isotope fractionation and mixing processes from the leaves to the wood. *Tree Physiology*, **38**, 796-818.

Gong X.Y., Chen Q., Lin S., Brueck H., Dittert K., Taube F., Schnyder H. 2011. Tradeoffs between nitrogen- and water-use efficiency in dominant species of the semiarid steppe of Inner Mongolia. *Plant and Soil*, **340**, 227-238.

Gong X.Y., Schäufele R. & Schnyder H. (2016) Bundle-sheath leakiness and intrinsic water-use efficiency of a perennial C_4 grass are increased at high vapour pressure deficit during growth. *Journal of Experimental Botany*, DOI: 10.1093/jxb/erw417.

Helle G. & Schleser G. (2004) Beyond CO_2-fixation by Rubisco–an interpretation of $^{13}C/^{12}C$ variations in tree rings from novel intra-seasonal studies on broad-leaf trees. *Plant, Cell & Environment*, **27**, 367-380.

Helliker B.R. & Ehleringer J.R. (2002) Grass blades as tree rings: environmentally induced changes in the oxygen isotope ratio of cellulose along the length of grass blades. *New Phytologist*, **155**, 417-424.

Hemming D., Fritts H., Leavitt S.W., Wright W., Long A. & Shashkin A. (2001) Modelling tree-ring $\delta^{13}C$. *Dendrochronologia*, **19**, 23-38.

Hill S.A., Waterhouse J.S., Field E.M., Switsur V.R. & Ap Rees T. (1995) Rapid recycling of triose phosphates in oak stem tissue. *Plant, Cell & Environment*, **18**, 931-936.

Hong Y., Jiang H., Liu T., Zhou L., Beer J., Li H., …, Qin X. (2000) Response of climate to solar forcing recorded in a 6000-year$\delta^{18}O$ time-series of Chinese peat cellulose. *The Holocene*, **10**, 1-7.

Kagawa A., Sugimoto A., Yamashita K. & Abe H. (2005) Temporal photosynthetic carbon isotope signatures revealed in a tree ring through $^{13}CO_2$ pulse-labelling. *Plant, Cell & Environment*, **28**, 906-915.

Kahmen A., Sachse D., Arndt S.K., Tu K.P., Farrington H., Vitousek P.M. & Dawson T.E. (2011) Cellulose $\delta^{18}O$ is an index of leaf-to-air vapor pressure difference (VPD) in tropical plants. *Proceedings of the National Academy of Sciences*, **108**, 1981-1986.

Kikuzawa K. (1984) Leaf survival of woody plants in deciduous broad-leaved forests. 2. Small trees and shrubs. *Canadian Journal of Botany*, **62**, 2551-2556.

Köhler I.H., Macdonald A. & Schnyder H. (2016) Last-century increases in intrinsic water-use efficiency of grassland communities have occurred over a wide range of vegetation composition, nutrient inputs and soil pH. *Plant Physiology*, **170**, 2881-2890

Lattanzi F.A., Schnyder H. & Thornton B. (2005) The sources of carbon and nitrogen supplying leaf growth. Assessment of the role of stores with compartmental models. *Plant Physiology*, **137**, 383-395.

Libby L.M., Pandolfi L.J., Payton P.H., Marshall J., Becker B. & Giertz-Sienbenlist V. (1976) Isotopic tree thermometers. *Nature*, **261**, 284-288.

Liu H.T., Gong X.Y., Schäufele R., Yang F., Hirl R.T., Schmidt A. & Schnyder H. (2016) Nitrogen fertilization and $\delta^{18}O$ of CO_2 have no effect on ^{18}O-enrichment of leaf water and cellulose in *Cleistogenes squarrosa* (C_4)–is VPD the sole control? *Plant, Cell & Environment*, **39**, 2701-2712.

MacAdam J.W. & Nelson C.J. (2002) Secondary cell wall deposition causes radial growth of fibre cells in the maturation zone of elongating tall fescue leaf blades. *Annals of Botany*, **89**, 89-96.

Ménot-Combes G., Burns S.J. & Leuenberger M. (2002) Variations of $^{18}O/^{16}O$ in plants from temperate peat bogs (Switzerland): implications for paleoclimatic studies. *Earth and Planetary Science Letters*, **202**, 419-434.

Monteith J. (1995) A reinterpretation of stomatal responses to humidity. *Plant, Cell & Environment*, **18**, 357-364.

Peñuelas J. & Azcón-Bieto J. (1992) Changes in leaf $\delta^{13}C$ of herbarium plant species during the last 3 centuries of CO_2 increase. *Plant, Cell & Environment*, **15**, 485-489.

Pilcher J.R., Baillie M.G., Schmidt B. & Becker B. (1984) A 7,272-year tree-ring chronology for western Europe. *Nature*, **312**, 150-152.

Roden J.S., Lin G. & Ehleringer J.R. (2000) A mechanistic model for interpretation of hydrogen and oxygen isotope ratios in tree-ring cellulose. *Geochimica et Cosmochimica Acta*, **64**, 21-35.

Scheidegger Y., Saurer M., Bahn M. & Siegwolf R. (2000) Linking stable oxygen and carbon isotopes with stomatal conductance and photosynthetic capacity: a conceptual model. *Oecologia*, **125**, 350-357.

Schleip I., Lattanzi F.A. & Schnyder H. (2013) Common leaf life span of co-dominant species in a continuously grazed temperate pasture. *Basic and Applied Ecology*, **14**, 54-63.

Schleser G.H., Helle G., Lücke A. & Vos H. (1999) Isotope signals as climate proxies: the role of transfer functions in the study of terrestrial archives. *Quaternary Science Reviews*, **18**, 927-943.

Schnyder H. (1992) long-term steady-state labeling of wheat plants by use of natural $^{13}CO_2/^{12}CO_2$ mixtures in an open, rapidly turned-over system. *Planta*, **187**, 128-135.

Schnyder H., Schäufele R., Lötscher M. & Gebbing T. (2003) Disentangling CO_2 fluxes: direct measurements of mesocosm-scale natural abundance $^{13}CO_2/^{12}CO_2$ gas exchange, ^{13}C discrimination, and labelling of CO_2 exchange flux components in controlled environments. *Plant, Cell & Environment*, **26**, 1863-1874.

Schollaen K., Heinrich I. & Helle G. (2014) UV-laser-based microscopic dissection of tree rings–a novel sampling tool for $\delta^{13}C$ and $\delta^{18}O$ studies. *New Phytologist*, **201**, 1045-1055.

Schulze B., Wirth C., Linke P., Brand W.A., Kuhlmann I., Horna V. & Schulze E.D. (2004) Laser ablation-combustion-GC-IRMS—a new method for online analysis of intra-annual variation of $\delta^{13}C$ in tree rings. *Tree Physiology*, **24**, 1193-1201.

Schulze E.D. (1986) Carbon dioxide and water vapor exchange in response to drought in the atmosphere and in the soil. *Annual Review of Plant Physiology*, **37**, 247-274.

Silvertown J., Poulton P., Johnston E., Edwards G., Heard M. & Biss P.M. (2006) The Park Grass Experiment 1856–2006: its contribution to ecology. *Journal of Ecology*, **94**, 801-814.

Skinner R. & Nelson C. (1995) Elongation of the grass leaf and its relationship to the phyllochron. *Crop Science*, **35**, 4-10.

Song X., Farquhar G.D., Gessler A. & Barbour M.M. (2014) Turnover time of the non-structural carbohydrate pool influences $\delta^{18}O$ of leaf cellulose. *Plant, cell & environment*, **37**, 2500-2507.

Sternberg L.D.S.L. (2009) Oxygen stable isotope ratios of tree-ring cellulose: the next phase of understanding. *New Phytologist*, **181**, 553-562.

Treydte K., Frank D., Esper J., Andreu L., Bednarz Z., Berninger F., …, Filot M. (2007) Signal strength and climate calibration of a European tree-ring isotope network. *Geophysical Research Letters*, **34**.

Treydte K.S., Schleser G.H., Helle G., Frank D.C., Winiger M., Haug G.H. & Esper J. (2006) The twentieth century was the wettest period in northern Pakistan over the past millennium. *Nature*, **440**, 1179-1182.

Webb E.A. & Longstaffe F.J. (2006) Identifying the $\delta^{18}O$ signature of precipitation in grass cellulose and phytoliths: refining the paleoclimate model. *Geochimica et Cosmochimica Acta*, **70**, 2417-2426.

Wittmer M.H.O.M, Auerswald K., Tungalag R., Bai Y.F., Schäufele R., Schnyder H. (2008) Carbon isotope discrimination of C_3 vegetation in Central Asian grassland as related to long-term and short-term precipitation patterns. *Biogeosciences*, **5**, 913–924.

Wright W.E. & Leavitt S.W. (2006) Needle cell elongation and maturation timing derived from pine needle cellulose $\delta^{18}O$. *Plant, Cell & Environment*, **29**, 1-14.

Yang F., Gong X.Y., Liu H.T., Schäufele R. & Schnyder H. (2016) Effects of nitrogen and vapour pressure deficit on phytomer growth and development in a C_4 grass. *AoB PLANTS*, DOI: 10.1093/aobpla/plw1075.

Figures and Tables

Table 1. Developmental stages of leaf blades at times of transfer to a new VPD environment and harvest/sampling 7 d later, and growth duration in the new environment following the transfer (for details, see Materials and Methods and Results). Developmental stage is given as leaf blade length expressed as a fraction of final length (f_{FBL}), and was inferred from the leaf appearance interval (2.4 d at both low and high VPD) and the time course of leaf blade elongation shown in Fig. 1. Growth duration after the transfer was calculated as the time needed to reach 98% of final blade length.

Leaf number	(f_{FBL}) at time of		Growth duration after
	transfer	harvest	transfer
	%	%	d
1	5	84	7.0
2	19	97	7.0
3	54	100	5.1
4	85	100	2.7
5	97	100	0.3
≥6	100	100	0

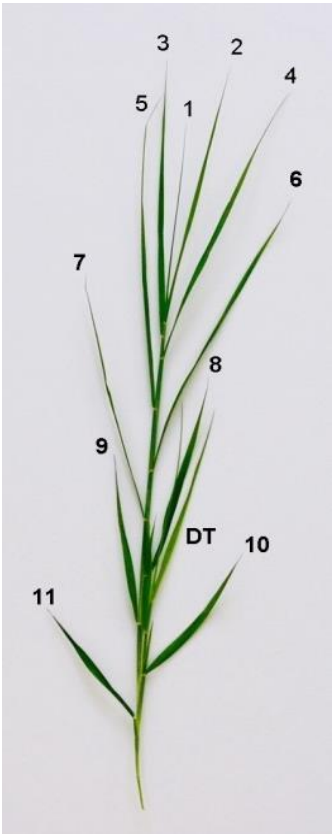

Figure 1. Photograph of a tiller of *Cleistogenes squarrosa*. Leaf blades are numbered consecutively from the tip to the base of the tiller, with no. 1 the youngest (exposed) leaf and no. 11 the oldest. DT refers to a daughter tiller which has emerged from the axillary bud of leaf no. 10 (photo taken from Supporting Information in Liu *et al*. 2016).

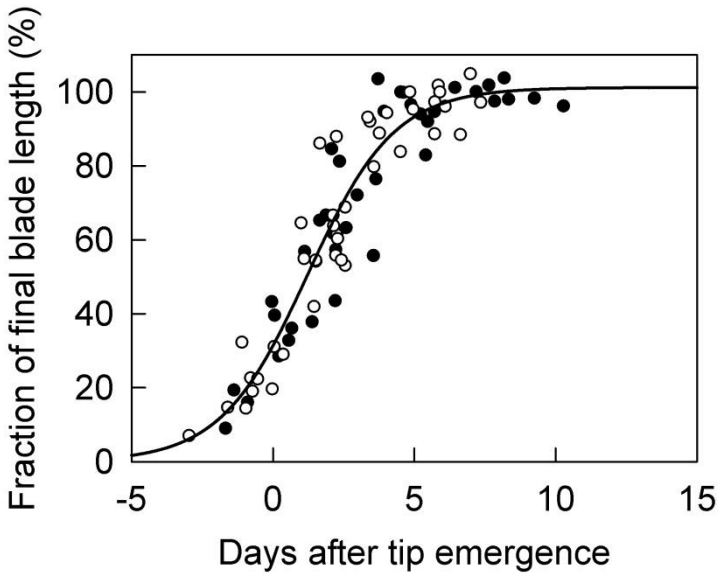

Figure 2. Time course of leaf blade elongation of *Cleistogenes squarrosa* in relation to the time of leaf tip emergence. Plants were grown at low VPD (closed circles) and high VPD (open circles). Leaf blade length is expressed as a fraction of final length (f_{FBL}). Emergence is defined as the time when the leaf tip grows past the highest visible ligule of the next fully expanded leaf. The solid curve denotes a 3-parameter sigmoidal function for all data: $y = 101.19/\{1 + \exp[(1.22 - x)/1.53]\}$, $R^2 = 0.89$. VPD had no effect on the parameters of the function ($P > 0.05$).

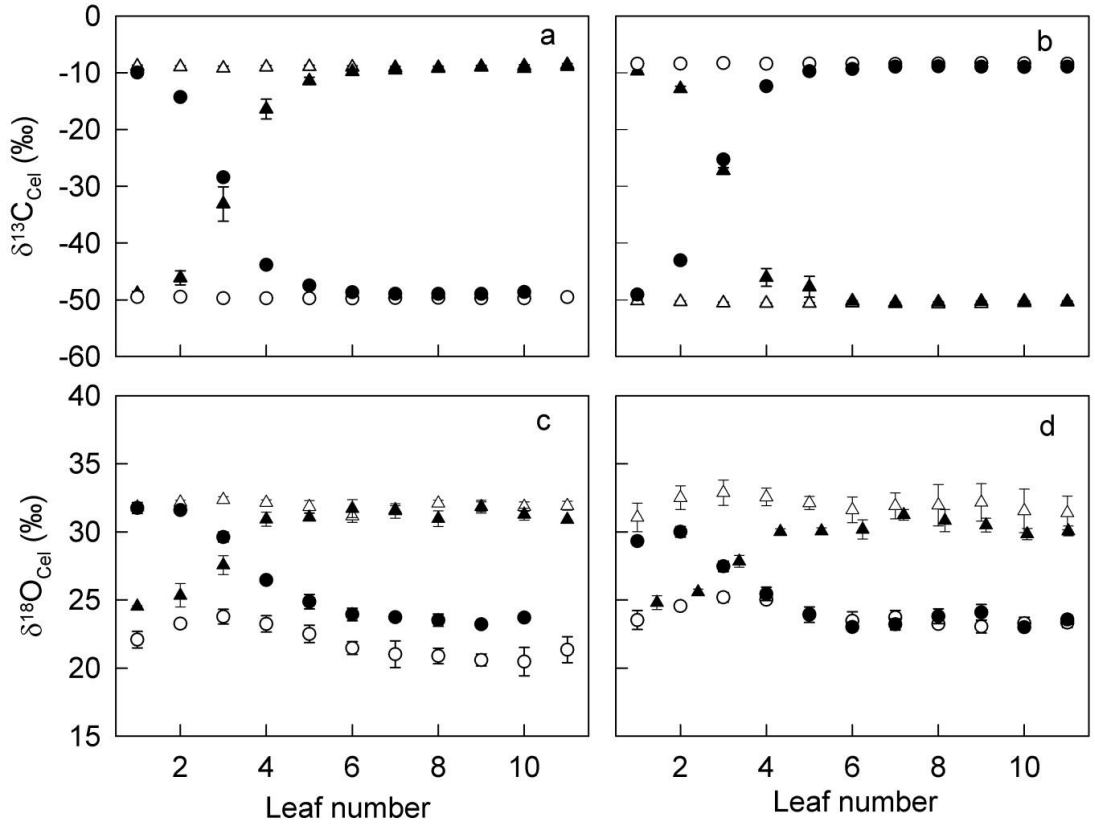

Figure 3. Carbon isotope composition, $\delta^{13}C_{Cel}$ (a, b), and oxygen isotope composition (c, d) of cellulose, $\delta^{18}O_{Cel}$, in the different leaves formed along a tiller of *C. squarrosa*. Leaves were numbered from youngest to oldest (cf. Fig. 2). Plants were either kept constantly in the same environment (open symbols) or transferred from one VPD environment to the other (low to high VPD or high to low VPD) and kept in the new environment for 7 d before sampling (closed symbols). In all cases, the transfer of plants was associated with exposure to an altered $\delta^{13}C_{CO2}$ (see Materials and Methods). The experiment had two replications: 1st experiment (a, c), 2nd experiment (b, d). Symbols: constant low VPD (open circles); constant high VPD (open triangles); low to high VPD transfer (closed circles); high-to-low VPD transfer (closed triangles). In the 1st (2nd) experiment the low VPD chamber received ^{13}C-depleted CO_2 (^{13}C-enriched CO_2) and the high VPD chamber ^{13}C-enriched CO_2 (^{13}C-depleted CO_2). For details of treatments see Fig. S1 and Materials and Methods. Values are means ± standard error (*n* = 3).

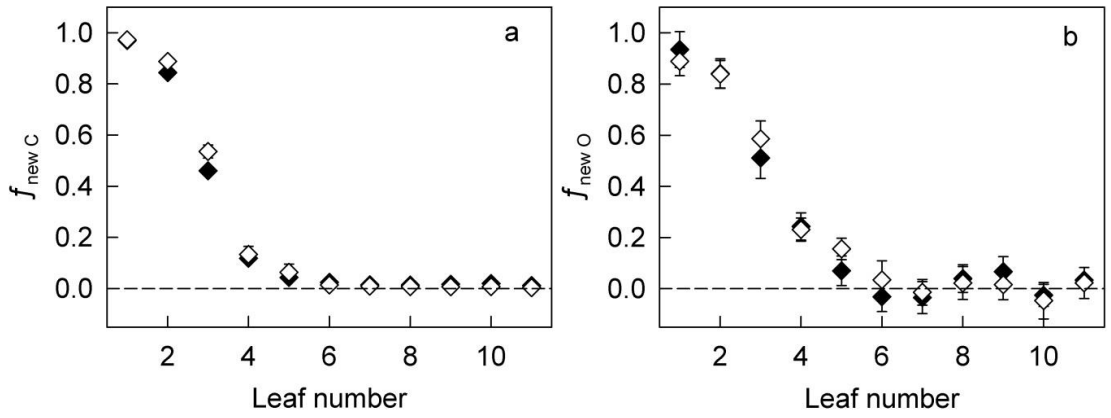

Figure 4. Fractions of new carbon, $f_{new\ C}$ (a) and new oxygen, $f_{new\ O}$ (b) in cellulose of leaf blades of different ages in plants transferred from low to high VPD (closed diamonds) and from high to low VPD (open diamonds). Leaves are numbered from the youngest to the oldest (cf Fig. 2). Transferred plants were exposed to the new VPD environment for a period of 7 d before sampling. In all treatments, transferred plants were exposed to an altered $\delta^{13}C_{CO2}$ that provided for a differential labeling of all carbon assimilation in the new VPD environment (see Materials and Methods and Fig. S1). Values are presented as mean ± standard error (n = 6).

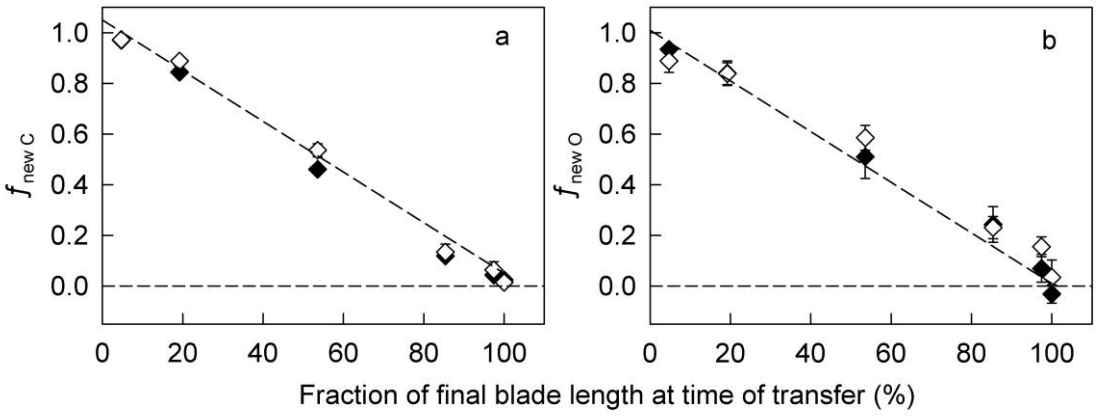

Figure 5. Fractions of new carbon, $f_{new\ C}$ (a) and new oxygen, $f_{new\ O}$ (b) in cellulose of leaf blades of different ages in plants transferred from low to high VPD (closed diamonds) and from high to low VPD (open diamonds) as a function of the fraction of leaf blade length that was already attained at the time of transfer. Leaves are numbered from the youngest to the 6th old blade which has already been fully expanded at time of transfer (cf. Fig. 2 and Table 1). Transferred plants were exposed to the new VPD environment for a period of 7 d before sampling. The dashed lines are linear regression lines for $f_{new\ C}$ in panel (a): y = −0.01 x + 1.05 (R^2 = 0.99), and for $f_{new\ O}$ in panel (b): y = −0.01 x + 1.01 (R^2 = 0.88). Values are presented as mean ± standard error (n = 6). For further details see Materials and Methods, Fig. 3 and Fig. S1.

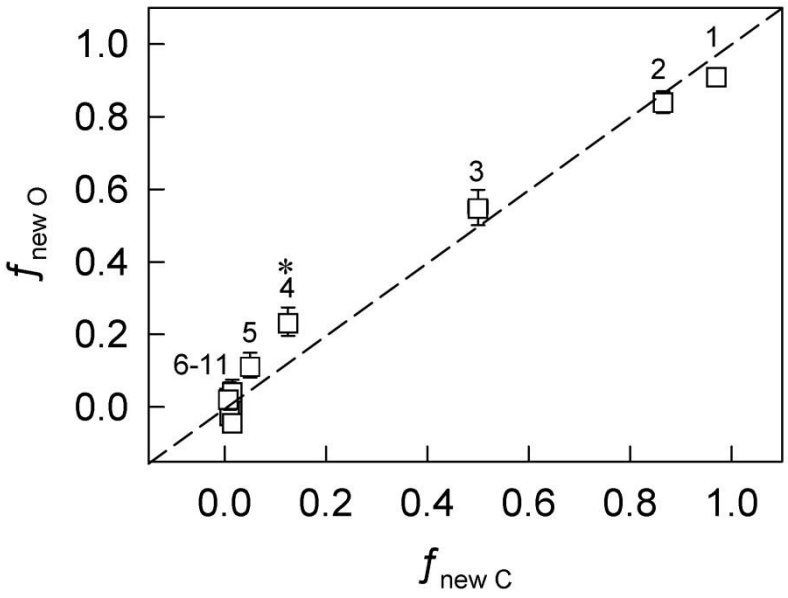

Figure 6. Relationship between the fractions of new carbon ($f_{new\ C}$) and oxygen ($f_{new\ O}$) in cellulose of leaf blades of different ages in plants. Data of $f_{new\ C}$ and $f_{new\ O}$ transferred from low to high VPD and from high to low VPD was combined together due to the similar general relationship between $f_{new\ C}$ and $f_{new\ O}$ with leaf age/developmental stage. Numbers refer to leaf age as indicated in Fig. 2, Table 1. * above a data point indicates a significant difference between $f_{new\ C}$ and $f_{new\ O}$ ($P < 0.05$). For other leaf categories there was no significant difference between $f_{new\ C}$ and $f_{new\ O}$ of. Dashed lines give the 1:1 relationship. Values are presented as means ± standard error ($n = 6$) for both $f_{new\ C}$ and $f_{new\ O}$.

SUPPORTING INFORMATION

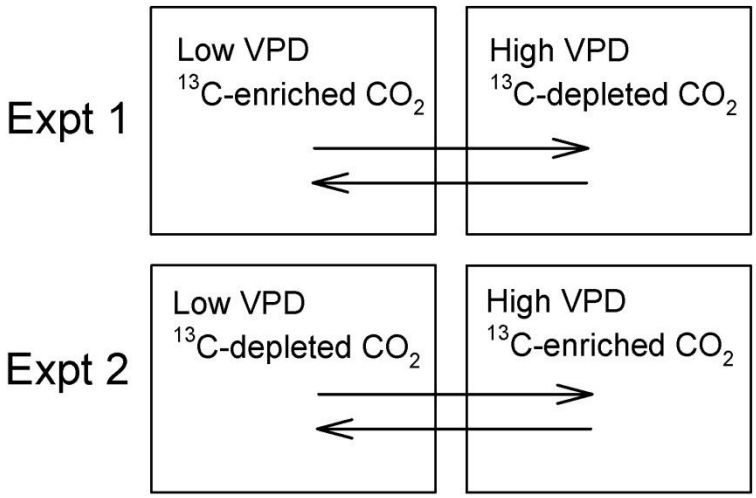

Figure S1. Experimental scheme. Two independent experiments were performed with plants of *C. squarrosa* exposed to four treatments in growth chambers: constant low VPD, constant high VPD, transfer from low to high VPD, and transfer from high to low VPD. In both experiments, the low and high VPD environments received CO_2 with contrasting $\delta^{13}C_{CO2}$ (^{13}C-depleted CO_2, −48.8‰; and ^{13}C-enriched CO_2, −6.2‰). Transferred plants were kept in the new environment (high or low VPD) for 7 d and then sampled in parallel with plants kept constantly at low and high VPD. Three samples were collected in each treatment in each experiment. Except for VPD and $\delta^{13}C_{CO2}$ all conditions were kept the same in all growth chambers.

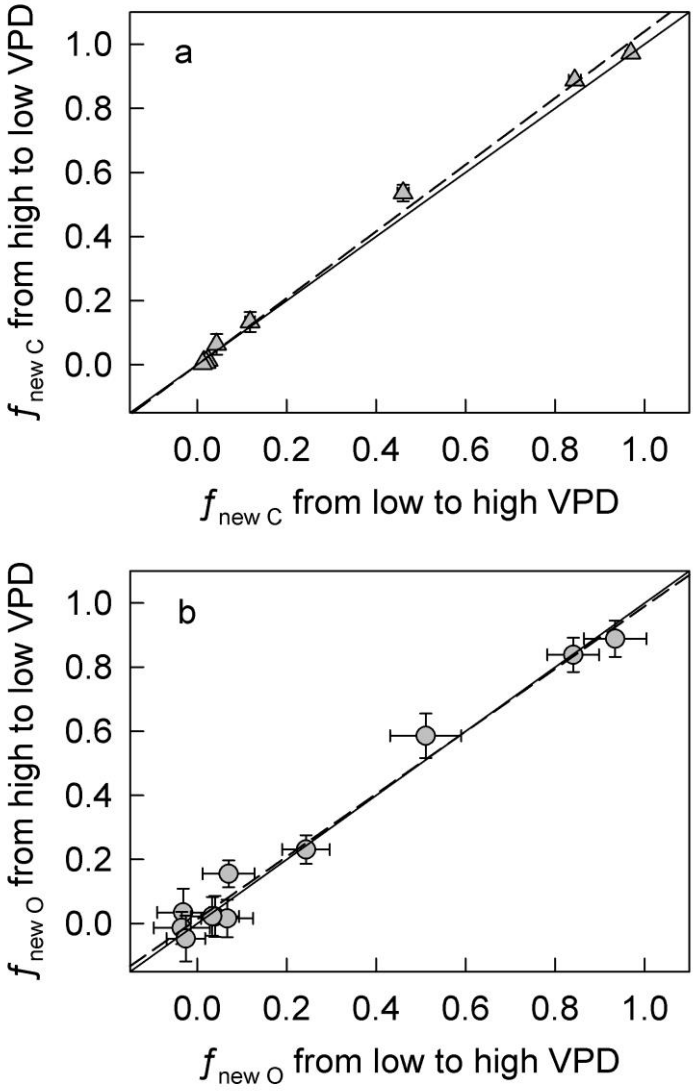

Figure S2. (a) Fraction of new carbon ($f_{new\ C}$) in leaf blade cellulose of plants transferred from high to low VPD (y-axis) *versus* $f_{new\ C}$ in plants transferred from low to high VPD (x-axis). (b) Fraction of new oxygen ($f_{new\ O}$) in plants transferred from low to high VPD (x-axis) *versus* $f_{new\ O}$ in plants transferred from high to low VPD (y-axis). Data points compare $f_{new\ C}$ (or $f_{new\ O}$) for same age leaves. The solid lines give the 1:1 relationship. The dashed lines are linear regression lines for $f_{new\ C}$ in panel (a): y = 1.04 x + 0.0004 (R^2 = 0.996), and for $f_{new\ O}$ in panel (b): y = 0.98 x + 0.01 (R^2 = 0.98). For both regressions, the intercept is not significantly different from 0 and the slope is not significantly different from 1. Data points show the mean ± standard error (n = 6).

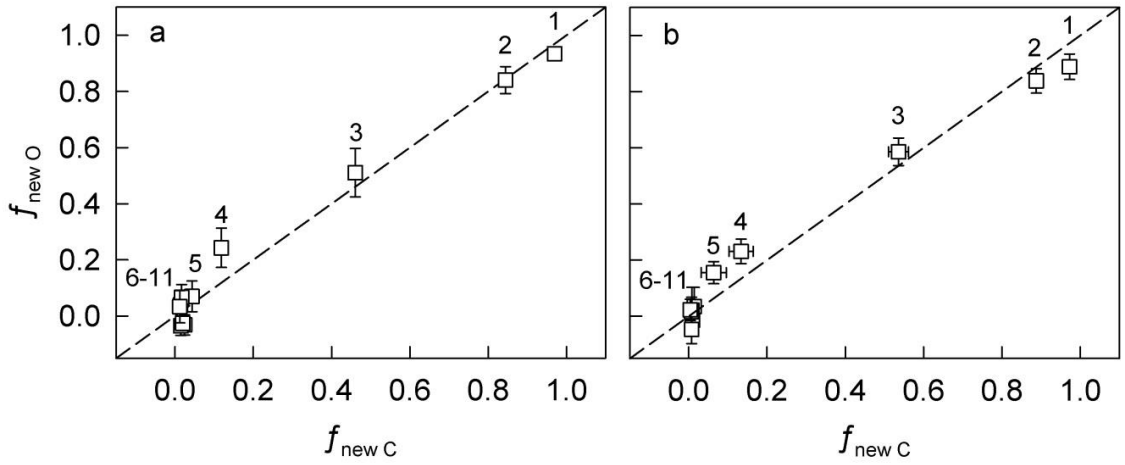

Figure S3. Relationship between the fractions of new carbon ($f_{new\ C}$) and oxygen ($f_{new\ O}$) in cellulose of leaf blades of different age in plants transferred from low to high VPD (a) and from high to low VPD (b). Numbers refer to leaf age as indicated in Fig. 1 and Table 1. The dashed lines are 1:1 lines, and values are presented as means ± standard error (n = 6).

Acknowledgments

I would like to express great gratitude to my supervisor, Prof. Hans Schnyder, for his supervision and support throughout my studies. His knowledge of plant biology and physiology, countless advice and attention helped me finish this thesis. Another person I would like to thank is my mentor Dr. Rudi Schäufele. I appreciated a lot his guidance and patience. Without your support, it would not have been possible to see the success of this work.

A big "thank you" goes to Dr. Xiao Ying Gong, for helping and encouraging me with the paper process. Also, I would like to thank Prof. Karl Auerswald, Dr. Ulrike Ostler, and Dr. Ceclilia Casas for helping me with research. I thank other members from the lab of Lehrstuhl für Grünlandlehre for helping me carry out all experiments.

A special thanks to my colleagues, as well as good friends, Melita, Anja, Ulrike, Regina, Cecilia, Hai Tao, and Chen Guo for their care and company. I was extremely happy to spend the past four years with you and to enjoy team sports with you. In addition, I would like to thank another two best Chinese friends, Chunyang Chen (University of Jena) and Cong Yang (University of Siegen), for encouragement and accompanying me through ups and downs.

I owe a debt of gratitude to the China Scholarship Council for providing me a fully-funded scholarship, enabling me to study in one of the leading universities in Germany.

Finally, I would like to express my love to my parents far away from Germany, for understanding and being with me.

Lebenslauf

Persönliche Angaben:

Name: Fang Yang

Geburtstag und Geburtsort: 10 Sept. 1986, Jilin, China

Nationalität: Chinesin

Familienstand: Ledig

Ausbildung:

2005 – 2009: B.Sc in Agronomy, Jilin Agricultural University, Changchun, Jilin, China

2009 – 2012: M.Sc in Ecology, Northeast Normal University, Changchun, Jilin, China

2012 – 2017: Ph.D in Ecophysiology, Technische Universität München, Freising, Germany

Berufliche Tätigkeiten

2012 – 2017: Wissenschaftliche Mitarbeiterin, Lehrstuhl für Grünlandlehre,

Technische Universität München